MINISTRY OF EDUCATION AND TRAINING

HO CHI MINH CITY

UNIVERSITY OF TECHNOLOGY AND EDUCATION

HO LE HUY PHUC

DEVELOPMENT OF NOVEL MESHLESS METHOD FOR LIMIT AND SHAKEDOWN ANALYSIS OF STRUCTURES & MATERIALS

DOCTORAL THESIS

MAJOR: ENGINEERING MECHANICS

Ho Chi Minh city, 3rd May 2020

MINISTRY OF EDUCATION AND TRAINING

HO CHI MINH CITY

UNIVERSITY OF TECHNOLOGY AND EDUCATION

HO LE HUY PHUC

DEVELOPMENT OF NOVEL MESHLESS METHOD FOR LIMIT AND SHAKEDOWN ANALYSIS OF STRUCTURES & MATERIALS

MAJOR: ENGINEERING MECHANICS

Supervisors:

1. Assoc. Prof Le Van Canh

2. Assoc. Prof Phan Duc Hung

Reviewer 1:

Reviewer 2:

Reviewer 3:

Declaration of Authorship

I declare that this is my own research.

The data and results stated in the thesis are honest and have not been published by anyone in any other works.

Ho Chi Minh city, 3rd August 2020
PhD candidate

HO LE HUY PHUC

Acknowledgements

The research presented in this thesis has been carried out in the framework of a doctorate at Faculty of Civil Engineering, Ho Chi Minh city University of Technology and Education, Vietnam. This work would have never been possible without the support and help of many people to whom I feel deeply grateful.

First and foremost, I would like to express my most sincere thanks to my supervisors, Assoc. Prof. Le Van Canh and Assoc. Prof. Phan Duc Hung, for their guidance, valuable academic advice, mental support and constant encouragement during the course of this work. I am deeply indebted to my major supervisor, Assoc. Prof. Le Van Canh. He is one of most influential people in my life, both professionally and personally. His guidance is precious, helping me develop the personal skills needed to succeed in future work.

I would like to thank the co-author of my papers - Prof. Tran Cong Thanh for his encouragement, support and guidance. I would also like to express my admiration for his unsurpassed knowledge of mathematics and numerical methods.

I really appreciate the financial support received from the Institute for Computational Science and Technology (ICST) - HCMC, the Science and Technology Incubator Youth Program - HCMC, and International University - VNU-HCMC throughout the research projects.

I take this opportunity to thank my colleagues in International University - VNU-HCMC, HCMC University of Technology and Education, and HUTECH University, especially Dr. Tran Trung Dung, PhD candidate Nguyen Hoang Phuong, PhD candidate Do Van Hien, Dr. Khong Trong Toan and Dr. Vo Minh Thien, for fruitful discussions about a range of topics and their mental support.

I sincerely thank my parents and my younger sisters for their unconditional love and support. I am also definitely indebted to my wife, Nguyen My Lam, for her love, understanding and encouraging me whenever I needed motivation.

Finally, I would like to dedicate this thesis to my little son - Ho Nguyen Nhat Duy. No word can describe my love for him.

Ho Chi Minh city, 3rd August 2020
PhD candidate

HO LE HUY PHUC

Abstract

The proposed research is essentially concerning on the development of powerful numerical methods to deal with practical engineering problems. The direct methods requiring the use of a strong mathematical tool and a proper numerical discretization are considered.

The current work primarily focuses on the study of limit and shakedown analysis allowing the rapid access to the requested information of structural design without the knowledge of whole loading history. For the mathematical treatment, the problems are formulated in form of minimizing a sum of Euclidean norms which are then cast as suitable conic programming depending on the yield criterion, e.g. second order cone programming (SOCP).

In addition, a robust numerical tool also requires an excellent discretization strategy which is capable of providing stable and accurate solutions. In this study, the so-called integrated radial basis functions-based mesh-free method (iRBF) is employed to approximate the computational fields. To eliminate numerical instability problems, the stabilized conforming nodal integration (SCNI) scheme is also introduced. Consequently, all constrains in resulting problems are directly enforced at scattered nodes using collocation method. That not only keeps size of the optimization problem small but also ensures the numerical procedure truly mesh-free. One more advantage of iRBF method, which is absent in almost meshless ones, is that the shape function satisfies Kronecker delta property leading the essential boundary conditions to be imposed easily.

In summary, the iRBF-based mesh-free method is developed in combination with second order cone programming to provide solutions for direct analysis of structures and materials. The most advantage of proposed approach is that the highly accurate solutions can be obtained with low computational efforts. The performance of proposed method is justified via the comparison of obtained results and available ones in the literature.

Tóm tắt

Luận án này hướng đến việc phát triển một phương pháp số mạnh để giải quyết các bài toán kỹ thuật, và phương pháp phân tích trực tiếp được sử dụng. Phương pháp này yêu cầu một thuật toán tối ưu hiệu quả và một công cụ rời rạc thích hợp.

Trước tiên, nghiên cứu này tập trung vào lý thuyết phân tích giới hạn và thích nghi, phương pháp được biết đến như một công cụ hữu hiệu để xác định trực tiếp những thông tin cần thiết cho việc thiết kế kết cấu mà không cần phải thông qua toàn bộ quá trình gia tải. Về mặt toán học, các bài toán được phát biểu dưới dạng cực tiểu một chuẩn của tổng bình phương các biến trong không gian Euclide, sau đó được đưa về dạng chương trình hình nón phù hợp với tiêu chuẩn dẻo, ví dụ chương trình hình hón bậc hai (SOCP).

Hơn nữa, một công cụ số mạnh còn đòi hỏi phải có kỹ thuật rời rạc tốt để đạt được kết quả tính toán chính xác với tính ổn định cao. Nghiên cứu này sử dụng phương pháp không lưới dựa trên phép tích phân hàm cơ sở hướng tâm (iRBF) để xấp xỉ các trường biến. Kỹ thuật tích phân nút ổn định (SCNI) được đề xuất nhằm loại bỏ sự thiếu ổn định của kết quả số. Nhờ đó, tất cả các ràng buộc trong bài toán được áp đặt trực tiếp tại các nút bằng phương pháp tụ điểm. Điều này không những giúp kích thước bài toán được giữ ở mức tối thiểu mà còn đảm bảo phương pháp là không lưới thực sự. Một ưu điểm nữa mà hầu hết các phương pháp không lưới khác không đáp ứng được, đó là hàm dạng iRBF thỏa mãn đặc trưng Kronecker delta. Nhờ vậy, các điều kiện biên chính có thể được áp đặt dễ dàng mà không cần đến các kỹ thuật đặc biệt.

Tóm lại, nghiên cứu này phát triển phương pháp không lưới iRBF kết hợp với thuật toán tối ưu hình nón bậc hai cho bài toán phân tích trực tiếp kết cấu và vật liệu. Thế mạnh lớn nhất của phương pháp đề xuất là kết quả số với độ chính xác cao có thể thu được với chi phí tính toán thấp. Hiệu quả của phương pháp được đánh giá thông qua việc so sánh kết quả số với những phương pháp khác.

Contents

List of Tables

List of Figures

List of Abbreviations

$\|.\|$	Euclidean norm.
2D	Two-dimensions.
3D	Three-dimensions.
BC	Boundary condition.
BEM	Boundary element method.
CCCC	Clamped-clamped-clamped-clamped (BC).
CCCF	Clamped-clamped-clamped-free (BC).
CFCF	Clamped-free-clamped-free (BC).
CPU	Central processing unit.
CS-HCT	Curvature Smoothing Hsieh-Clough-Tocher.
DLO	Discontinuous Layout Optimization.
dRBF	Direct radial basis function.
EFG	Element-free Galerkin.
FCCC	Free-clamped-clamped-clamped (BC).
FCFC	Free-clamped-free-clamped.
FDM	Finite difference method.
FE	Finite element.
FEM	Finite element method.
IQ	Inverse quadric.
iRBF	Indirect/integrated radial basis function.
LMEA	Local maximum-entropy approximation.
LP	Linear programming.
MF	Mesh-free.
MFM	Mesh-free method.
MLPG	Meshless local Petrov-Galerkin.
MLS	Moving least square.
MRKPM	Moving Reproducing kernel particle method.
MQ	Multi-quadric.

MQ-RBF	Multi-quadric radial basis function.
NEM	Natural neighbour method.
NNI	Natural neighbour interpolation.
P-D	Primal-Dual.
PDE	Partial differential equation.
PDEs	Partial differential equations.
PIM	Point interpolation method.
PU	Partition of Unity.
PUFEM	Partition of Unity Finite element method.
RBF	Radial basis function.
RBFs	Radial basis functions.
RBFNs	Radial basis function networks.
RKP	Reproducing kernel particle.
RKPM	Reproducing kernel particle method.
RPIM	Radial point interpolation method.
SDP	Semi-definite programming.
RVE	Representative Volume Element.
SCNI	Stability conforming nodal integration .
SFEM	Smoothed finite element method.
SOCP	Second-order cone programming.
SPH	Smooth Particle Hydrodynamics.
SSSS	Simply-simply-simply-simply (BC).
VEM	Volume element method.
XFEM	eXtended Finite Element Method.
YL	Yield line.

Chapter 1

Introduction

1.1 General

Limit and shakedown analysis or so-called direct analysis are well-known as the efficient approaches for safety assessment as well as structural design. The objective of both analysis models is to determine the maximum load that structures can be supported under the effect of different loading conditions. While limit analysis is usually used for the structures subjected to instantaneous loads increasing gradually until the collapse appears, shakedown analysis is appropriate for the structures under repeat or cyclic loads. The best advantage of direct analysis is the ability to estimate the ultimate load without obtaining the exact knowledge of loading path.

Based on the bounding theorems, direct analysis results in an optimization problem, in which the unknowns to be found are the velocity vector of kinematic form or the stress vector of static form, or both velocity and stress vectors of mixed formulation. Owing to the complexity of engineering problems, the numerical approaches are required to discretize the computational domain and approximate the unknown fields. Various numerical schemes have been proposed in framework of direct analysis, e.g. mesh-based or mesh-free methods. Besides that, one of major challenges in the field of limit and shakedown analysis is dealing with the nonlinear convex optimization problems. From the mathematical point of views, the resulting problems can be solved using different optimization techniques using linear or nonlinear algorithms.

In addition, owing to the increasing use of composite and heterogeneous materials in engineering, the computation of micro-structures at limit state becomes attracted in recent years. Known as the innovative micro-mechanics technique, ho-

mogenization theory is such an efficient tool for the prediction of physical behavior of materials. The macroscopic properties of heterogeneous materials can be determined by the analysis at the microscopic scale defined by the representative volume element (RVE). The implementation of limit analysis for this problem is similar to one formulated for macroscopic structures. A number of numerical approaches for direct analysis of isotropic, orthotropic, or anisotropic micro-structures have been developed and achieved lots of great accomplishments.

Figure 1.1 illustrates the whole numerical implementation for limit and shakedown analysis of structures and materials.

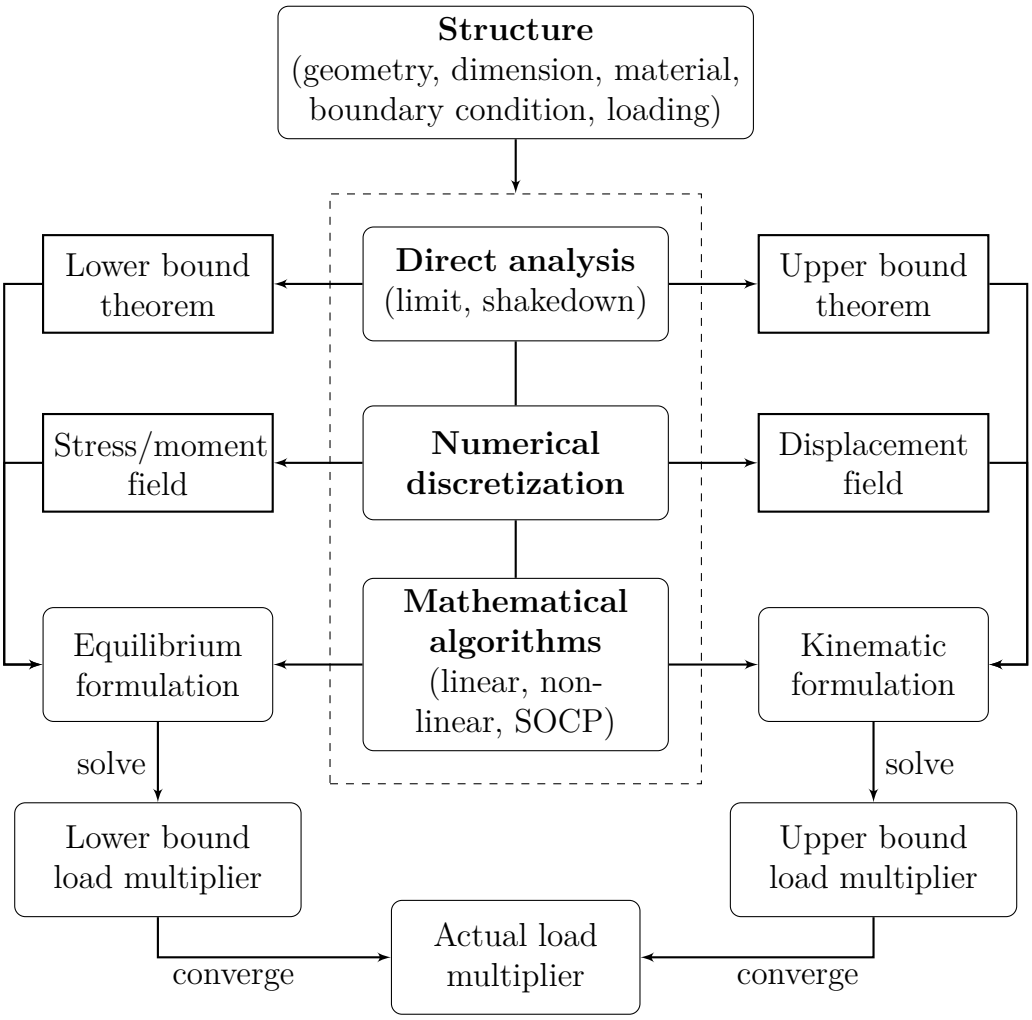

Figure 1.1: Direct analysis: numerical procedures.

1.2 Literature review

1.2.1 Limit and shakedown analysis

Theory of limit analysis was developed in early 20^{th} century based on the elastic- or rigid-perfectly plastic material model to support the engineers evaluate the collapse load of structures. The early theories of limit analysis was given by Kazincky in 1914 and Kist in 1917, then the complete formulation of both upper-bound and lower-bound theorems was firstly introduced by Drucker et al. [1]. Latterly, Hill [2] proposed an alternative formulation using the rigid-plastic material model. The landmark contributions to the development of limit analysis belong to Prager [3]; Martin [4]. The significantly contributions to the application of limit analysis in engineering problems can be founded in works of Hodge [5–7], Massonnet and Save [8], Save and Massonnet [9], Massonnet [10], Chakrabarty and Drugan [11], Chen and Han [12], Lubliner [13]. Since then, the researchers concern not only theory aspect but also the application of limit analysis in practical engineering problems.

In reality, structures are usually subjected repeat, cycle or even time-dependent loading. As a result, the structures may collapse when the loads are lower than those determined using limit analysis formulation. That means limit analysis may fail to provide a proper measure of structural safety. In this case, shakedown analysis can be used. The first formulation of shakedown analysis theorem was expressed by Bliech in 1932, then the static and kinematic principles were generally proved by Melan [14] and Koiter [15], respectively, which are well-known as lower bound and upper bound approaches. Next, the first separate criterion of shakedown (the incremental collapse criterion) was formulated by Sawczuk [16] and Gokhfeld [17]. Konig [18] completed the theory with his work on the alternative criterion. The separated shakedown theory is based on the fact that two different types of failure modes cause the in-adaptation of structures. It suggests the use of different formulations in dealing with two corresponding load factors, see e.g. Koenig [18]. The extensions of classical theorems to more realistic structures have attracted in recent years such as: geometrically linear structures, elastic perfectly-plastic material models, quasi-static mechanical and thermal loading, temperature-independent mechanical properties, negligible time-dependent effects. Among them, hardening and non-associative flow rules have been studied by Maier [19], Pycko and Maier [20], Heitzer et al. [21]. Studies on shakedown problem under geometric non-linearity

can be found in works of Weichert [22], Weichert and Hachemi [23], Polizzotto and Borino [24]. Shakedown has been extended to composites in study of Weichert et al. [25], damaged and cracked structures in studies of Feng and Gross [26], Hachemi and Weichert [27], Belouchrani and Weichert [28]. Another important area concerning the effects of temperature on yield surface was carried-out by Kleiber and Konig [29], Borino [30]. Recently, Pham [31] pointed out that real engineering materials may not yield but may fail under high hydrostatic stresses. In that work, the author has proposed a modified shakedown kinematic theorem using a fictitious material that can yield in bulk tension and compression. Le et al. [32] demonstrated that under repeat or cyclic load, structures can be collapse by the rotating plasticity, a general form of alternating plasticity, incremental plasticity and instantaneous plasticity.

The only difference between limit analysis and shakedown analysis is the loading conditions applying to structures. Limit analysis considers structures under one vertices loading, whereas shakedown model takes into account structures under a loading domain formed by various vertices. Consequently, the size of shakedown problem is lager than limit ones. It is important to note that limit analysis is the special case of shakedown analysis when number of loading vertices reduces to one. Therefore, in general, two models are very similar. There are two issues when handling that problems: first, it is in need of a robust tool for solving the nonlinear yield functions; and second, it is necessary to develop an appropriate numerical method for the approximation of problems. The brief overview of historical development of related matters will be expressed in the following.

1.2.2 Mathematical algorithms

One of challenges in solving limit and shakedown problem is finding out an appropriate optimization programming. In whole history of direct analysis, a number of optimization tools have been developed. Linear programming (LP) is simplest and widely used owing to the allowance of solutions for large scale problems. The contribution to this field can be found in works of Anderheggen and Knopfel [33], Cohn et al. [34], Nguyen [35], Sloan [36]. LP is simple for the implementation, but the expected solutions may not be obtained due to the yield functions can not be exactly described. Overcoming this drawback, the non-linear yield surface is treated by the approximation of itself piecewise linear, see e.g. Maier [37], Tin-Loi

[38], Christiansen [39]. Then, existing optimization algorithms, such as the Simplex method or Interior-point methods can be applied. The disadvantage of this scheme is the highly computational cost caused by linearizing the yield functions.

The nonlinear yield functions can be directly used in nonlinear programming formulations by means of Newton-type algorithm, for which eliminating the linear or nonlinear constrains using Lagrange multipliers is an important step in solving the problems. Then, an unconstrained functional formulation can be dealt with using several iterative methods. Devoting to the development of such algorithms, it should refer to works of Gaudrat [40], Zouain et al. [41], Liu et al. [42], Andersen and Christiansen [43], Andersen et al [44]. By other procedure, Mackenzie and Boyle [45], Ponter and Carter [46], Maier et al. [47], Boulbibane and Ponter [48] used the elastic compensation method considered as a direct method for nonlinear programming technique. In those studies, Young's modulus of each element is modified during the iterative linear-elastic finite element, then the optimized statically admissible stress field is obtained after each iteration leading to an upper bound and a pseudo-lower bound solution. Similarly to the linearizing technique, the high expense of computation is the major obstacle of this procedure.

Recently, a state of art primal-dual interior point algorithm has been introduced, the nonlinear conditions of the yield functions can be transformed into the form of the second order cone programming (SOCP) problem with a large number of variables and nonlinear constraints. Then the solution of a minimization problem with linear objective function and feasible region defined by some cones. The advantage of this method is the ability to solve large problems with thousands of variables in tens of seconds only. The important contributions to this method can bee seen in studies of Nesterov et al. [49], Andersen et al. [50], Ben-Tal and Nemirovski [51], Renegar [52], Makrodimopoulos and Bisbos [53], Bisbos et al. [54], Makrodimopoulos [55].

1.2.3 Discretization techniques

Theorems of limit and shakedown analysis lead to two classic problems including static and kinematic formulations corresponding to the lower-bound and upper-bound problems, respectively. The lower-bound solution will be obtained using equilibrium formulation, and the stress or moment fields associated with the nodal values are dicretized. The approximated fields must satisfy the boundary conditions,

the equilibrium conditions and the fulfill of yield criterion. In order to satisfy this statically admissible conditions, a set of linear constrains on the stress or moment parameters needs to be introduced. Therefore, approximating the stress field is more difficult than those of displacement or velocity fields. The displacement or velocity formulation requires an approximation of a kinematically admissible displacement velocity field, and the upper-bound solution will be obtained. The internal compatibility condition can be straightforwardly satisfied in the assembly scheme, and the boundary conditions can be enforced directly. A number of studies based on numerical method, such as finite element method (FEM), smoothed finite element method (SFEM), or mesh-free methods were carried out for limit and shakedown problems.

Nowadays, finite element method has become the most popular tool in academic as well as industrial applications. In the literature, there are three basic types of finite element models, i.e., displacement, equilibrium and mixed formulations. In case of limit analysis, equilibrium model has been investigated in studies of Hodge and Belytschko [56], Nguyen [57], Krabbenhoft and Damkilde [58], Lyamin and Sloan [59], Le et al. [60]. Displacement finite element models can be found in works of Hodge and Belytschko [56], Le et al. [60], Anderheggen [61], Krabbenhoft et al. [62], Capsoni and Corradi [63], Bleyer and Buhan [64]. The mixed formulation allows both stresses and displacements to be determined directly, and volumetric locking can be avoided, but there is one drawback exiting, that is the solution obtained is lack of information on the status, it is unclear whether the solution is upper bound or lower bound. Mixed approach for limit analysis was developed by Christiansen [39], Capsoni [65], Yu and Tin-Loi [66]. Finite shakedown formulation combined with different optimization algorithms, e.g., piecewise-linear yield criteria, Newton-type scheme or interior-point method were developed. The contribution of this field can be seen in works of Belytschko [67], Tin-Loi [38], Carvelli et al. [68], Heitzer et al. [21], Yan and Nguyen [69], Vu et al. [70, 71], Simon [72], Simon and Weichert [73–76]. Recently, FEM in combination with second-order cone programming was also applied to solve limit and shakedown analysis in works of Tran et al. [77], Le et al. [32]. An improved form of standard FEM so-called SFEM has been extended to direct analysis in studies of Le et al. [78, 79], Tran et al. [80], Nguyen-Xuan et al. [81], Ho et al. [82]. Besides FEM and SFEM, an other mesh-based procedure named Boundary Element method (BEM) has been successfully applied for limit and shakedown analysis, the contribution can be found in works of Maier and

Polizzotto [83], Panzeca [84], Zhang et al. [85], Liu et al. [86, 87].

In recent years, taking advantage of computational efficiency, mesh-free methods have been continuously developed and significantly devoted to the development of limit and shakedown analysis. Natural Element method was employed to handle limit and shakedown problems, see e.g. Zhou et al. [88, 89]. Application of Element-free Galerkin method combined with the non-linear programming for solving optimization problems can be found in works of Chen et al. [90, 91]. Le et al. [92–95] also adopted EFG method by combining with stabilized conforming nodal integration (SCNI) and SOCP, then employed to solve upper bound as well as lower bound limit analysis. Similarly, the meshless based radial basis function so-called Radial Point Interpolation method was also using to deal with the upper-bound limit analysis problems, see e.g. Liu and Zhao [96].

1.2.4 The direct analysis for microstructures

The computation of heterogeneous microstructure were early carried out from 19^{th} century by Voigt (1887) with the rule of mixtures. Then, several homogenization techniques, such as self-consistent [97], variational bounding methods [98, 99] and asymptotic homogenization [100, 101] have been proposed to handle the microstructures with assumptions of linear elastic behavior, simple geometries and small strains. Since the increasing use of composite materials and the requirement of dealing with the complex behavior of microstructures, a new class of so-called unit cell methods was early proposed by Eshelby [97] and widely applied in this field [102, 103]. This approach can provide the effective properties of the material as well as the valuable information on the local micro-structural fields. However, the unit cell methods are based on a priori assumed macroscopic constitutive relations, which is usually infeasible when the constitutive behaviour becomes non-linear. Therefore, most of above techniques are unable in large deformations, complex loading paths or the change of geometries. In recent years, the multi-scale homogenization technique or also called global-local analysis firstly proposed by Suquest [104] has been widely exploited. The computational homogenization methodology have been mostly applied to the periodic composite and heterogeneous materials. Techniques of computational homogenization can overcome the major drawbacks of unit cell methods, provide transition between micro-scale features and macro-response, and allow the use of modelling technique on microscopic structures as finite element

method [105–107], the Voronoi cell method [108, 109], a crystal plasticity framework [110], boundary element method [111], mesh-free methods [112, 113].

Extending to predict the macroscopic behavior of composite materials, Suquet [114] introduced the homogenization theory to plastic mechanics. Based on the concept of RVE and homogenization technique of Suquet, Buhan and Taliercio [115] proposed the first formulation of limit analysis in terms of solving the composite structure at micro-scale. The theoretical formulation then developed in the studies of Taliercio [116], Taliercio and Sagramoso [117] for fiber-reinforced composite using Drucker-Prager, Mohr-Coulomb or von Mises yield criterion. The first numerical implementation for this field belongs to Francescato and Pastor [118] with the use of finite element method and linear mathematical programming. By means of static direct methods, Weichert et al. [25, 119] developed a 3-dimensions finite element procedure for analysis of isotropic microstructures. Using a similar approach, Zhang et al. [120] presented the quasi-lower bound formulation for periodic composite and heterogeneous materials using the nonlinear programming. Besides that, the kinematic formulations in combination with nonlinear algorithms can be found in studies of Li et al. [121–125]. In these works, both isotropic and anisotropic materials obeying the von Mises or elliptic yield criterion were considered. For the purpose of improving the computational aspect, Le et al. [126] proposed a numerical method based on the finite element method and the combination of kinematic theorem and homogenization theory for limit analysis of periodic composite. The study proved that the accurate solutions can be obtained rapidly using SOCP.

1.2.5 Mesh-free methods - state of the art

The necessary of mesh-free methods

Parallel with the development of information technology and computer, the numerical methods become indispensable tools for simulation and design of practical structures. The engineering problems are usually formulated in form of Partial differential equations (PDEs) relating to the boundary conditions, and solved using analytical method. The complex problems need to be approximated using the numerical methods, for which the PDEs are transferred to an equilibrium form so-called variational form or weak form, then a set of simultaneous algebraic equations is established for overall computational domain via the approximate functions. The

boundary conditions are required to applied before solving problem to determine the approximate solutions.

As mentioned, among numerical schemes, FEM have been rapidly developed and became the most popular tools in simulation as well as analysis of engineering problems. Various codes or commercial software packages based on FEs background are developed and widely used in almost areas, for example structural mechanics, thermal analysis, fluid dynamics, and even multi-physics simulation. In FEM, the computational domain is sub-divided to various finite elements connected together at nodes. This work is called discretization; and the nodal connectivity well-known as the mesh is the fundamental feature of mesh-based method. The creation of the mesh plays an important role in FEM implementation and takes most of total computational cost. There are several issues generated by the mesh, for example in large deformation problems, the continuous remeshing of domain may be required to avoid the breakdown of the computation caused by the excessive mesh distortion. The very fine mesh may be required for the accurate solutions, that makes the computational cost increase. In one other case, fracture problems, FEM may fail in dealing with the discontinuities at crack paths and crack tips where the refinement is required after every computational step. Therefore, no-mesh is necessary in whole process of solving problems, and that is the ideal for a novel scheme named mesh-free or meshless method.

Generally, dealing with engineering problems, the numerical implementation of mesh-free (MF) methods is similar to mesh-based ones, see Figure 1.4. The major difference between MF scheme and FEM is the strategy to discretize the computational domain and construct the shape function. The nodal connectivity is not required in mesh-free methods (Figure 1.2). The absence of mesh is the most attractive characteristic of MF methods leading to the reduction of computational cost [127] and the flexibility in operation of nodes (adding, eliminating or moving nodes) within the computational domain. Owing to that advantage, the adaptive technique as $p-$adaptive or $h-$adaptive can be conveniently applied in MF method [127]. The computation is also flexibly implemented using several procedures. Some mesh-free models use Gauss points relating to background cells as Figure 1.3(a), that is similar to FEM and does not ensure the truly meshless feature. In other methods, the Gauss points are replaced by the scattered nodes within the problem domain. Then, the nodal computational domain (or representative domain) can be determined using various different means, for example Voronoi diagram known as

the duality of Delaunay triangles as Figure 1.3(a). For convenience, the available *Vononoi* function in programming language software, e.g. *Matlab*, C^{++} or *Python*, can be utilized.

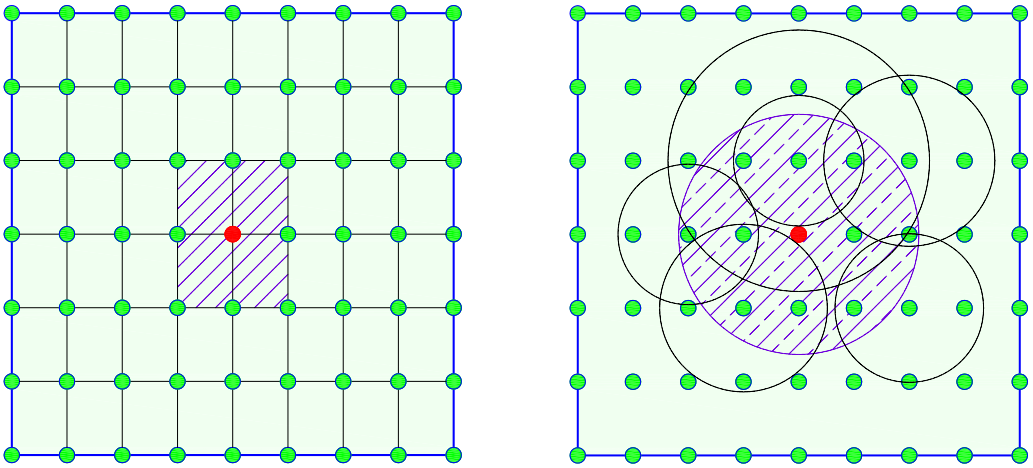

(a) FEM discretization (b) MF discretization

Figure 1.2: The discretization of FEM and MF method

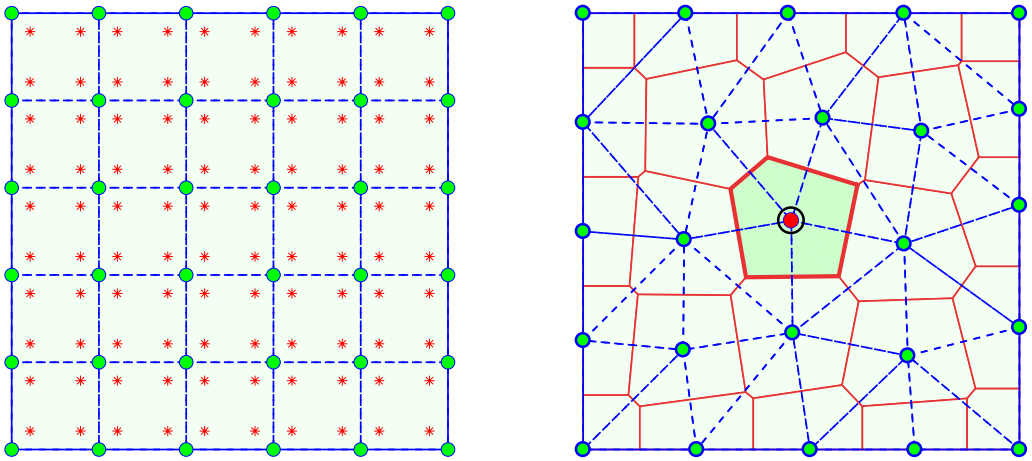

(a) Based on Gauss points (b) Based on scattred nodes

Figure 1.3: The computational domain in mesh-free method

An other difference of mesh-free methods compared with mesh-based procedures is the influent domain (or support domain). The concept *influent domain* is used in case of the computation is the carried out on scattered nodes, whereas the concept *support domain* is used when the implementation bases on arbitrary point within the computational domain, e.g. Gauss point. For convenience, the concept *influent domain* used in the thesis. While the nodal influent domains in mesh-based methods

are limited by all elements attached to nodes, in meshless method, the influent domains of nodes can be flexibly chosen (rectangle domain, square domain or circular domain). That domains can overlap as seen in Figure 1.2(b), and can be resized easily. That ensures the good continuity for MF approximation in comparison with the traditional approaches. Figure 1.2(b) illustrates the strategy to determined the influent domain using the circle where the influent radius R_I can be modified via a dimensionless parameter β_s as

$$R_I = \beta_s d_I, \quad \beta_s \geq 1 \tag{1.1}$$

where d_I denotes the minimal distance from considered node to its neighbours in the computational domain. The accuracy and computational expensive depend on the choice of influent radius. Therefore, parameter R_I needs to be investigated in the numerical implementation.

The most important advantages of mesh-free methods in comparison with FEM is the high-order continuous shape function. As a consequence, the MF methods can provide highly accurate solutions with the good convergence rate [128]. Moreover, the accuracy of solutions in MF method can be easily improved via the modification of influent domain. The most common drawbacks of MF methods are probably the computational cost when constructing the shape function, the density of matrices and the lack of Kronecker-delta property in several approximation techniques.

Recently, various modes of meshless method have been developed, improved and widely applied in different areas, such as solid mechanics, fluid mechanics, molecular dynamics or even molecular biology. Each method bases on an individual basis function and uses an individual approximation or interpolation technique, more details will be presented in the following sections.

Overview of popular mesh-free methods

The original mesh-free method is Smooth Particle Hydrodynamics (SPH) introduced by Gingold and Monaghan [129] and Lucy [130]. SPH method firstly applied to simulate the phenomena such as supernova, and then was employed in fluid dynamics. Libersky and Petschek [131] extended this method to solid mechanics analysis. The main advantage of the SPH method is its ability to treat local deformations, which is considered to be better than mesh-based methods. Then, this

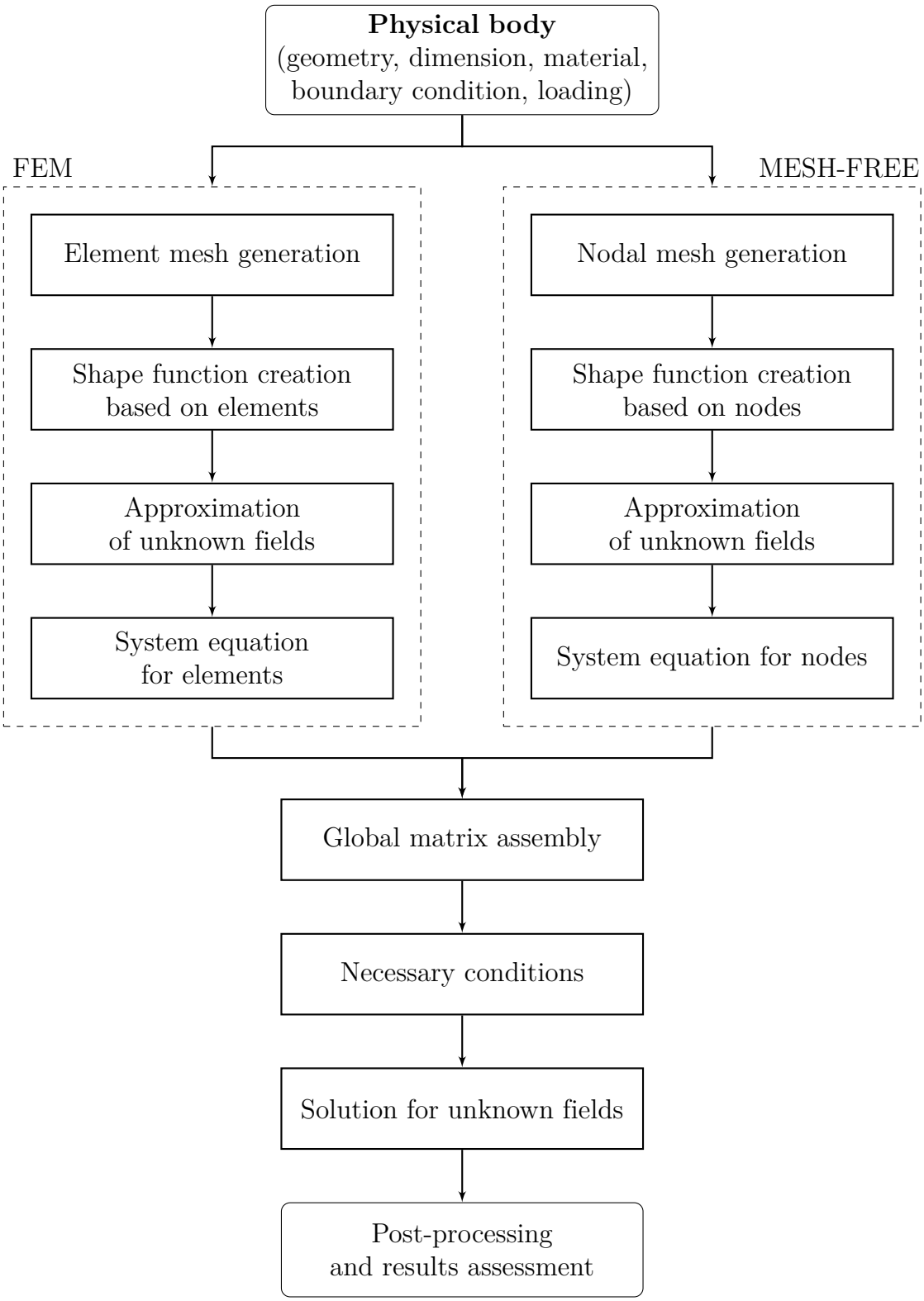

Figure 1.4: Numerical procedures: Mesh-free method vesus FEM

feature was utilized to handle a number of problems as metal form or crack propagation analysis, etc. However, the classical formulations of SPH lack of stability and consistency, thus various modifications have been carried out to improve the accuracy in recent years.

Based on the ideal of SPH method, Belytschko et al. [132] developed the Element-free Galerkin (EFG) method using Moving Least Square (MLS) approximation priorly proposed by Lancaster and Salkauskas (1981) [133]. EFG method avoids the discontinuous feature of previous SPH versions and becomes the most widely used meshless method. Liu et al. [134] proposed the meshless method named Reproducing Kernel Particle Method (RKPM). Although the method is similar to EFG procedure, RKMP originally bases on the wavelets rather than on curve-fitting. Surprisingly, the polynomial reproduction leads to the shape function of RKPM almost identical to one of EFG scheme. At the same time, Duarte and Oden [135] introduced hp-cloud method. That is the first mesh-free method developed without relying on the idea of SPH. In contrast to the EFG and RKPM method, hp-cloud method uses an extrinsic basis to increase the consistency (or completeness) of expression. Based on the similarities between meshless method and finite element those, Melenk et al. [136] formulated a consolidated form of them so-called Partition of Unity Finite Element Method (PUFEM). One of popular mesh-free procedures named Meshless Local Petrov-Galerkin (MLPG) was developed by Atluri et al. [137]. The difference of MLPG compared to above mentioned methods is the local weak form constructed on overlap sub-domains alternating to the global weak form, and then the integrals are calculated in that local domains. Using MLPG approach, the integration can be implemented without the background cells, ensuring that MLPG is a truly meshless method. Arroyo and Ortiz [138] proposed a mesh-free method based on the Local maximum-entropy approximation (LMEA). The basis function used in this method is similar to one in MLS, but its advantage is that the local approximation function produces a shape function nearly satisfying Kronecker-delta property at the boundaries of problem domain. Using Natural Neighbour Interpolation (NNI) technique introduced by Sibson [139], Brauand Sambridge [140] developed the Natural Element method (NEM) for the purpose of solving PDEs. NEM was then extended to solid mechanics analysis by Sukumar et al. [141].

Besides, several meshless methods were developed based on the interpolation technique, and the radial basis functions (RBFs) are commonly utilized. The fun-

damentals of RBF method were firstly introduced by Hardy [142] for cartography problem. In this study, the multiquadric (MQ) radial function was presented. Lately, Franke [143] investigated 32 most commonly used interpolation methods and proved that MQ is the best one. The main feature of MQ method is the basis function only depends on the Euclidean distance which is radially symmetric to its center. From MQ method, different radial functions was generalized as the thin plate spline, the Gaussian, the cubic, etc, constituting the so-called Radial basis function method, see e.g. Duchon [144]. Recently, Kansa [145, 146] introduced RBF collocation method considered as a way to solve the partial differential equations (PDEs) for parabolic elliptic and hyperbolic. Kansa's method bases on the collocation method and the MQ-RBF, yielding to the global approximation. In this scheme, the dense stiffness matrix is obtained. As a result, it takes a very expensive cost to solve the problems with a large number of collocation points. Avoiding that drawback, the RBF Hermite-Collocation was proposed, both globally and locally supported RBF was used. The results proved that globally supported RBF gives the more accurate solution than locally supported case, but its computational expense is higher. Recently, the RBF method named Local Multiquadric was proposed by Lee et al. [147], for which the approximate function is constructed using sub-domains, then the local approximation and a sparse stiffness matrix are obtained. Applying weak form, Wendland [148] developed a Galerkin mesh-free method using radial basis functions. RBFs have also been used in Boundary element method (BEM) or Meshless local Petrov-Galerkin (MLPG) and successfully applied to solve various nonlinear problems in computational mechanics.

With the purpose of handling the matters generated by the lack of Kronecker-delta property in mesh-free approximations, Liu and Gu developed the Point Interpolation Method (PIM) using the polynomial basis function. PIM encounters drawback in inverting matrices vanished in some situations, thus an alternative one so-called Radial Point Interpolation Method (RPIM) was introduced [149]. The major advantage of using radial basis function in PIM is the invertibility of moment matrix. Unfortunately, the accuracy of results may not be given as expected. As a result, a polynomial term is added into the basis function to improve the accuracy as well as the stability of solutions. Using the radial basis functions but approaching in the opposite direction compared with RPIM, Tran-Cong et al. [150–153] developed the Integrated radial basis function (iRBF) method. Generally, iRBF method possesses all the good features of RPIM, but its approximation is better than RPIM

one owing to the use of multiple integration, yielding to the higher-order shape function.

Approximation technique based on RBFs

The key ideal of mesh-free methods is that the approximation or interpolation bases on a set of arbitrary scattered nodes. To ensure the convergence and stability, the approximate functions must satisfy following requirements.

- *Consistency:* If s is the order of the highest derivative occurring in the weak form, the approximate function should be differentiable at least up to the order s^{th} inside influent domain.

- *Completeness:* The shape function must have ability to reproduce polynomials up to order s^{th} to ensure the stability and convergence of numerical method. If the shape function $\Phi_I(\mathbf{x})$ is complete up to order s^{th}, any degree s^{th} polynomial can be reproduced as

$$\sum_I x^p \Phi_I(\mathbf{x}) = x^p, \quad 0 \leq p \leq s \tag{1.2}$$

  or

$$\sum_I \mathbf{p}(\mathbf{x}) \Phi_I(\mathbf{x}) = \mathbf{p}(\mathbf{x}), \quad \forall \mathbf{x} \in \Omega \tag{1.3}$$

  where $\mathbf{p}(\mathbf{x})$ denotes the basis function.

- *Partitions of unity:* The sum of all nodal shape function values at any point in the computational domain must be unit, ensuring the proper representation of a constant field of the solid

$$\sum_I \Phi_I(\mathbf{x}) = 1, \quad \text{in } \Omega_I \tag{1.4}$$

As mentioned, up to now, mesh-free method have been considerably developed with a number of schemes based on different approximation or interpolation techniques such as SPH method [129, 130], RKPM method [134], PU method [136, 154, 155], RBFs method [145–153], MLS approximation [132], LMEA approximation [138], NNI approximation [139–141], and various other approaches, more details can be found in [156–158]. Owing to its high-order shape function and the

advantage in enforcing essential boundary conditions, this thesis only focuses on the iRBF method proposed by Tran-Cong et al. [150–152], where the radial basis functions are used.

Several popular radial basis functions in the literate can be listed as follows

$$g_I(\mathbf{x}) = \begin{cases} (r^2 + a_I^2)^q & \text{for general multiquadrics} \\ \sqrt{r^2 + a_I^2} & \text{for multiquadrics (MQ)} \\ \dfrac{1}{\sqrt{r^2 + a_I^2}} & \text{for inverse multiquadrics} \\ \dfrac{1}{r^2 + a_I^2} & \text{for inverse quadrics} \\ e^{-\left(\frac{r}{a_I}\right)^2} & \text{for Gaussian} \\ r^2 log(r) & \text{for thin plate spline} \end{cases} \tag{1.5}$$

where $r = \|\mathbf{x} - \mathbf{x}_I\|$ is the radius from node I^{th} and others in the influent domain; the shape parameter $a_I = \alpha_s d_I$, with $\alpha_s > 0$ is the dimensionless factor; and d_I denotes the minimum distance from node I^{th} to its neighbours.

Direct (dRBF) and indirect/integrated (iRBF) formulations

A smooth function $u(\mathbf{x})$ can be directly approximated based on a set of N scattered nodes and a radial basis function as

$$u^h(\mathbf{x}) = \sum_{I=1}^{N} g_I(\mathbf{x}) a_I \tag{1.6}$$

where $u^h(\mathbf{x})$ is the approximate function of $u(\mathbf{x})$; $\{a_I\}_{I=1}^N$ is a set of expanded (or unknown) parameter; $\{g_I(\mathbf{x})\}_{I=1}^N$ is the radial basis function.

From (1.6), the derivatives of $u(\mathbf{x})$ can be calculated as

$$u^h_{j\ldots l}(\mathbf{x}) = \frac{\partial^k u^h}{\partial x_j \ldots \partial x_l} = \sum_{i=1}^{N} \frac{\partial^k g_I(\mathbf{x})}{\partial x_j \ldots \partial x_l} u_I \tag{1.7}$$

It is worth mentioning that errors in the approximate function computed by

Equation (1.6) is low, but errors in its derivatives are still high [152]. Moreover, the derivative functions, especially higher order ones, are strongly influenced by the local behavior of the approximation. Consequently, the so-called indirect RBF method was also developed in [150–153] and will be recalled the following.

In iRBF approach, the highest derivative (order s^{th}) of approximate function is firstly constructed using RBF as

$$u^h_{,jk\ldots rs}(\mathbf{x}) = \sum_{I=1}^{N} g_I(\mathbf{x}) a_I \tag{1.8}$$

Next, the lower-order derivatives and the original function will be calculated using the multiple integration as follows

$$u^h_{,jk\ldots r}(\mathbf{x}) = \int \sum_{I=1}^{N} g_I(\mathbf{x}) a_I dx_s + C_s(\mathbf{x}) \tag{1.9a}$$

$$\ldots$$

$$u^h_{,j}(\mathbf{x}) = \int \cdots \int \sum_{I=1}^{N} g_I(\mathbf{x}) a_I dx_s \ldots dx_k + C_{s\ldots k}(\mathbf{x}) \tag{1.9b}$$

$$u^h(\mathbf{x}) = \int \cdots \int \sum_{I=1}^{N} g_I(\mathbf{x}) a_I dx_s \ldots dx_j + C_{s\ldots j}(\mathbf{x}) \tag{1.9c}$$

where $C_s(\mathbf{x}), \ldots, C_{s\ldots j}(\mathbf{x})$ is the function order 0 up to order $(s-1)^{th}$ with the parameters are integral constant.

Playing the prior inversion of matrix in (1.9c) and substituting to Equations (1.8) and (1.9a - 1.9c), the reflection of the approximate function and its derivatives pass through the nodal values can be obtained. It should be noted that the iRBF shape function satisfies Kronecker-delta property leading to the essential boundary conditions can be applied similarly to the finite element method.

Numerical implementation in mesh-free method

The engineering problems are firstly formulated in form of PDEs with the boundary conditions, and then solved to obtain solutions. Consider a PDEs in domain Ω with kinematic boundary Γ_u and static boundary Γ_t such that $\Gamma_u \cup \Gamma_t = \Gamma$ and

$\Gamma_u \cap \Gamma_t = \varnothing$ as follows

$$\nabla_s^T \boldsymbol{\sigma} + \mathbf{b} = 0, \qquad \text{in } \Omega \tag{1.10a}$$

$$\boldsymbol{\sigma} = \mathbf{D}\nabla_s \mathbf{u} \tag{1.10b}$$

where $\boldsymbol{\sigma}$ is the Cauchy stress tensor; $\mathbf{b}$ is the body force per a volume unit; ∇ is the differential operation; $\mathbf{D}$ is the matrix consisting material constants; $\mathbf{u}$ is the vector including displacement components. The PDEs (1.10a) can be rewritten as

$$\nabla_s^T \mathbf{D} \nabla_s \mathbf{u} + \mathbf{b} = 0 \tag{1.11}$$

The boundary conditions are defined by

$$\mathbf{n}.\boldsymbol{\sigma} = \bar{\mathbf{t}}, \qquad \text{on } \Gamma_t \tag{1.12a}$$

$$\mathbf{u} = \bar{\mathbf{u}}, \qquad \text{on } \Gamma_u \tag{1.12b}$$

with $\mathbf{n}$ is the outward normal vector of static boundary.

The equation system (1.11) is the strong form describing the mechanical behaviors where displacements is the main variables. Almost engineering problems will be solved using numerical procedures after transforming to PDEs form. There are two main strategies for solving problems, which are known as strong form and weak form, respectivelly, and will be clarified in the following.

Strong form - Collocation method

Consider an approximation for set of N discretized nodes as

$$\mathbf{u}^h(\mathbf{x}) = \sum_{I=1}^{N} \Phi_I(\mathbf{x}) u_I \tag{1.13}$$

with $\Phi_I(\mathbf{x})$ is the shape function obtained using the approximate/interpolated techniques previous presented; u_I denotes the unknown values at nodes. For the strong form methods, the order of approximate functions must be higher or equal to the order of derivative of strong form equation system, and that requirement is called *strong*.

In collocation method, the equation system (1.11) is satisfied at every points in

the problem domain, and the conditions in (1.12) are applied

$$\nabla_s^T \mathbf{D} \nabla_s \mathbf{u}(\mathbf{x}_J) + \mathbf{b}_J = 0, \qquad \forall J \in \Omega \tag{1.14a}$$

$$\mathbf{n}\mathbf{D}\nabla_s \mathbf{u}(\mathbf{x}_K) = \bar{\mathbf{t}}_K, \quad \forall K \in \Gamma_t \tag{1.14b}$$

$$\mathbf{u}(\mathbf{x}_L) = \bar{\mathbf{u}}_L, \quad \forall L \in \Gamma_u, \quad (J + K + L = N) \tag{1.14c}$$

The advantage of collocation approaches is the simple implementation and computational speed. There are no-need of integrals, and the shape conditions are directly enforced at nodes instead of at Gauss points. However, unexpected solutions can be obtained due to the instability. In this thesis, the so-called Stability conforming nodal integration (SCNI) scheme will be employed to handle this drawback. Using SCNI technique, problems can be implemented by the similar way of collocation method, but the stability and accuracy of solutions are ensured.

Galerkin weak form

The unknown field will be approximated via a trial function $\mathbf{u}$. Multiplying both sides of strong form (1.11) with a arbitrary trial function φ and carrying out the integration on overall domain Ω, the weak form will be obtained as

$$\int_\Omega \varphi^T \nabla_s^T \mathbf{D} \nabla_s \mathbf{u} d\Omega + \int_\Omega \varphi^T \mathbf{b} d\Omega = 0 \tag{1.15}$$

Using the partial integral, then applying the static boundary condition (1.12a) and the condition $\varphi = 0$ on Γ_u, the weak form (1.15) can be rewritten as

$$\int_\Omega (\nabla_s \varphi)^T \mathbf{D} (\nabla_s \mathbf{u}) d\Omega = \int_\Omega \varphi^T \mathbf{b} d\Omega + \int_{\Gamma_t} \varphi^T \bar{\mathbf{t}} d\Gamma \tag{1.16}$$

If in the strong form, the PDEs are required to be satisfied at every points in problem domain and the approximate function must have order at least equal to those in the highest derivative of PDEs, in the weak form, applying the partial integral for (1.15) leads to the reduction of the order of operator ∇. Therefore, the requirement of continuity is *weak*, meaning that the order of trial function can be smaller than the order of highest derivative in PDEs and all conditions need to be satisfied only inside domain Ω. Noting that when transforming from strong form to weak form, the static condition (1.12a) is used, thus there is only the displacement

condition (1.12b) in the weak form.

Using weak form, the engineers usually prefer to directly access the Galerkin weak form

$$\int_{\Omega}(\nabla_s \delta\mathbf{u})^T \mathbf{D}(\nabla_s \mathbf{u})d\Omega - \left[\int_{\Omega} \mathbf{u}^T \mathbf{b} d\Omega + \int_{\Gamma_t} \delta\mathbf{u}^T \bar{\mathbf{t}} d\Gamma\right] = 0 \tag{1.17}$$

with δ is the variational operator. Considering physical meaning, a displacement field satisfying Equation (1.17) with the arbitrary test function φ will minimize the total power in the whole system and keep the system in the stable and equilibrium state. Equation (1.17) is completely similar to equation (1.16) constructed from the strong form.

The mesh-free method based on Galerkin formulation can be found in the studies of Belytschko et al. [132, 159, 160], Liu et al. [134], Duarte and Oden [135] or Melenk and Babuska [136]. Two major aspects of this method including applying the essential boundary condition and estimating the integrals in the weak form equations will be discussed in following sections.

Enforcement of essential boundary conditions

Usually in mechanics problems, when considering behavior at elastic state, after constructing the stiffness matrix, it is in need to eliminate the singularity caused by the physical movement of the body, this work is called enforcing the essential boundary conditions. In order to easily impose this conditions, the shape functions are required to satisfy Kronecker-delta property, it means

$$\Phi_I(\mathbf{x}_J) = \delta_{IJ} = \begin{cases} 1 & \text{if } I = J, \\ 0 & \text{if } I \neq J. \end{cases} \qquad I, J = 1, 2, \ldots, N \tag{1.18}$$

While Kronecker-delta property obviously exists in FEM, most of meshless approaches lack this feature. Consequently, when applying the boundary conditions, several special techniques will be employed such as Lagrange multiplier [132, 134–136], penalty method [161, 162], modified variational principle [159], point collocation method [161], coupling to with FEM [160, 163] or specially modified shape function [164]. For the case of RPIM and iRBF approaches, the essential boundary conditions can be imposed similarly to the finite element method.

Numerical integration

In the numerical methods, the use of numerical integration is the essential work to evaluate the integrals on the computational domain. Mesh-free methods usually employ two main schemes, there are using Gauss integral based on the background cells and using nodal integral based on discretized nodes. Among them, Gauss integral is the most popular technique for numerical methods. The drawback of this scheme is the requirement of background cells, making the procedure not truly meshless. In order to obtain a good description of the high-order shape function, a number of Gauss points are required in the domain, increasing the computational cost. Moreover, if the background cells are used in Galerkin weak form, the numerical integration errors (with Gauss quadrature) occurs in all mesh-free approximation owing to the support domains for the basis functions do not coincide with the background cells. Consequently, instead of using Gauss integral, Beissel and Belytschko [165] proposed the modification of power functional by adding a square of residual weight to the equilibrium equation in order to eliminate the singularity. In other research, Chen et al. [166] introduced the Stability conforming nodal integration (SCNI) technique based on the idea of smoothing strain rate at node. Then, to improve this technique in terms of accuracy, stability and convergence rate, Chen et al. [167] proposed to add a reinforced linear function into the approximation. The scheme was used in combination with Moving Reproducing Kernel Particle Method (MRKPM) in [167].

1.3 Research motivation

Numerical methods are the most efficient tools for current studies in the field of limit and shakedown analysis. As mentioned above, a number of researchers have devoted their effort to develop the robust approaches for this area. The numerical procedures using continuous field, semi-continuous field (Krabbenhoft et al. [62]), or truly discontinuous field (Smith and Gilbert [168]) have been executed with the support of finite element method (FEM). However, there are several matters of mesh-based procedures, which need to be handled, for instance, locking problems, mesh distortion and highly sensitive to the geometry of the original mesh, particularly in the region of stress or displacement singularities. In order to improve the computational aspect of FEM, a number of studies proposed the adaptive tech-

nique for limit and shakedown analysis, the achievement can be found in the works of Christiansen and Pedersen [169], Borges et al. [170], Franco et al. [171], Lyamin and Sloan [172], Cecot [173], Ngo and Tin-Loi [174], Ciria et al. [175], Le [176]. However, the whole process is complicate and requires the fine meshing to obtain the expected results. An improving form of FEM named SFEM (smoothed finite element method) is also applied in works of Le et al. [78, 79], Tran et al. [80], Nguyen-Xuan et al. [81]. Generally, SFEM is better than FEM in terms of stability and convergence, but this method does not surmount all disadvantages of FEM caused by the mesh. Recently, mesh-free methods are also extended to direct analysis. Among them, Element-free Galerkin (EFG) method is the most interested choice, several typical studies can be noted here as Chen et al. [90, 91], Le et al. [92–95]. Besides, some other meshless procedures have been also successfully applied to this area such as Natural Element method (NEM - Zhou et al. [88, 89]), Radial Point Interpolation method (RPIM - Liu and Zhao [96]). In comparison with the traditional approaches, mesh-free methods possess the high-order shape function, hence above disadvantages can be overcame. However, it should be noted that several meshless methods lack Kronecker-delta property leading to the difficulty in imposing the essential boundary conditions. Owing to the advantages of shape function as mentioned in previous sections, iRBF method can provide an efficient treatment for those obstacles arising in whole process of formulating and solving optimization problems. According to the author's knowledge, the applications of iRBF method are focused on the fields of solving PDEs [150–153], fluid mechanics [177], or elastic analysis of solid and fracture mechanics [178]. The development of iRBF method for limit and shakedown analysis will be a new contribution to this area. In addition, in previous studies using iRBF, the numerical integration is carried out utilizing Gauss points, increasing the computational cost. Therefore, the stabilized approximation based on the combination of iRBF approximation and SCNI will improve the computational aspect of proposed numerical method.

Moreover, solving limit and shakedown problem requires to handle the optimization problem involving either linear or non-linear constrains. The traditional way to overcome this drawback is linearizing non-linear convex yield criteria. The efficient tools, for instance, Simplex algorithm (Anderheggen and Knopfel [33], Christiansen [179]), can be used. However, a large number of constrains and variables in the optimization problems are required to obtain the sufficiently accuracy results, which increase the computational cost. On one other hand, that is the attempts to deal

with the convex yield criteria using non-linear packages. Although the highly accurate solutions can be obtained, the expensive cost is the major trouble of this scheme. In framework of limit analysis, the primal-dual interior-point algorithm (Christiansen and Kortanek [180], Andersen and Christiansen [181]) is well-known as one of most robust and efficient algorithms in handling the optimization problems with large-scale nonlinear constrains. Therefore, extending of this scheme to the shakedown formulation will lead to more advantages for direct analysis of either structures or materials.

Besides, the earliest application of direct analysis for microscopic structures can be found in studies of Buhan and Taliercio [115], Taliercio [116], Taliercio and Sagramoso [117], where the limit load of typical problems were determined. The homogenization theory was applied to limit analysis using linear programming in works of Francescato and Pastor [118], Zhang et al. [120], Weichert et al. [25, 119], Chen et al. [182]. Besides that, the nonlinear programming were also employed for direct analysis of heterogeneous materials by Carvelli et al. [183], Li et al. [121–125], Hachemi et al. [184], Le et al. [126]. Actually, almost studies dealt with the isotropic or anisotropic materials using linear or nonlinear programming with the support of finite element method, the application of mesh-free method in framework of computational homogenization analysis of materials at limit state is still unavailable.

In conclusion, it can be observed that many challenges still remain in developing a robust tool to improve the computational aspect of limit and shakedown analysis for structures and materials. The absence of the integration of an optimization algorithm in structural analysis software packages, e.g. ANSYS or ABAQUS, leads to the fact that limit and shakedown analysis has not yet been commercialized and widely applied in structural design. Present study focuses on the combination of a discretization scheme and an optimization programming to propose an efficient numerical approach for direct analysis method, i.e., (i) the stabilized iRBF mesh-free method will be developed; (ii) the optimization problems will be formulated using the so-called second-order cone programming (SOCP) to deal with the convex yield criterion; (iii) the numerical approach will be applied to handle the direct analysis problems for structures and materials.

1.4 The objectives and scope of thesis

The major objective of thesis is developing the integrated radial basis functions-based mesh-free method (iRBF method) and the optimization algorithm based on conic programming, then extending the numerical approach to limit and shakedown analysis of structures and materials. In order to obtain above mentioned aims, the following tasks will be carried out.

First, the mesh-free method based on integrated radial basis functions, for which the stability conforming nodal integration (SCNI) is employed to obtained the smoothed versions of shape function derivatives, is developed to discretize the computational domain; then the general approximate fields for different types of problems (displacement and stress fields) are established.

Second, the kinematic and static formulations of limit and shakedown analysis for structures and materials, governed by several well-known yield criterion, e.g., von Mises or Nielsen, are formulated, and then the optimization problems are cast as second-order cone programming.

Finally, the resulting optimization problems are solved using the highly efficient tools such as Mosek software package combined with Matlab programming. The obtained solutions are compared with other those in available studies in order to estimate the computational aspect of proposed approaches.

It is important to note that, within the scope of the thesis, proposed numerical method will be employed to deal with several common engineering structures, such as continuous beam, simple frame, plates, reinforced concrete slabs, or computational homogenization analysis of micro-structures. The material model is assumed as rigid-perfectly plastic or elastic-perfectly plastic. The 2D and 3D structures are considered under both constant and variable loads, corresponding to limit and shakedown analysis, respectively. The benchmark problems will be investigated for the comparison purpose; thereby, the computational aspect of proposed approach is evaluated.

1.5 Original contributions of the thesis

According to the author's knowledge, the following points have never been published in other studies, and they can be considered as the original contributions of

the thesis

- The development of stabilized iRBF method, which is based on the combination of iRBF approximation and SCNI scheme, for the field of limit and shakedown analysis.
- The development of stabilized iRBF method for computational homogenization analysis of micro-structures at limit state. This is the first time a mesh-free method is employed to treat that problem.
- Based on iRBF approximation and bounding theorems, the kinematic and static limit and shakedown analysis are formulated in form of SOCP. Proposed method is used to deal with various types of structures and materials obeying different yield criterion.

1.6 Thesis outline

The thesis includes 7 chapters, in which chapters 3, 4, 5 and 6 present the contents and numerical solutions collected from the manuscripts published or submitted to publication. The outline of the thesis is the following.

Chapter 1 generally introduces the thesis; the review of contents relating to the thesis, summarizes the historical development, applications and the contributions of available numerical procedures for engineering problems. Besides, the research motivations, objectives and scope of the thesis are also clarified.

Chapter 2 expresses the fundamental theories applied in the thesis involving limit and shakedown analysis, the optimization algorithms (second-order cone programming), the homogenization theory and the integrated radial basis function-based mesh-free method.

Chapter 3 presents the application of iRBF method for limit analysis of plane problem where both kinematic and static field corresponding to the upper and lower bound formulations are investigated. The obtained limit load multipliers for various benchmark problems are compared with those reported in previous studies.

Chapter 4 expresses the other application of iRBF method for limit analysis of reinforced concrete slabs under bending loads. The kinematic formulation of problems are considered, then the limit load and the collapse mechanism of slabs with

various different shapes are determined. The computational efficiency of proposed method is evaluated via the comparison with other studies.

Chapter 5 presents the stabilized iRBF method in the application for limit and shakedown analysis of plane problems using either two dimensional or three dimensional models. The equilibrium formulation is employed in this section. The quasi-lower bound of limit and shakedown loads are obtained owing to several special techniques. The elastic stress field, residual stress field as well as the plastic stress field for various different problems are illustrated. As previous chapters, the computational aspect is also analysis.

Chapter 6 investigates the computational homogenization analysis of materials using stabilized iRBF method. The approximate results involving limit load multipliers and the yield surface of materials are expressed.

Chapter 7 presents the discussions on the numerical solutions, the convergence and reliability of results obtained using proposed method. Finally, several conclusions are drawn and the recommendation for future works are also presented.

Chapter 2

Fundamentals

Previous chapter presents the literature review of limit and shakedown theory, homogenization technique as well as different approximation schemes of mesh-free methods. This chapter will clarify fundamentals applied to this thesis. The iRBF based meshless method proposed by Tran-Cong et al. [150–153] will be used to handle all problems in the thesis.

2.1 Plasticity relations in direct analysis

2.1.1 Material models

In plasticity theory, for convenience, the real behaviour of materials are replaced by the idealized models for which the hardening or softening behaviour can be ignored. Figure 2.1(a) illustrates the elastic-perfectly plastic model where material behavior is considered in two stages including elasticity and plasticity. In this model, materials behave elastically when stress is below the ultimate strength; otherwise, the yield occurs. In fact, the elastic deformations are very small in comparison with plastic ones; therefore, it can be ignored. In other words, the elastic-perfectly plastic model can be replaced by the rigid-perfectly plastic one as seen in Figure 2.1(b).

The plastic deformations obey the flow rule as

$$\dot{\boldsymbol{\epsilon}} = \dot{\mu}\frac{\partial \psi}{\partial \sigma} \tag{2.1}$$

where $\dot{\mu} > 0$ is plastic parameter; $\psi(\boldsymbol{\sigma})$ denotes yield function forming the space limited by a time-independent yield surface such that

- $\psi(\boldsymbol{\sigma}) < 0$: elastic behavior;

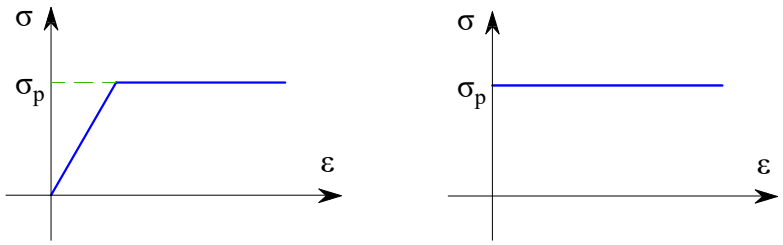

(a) Elastic-perfectly plastic model (b) Rigid-perfectly plastic model

Figure 2.1: Material models

- $\psi(\boldsymbol{\sigma}) = 0$: appearance of plastic deformations;
- $\psi(\boldsymbol{\sigma}) > 0$: inaccessible region.

The material models are required to obey the stability postulate proposed by Drucker and its important consequences called the normality rule and convexity.

Drucker's stability postulate

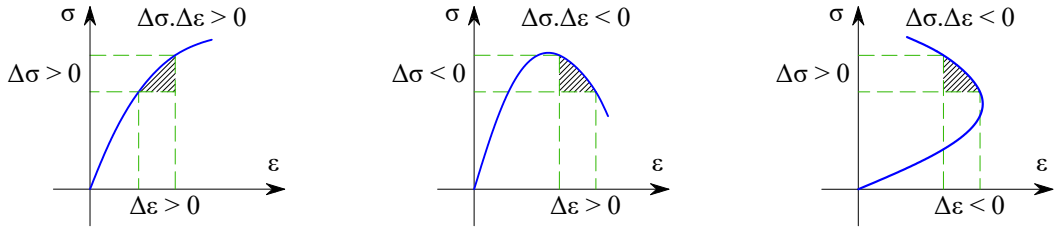

(a) Stable (b) Unstable (c) Unstable

Figure 2.2: Stable and unstable material models

Following Drucker, material models are stable if the work produced over the cycle of applied and removed loads is non-negative

$$\oint (\boldsymbol{\sigma} - \boldsymbol{\sigma}^0) d\boldsymbol{\epsilon} \geq 0 \tag{2.2}$$

where $\boldsymbol{\sigma}$ is the current stress tensor on the yield surface ($\psi(\boldsymbol{\sigma}) = 0$); $\boldsymbol{\sigma}^0$ denotes the plastically admissible stress tensor ($\psi(\boldsymbol{\sigma}^0) < 0$).

Above formulae is also simply known as *Drucker's inequality* and it is appropriate

for perfectly plastic and hardening materials

$$(\boldsymbol{\sigma} - \boldsymbol{\sigma}^0)\boldsymbol{\epsilon} \geq 0 \tag{2.3}$$

Figure 2.2 describes the stable behavior (producing positive work) and unstable behavior (producing negative work). Following that, materials satisfy the behavior illustrated in Figure 2.2(a) will be called stable or standard materials; and the materials possess behavior according to those in Figures 2.2(b) and 2.2(c) will be called unstable or nonstandard materials.

The normality rule

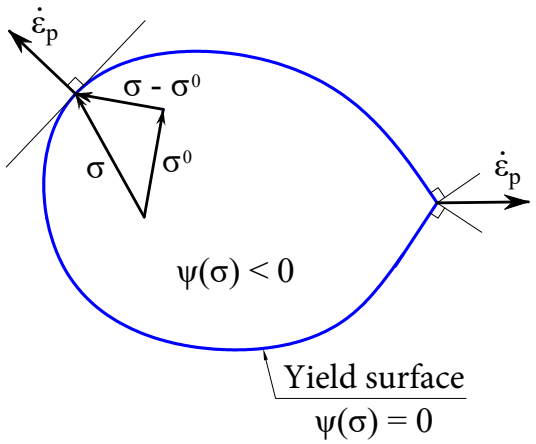

Figure 2.3: The normality rule

The plastic strain rates are proportional to the gradient of yield functions at any point on the smoothed yield surface $\psi(\boldsymbol{\sigma}) = 0$, and are normal of yield surface. If there are singular points on the yield surface where the normal direction is not unique, the plastic strain vector must lie between adjacent normal at the corners as Figure 2.3. When n yield surfaces intersect at a singular point, formulae (2.1) is replaced by

$$\dot{\boldsymbol{\epsilon}} = \sum_{i=1}^{n} \dot{\mu} \frac{\partial \psi}{\partial \sigma} \tag{2.4}$$

The convexity

From Figure 2.3, it can be seen that corresponding to any stress $\boldsymbol{\sigma}^0$ lies on the outward side of the tangent, Drucker's inequality will be violated. In other word, if all of elastic stresses lie on one side of the tangent, the yield surface is convex. The material obeying to Drucker's postulate is required that its yield function $\psi(\boldsymbol{\sigma})$ must be convex in the stress space $\boldsymbol{\sigma}$. The convexity plays an important role in plasticity theory allowing the use of convex programming in direct analysis.

Yield criterion

A yield criterion defines the limit of elasticity under the complex stress state. For isotropic materials, the direction of principle stresses are independent with type of materials, thus the yield criterion can be preformed in terms of principle stresses as

$$\psi(\sigma_1, \sigma_2, \sigma_3) = k \tag{2.5}$$

where k denotes the material constant, for example $k = \sigma_p$ in case of unaxial tension loading, or $k = \tau_p$ for unaxial shear loading.

For perfectly plastic materials, the yield function is independent with plastic strain rate, and due to the physical isotropic characteristic, it depends on the invariant of stress tensor. The yield criterion can be rewritten as

$$\psi(I_1, J_2, J_3) = k \tag{2.6}$$

where I_1 is the first stress invariant; J_2 and J_3 are the second and third invariant of deviatoric stress tensor.

In various problems, the results from experience demonstrate that for several materials, e.g. metal, the influence of hydrostatic stress is negligible. As a result, the yield function depends on the deviatoric stress tensor only, it means

$$\psi(J_2, J_3) - k_v = 0 \tag{2.7}$$

where $k_v^2 = \dfrac{\sigma_p}{\sqrt{3}}$, with σ_p is the yield stress obtained form the unaxial tension test.

There are various yield criterion have been proposed for amount of materials, e.g. the Tressca or von Mises for metal, Drucker-Prager or Nielsen for reinforced

concrete materials, Mohr-Column for soil, etc.

2.1.2 Variational principles

Consider an elastic-perfectly plastic or rigid-perfectly plastic body bounded by volume V with kinematic boundary Ω_u where displacement components are constrained (Dirichlet boundary) and static boundary Ω_t where stress components are known (Neuman boundary) such that $\Omega_u \cup \Omega_t = V$, $\Omega_u \cap \Omega_t = \varnothing$. The structure is subjected to the body force $\mathbf{f}$ and surface load $\mathbf{t}$ as Figure 2.4.

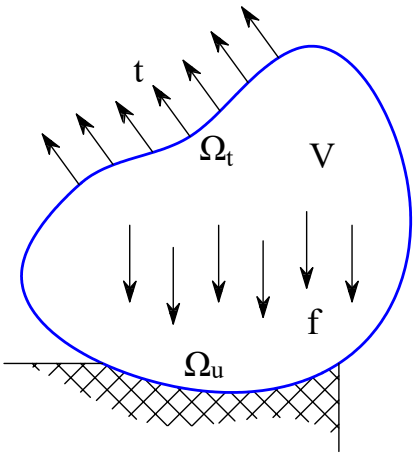

Figure 2.4: The equilibrium body

The basic concepts

A stress field $\boldsymbol{\sigma}$ is called *admissible static* if it satisfies the equilibrium condition and static boundary condition

$$\nabla\boldsymbol{\sigma} = \mathbf{f} \quad \text{in } V \tag{2.8a}$$

$$\mathbf{n}\boldsymbol{\sigma} = \mathbf{t} \quad \text{on } \Omega_t \tag{2.8b}$$

where ∇ is the differential operator.

$$\nabla = \begin{bmatrix} \frac{\partial}{\partial x} & 0 & 0 & \frac{\partial}{\partial y} & 0 & \frac{\partial}{\partial z} \\ 0 & \frac{\partial}{\partial y} & 0 & \frac{\partial}{\partial x} & \frac{\partial}{\partial z} & 0 \\ 0 & 0 & \frac{\partial}{\partial z} & 0 & \frac{\partial}{\partial y} & \frac{\partial}{\partial x} \end{bmatrix} \tag{2.9}$$

and $\mathbf{n}$ represents the outward normal matrix of surface Ω_t

$$\mathbf{n} = \begin{bmatrix} nx & 0 & 0 & ny & 0 & nz \\ 0 & ny & 0 & nx & nz & 0 \\ 0 & 0 & nz & 0 & ny & nx \end{bmatrix} \tag{2.10}$$

A stress field $\boldsymbol{\sigma}$ is called *plastically admissible* if the yield condition is not violated at anywhere

$$\psi(\boldsymbol{\sigma}) \leq 0 \tag{2.11}$$

A strain velocity field $\dot{\boldsymbol{\epsilon}}$ is called *kinematically admissible* if it satisfies the compatible condition and kinematic boundary condition

$$\dot{\boldsymbol{\epsilon}} = \nabla \dot{\mathbf{u}} \quad \text{in } V \tag{2.12a}$$

$$\dot{\mathbf{u}} = 0 \qquad \text{on } \Omega_u \tag{2.12b}$$

A strain velocity field $\dot{\boldsymbol{\epsilon}}$ is called *plastically admissible* if strain vector is the normal of the yield surface and the external work is positive

$$\dot{W}_E = \int_V \mathbf{f}\dot{\mathbf{u}} dV + \int_{\Omega_u} \mathbf{t}\dot{\mathbf{u}} d\Omega_u > 0 \tag{2.13}$$

Markov's principle

Following Markov, among all kinematically admissible and incompressible strain fields, the actual strain field will minimize the functional

$$\boldsymbol{\psi}(\dot{\mathbf{u}}) = \underbrace{\int_V D_p(\dot{\boldsymbol{\epsilon}}) dV}_{W_I} - \underbrace{\left[\int_V \mathbf{f}\dot{\mathbf{u}} dV + \int_{\Omega_u} \mathbf{t}\dot{\mathbf{u}} d\Omega_u\right]}_{W_E} \tag{2.14}$$

where W_I and W_E are the power of internal load and external load, respectively; $D_p(\dot{\boldsymbol{\epsilon}})$ denotes the plastic dissipation function defined by

$$D_p(\dot{\boldsymbol{\epsilon}}) = \max_{\boldsymbol{\sigma}} \boldsymbol{\sigma}\dot{\boldsymbol{\epsilon}} \quad \text{such that } \psi(\boldsymbol{\sigma}) \leq 0 \tag{2.15}$$

By solving problem (2.15), the stress state $\boldsymbol{\sigma}_{(\boldsymbol{\epsilon})}$ corresponding to the strain field $\dot{\boldsymbol{\epsilon}}$ obeyed the normality rule will be obtained. The plastic dissipation function is now rewritten as

$$D_p(\dot{\boldsymbol{\epsilon}}) = \boldsymbol{\sigma}_{(\boldsymbol{\epsilon})}\dot{\boldsymbol{\epsilon}} \tag{2.16}$$

Noting that function $D_p(\dot{\boldsymbol{\epsilon}})$ depends on the materials and the yield criterion used.

Hill's principle

Following Hill, among all statically and plastically admissible stress fields, the actual field will minimize the functional

$$\Pi(\boldsymbol{\sigma}) = -\int_{\Omega_u} (\mathbf{n}\boldsymbol{\sigma})\dot{\mathbf{u}}d\Omega \tag{2.17}$$

It is interesting to note that the consequences of principles formulated by Markov and Hill are well-known as the upper bound and lower bound of direct analysis which will be recalled following.

2.2 Shakedown analysis

In practice, structures can be subjected to various different forms of mechanical or thermal loading, for example monotonic or proportional loads, repeat loads, or even arbitrarily varying loads. Therefore, the failure of structures can be caused by various reasons. Under different intensities of applied loads, several behaviors of the structures can be obtained as follow

1. The respond of structure is only perfectly elastic if the load intensities are significantly small (Figure 2.5(a)).

2. If intensities of load beyond the elastic limit but are not too high, the plastic deformation occurs, increases and stops after some cycles. The behavior of

structure becomes elastic again. That state is called shakedown or adaptation (Figure 2.5(b)).

3. Under the load which is higher than the elastic limit, plastic deformation occurs and develops but it is not stable, the total strain is too large and structure becomes unserviceable. The phenomenon is called incremental collapse (Figure 2.5(c)).

4. Another behavior is called alternating plasticity. The plastic deformation change sign after every loading cycle, so the total strain is kept in small value. The structure will fail after a number of cycles because of the low-cycle fatigue failure (Figure 2.5(d)).

5. The structure can be collapse at the first cycle of loading due to the intensity of applied load is higher than its instantaneous load-carrying capacity. This situation is called plastic collapse (Figure 2.5(e)).

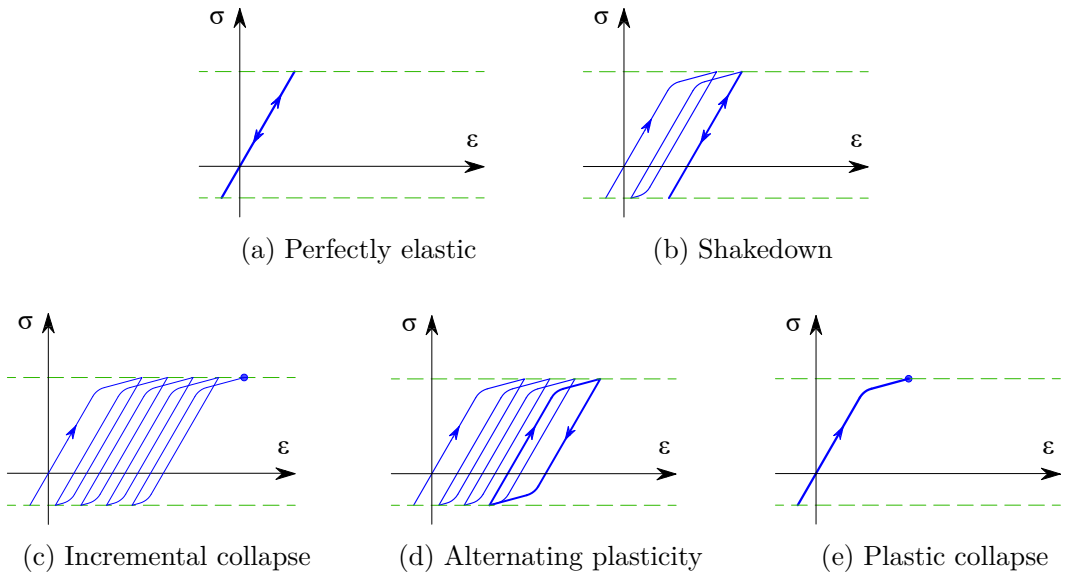

(a) Perfectly elastic (b) Shakedown

(c) Incremental collapse (d) Alternating plasticity (e) Plastic collapse

Figure 2.5: The different behaviors of structures under the cycle load

.

Viewing the above-mentioned situations, it can be observed that two-first cases may not dangerous; however, shakedown behavior (Figure 2.5(b)) thoroughly exploits the capacity of materials.

Consider a body made of elastic-perfectly plastic materials and is subjected to a load **F**. The displacement and deformation are assumed to be small enough to

ignore the geometrical change in equilibrium equations. The external load $\mathbf{F}$ are decomposed into two parts including body force $\mathbf{f}$ and surface load $\mathbf{t}$. Denoting $\mathbf{F}_0(\mathbf{f}_0, \mathbf{t}_0)$ for the initial load applying to the structure, thus

$$\mathbf{F} = \lambda \mathbf{F}_0 \tag{2.18}$$

where λ is the load multiplier; the load $\mathbf{F}$ is assumed that proportionally increase with λ. Denoting Ω_u and Ω_t for the kinematic and static of body, stress and strain components must satisfy the equilibrium condition, the compatibility condition as well as the kinematic and static boundary conditions completely

$$\boldsymbol{\sigma} + \mathbf{f} = 0 \qquad \text{in } V \tag{2.19a}$$

$$\dot{\boldsymbol{\epsilon}} = \nabla \dot{\mathbf{u}} \quad \text{in } V \tag{2.19b}$$

$$\mathbf{n}\boldsymbol{\sigma} = \mathbf{t} \qquad \text{on } \Omega_t \tag{2.19c}$$

$$\dot{\mathbf{u}} = \overline{\dot{\mathbf{u}}} \qquad \text{on } \Omega_u \tag{2.19d}$$

where $\dot{\mathbf{u}}$ is the deformation velocity; $\overline{\dot{\mathbf{u}}}$ is the known displacement velocity value; $\mathbf{n}$ is the outward normal of static boundary Ω; $\boldsymbol{\sigma}$ and $\boldsymbol{\epsilon}$ are stress and strain components, respectively.

The development of shakedown analysis bases on the fundamentals of the kinematic and static theorems well-known as the upper bound and lower bound of direct method.

2.2.1 Upper bound theorem of shakedown analysis

Using plastic strain field, the kinematic theorem of shakedown analysis was formulated by Koiter [15]. Following Koiter, the plastic strain rate $\dot{\boldsymbol{\epsilon}}^p$ is not required to satisfy the compatibility condition at each instant during the cycle, but the total plastic deformation $\Delta\dot{\boldsymbol{\epsilon}}^p$ accumulated after each cycle must satisfy the kinematically compatible condition, it means

$$\Delta\dot{\boldsymbol{\epsilon}}^p = \int_0^T \dot{\boldsymbol{\epsilon}}^p dt \quad \text{in } V \tag{2.20a}$$

$$\Delta\dot{\boldsymbol{\epsilon}}^p = \nabla \Delta\dot{\mathbf{u}} \qquad \text{on } \Omega_u \tag{2.20b}$$

$$\dot{W}_E = \int_0^T dt \left[\int_V \mathbf{f}\dot{\mathbf{u}} dV + \int_{\Omega_t} \mathbf{t}\dot{\mathbf{u}} d\Omega \right] > 0 \tag{2.20c}$$

Theorem 1. Upper bound theorem of shakedown analysis

1. Shakedown may happen if the following inequality is satisfied

$$\int_0^T dt \left[\int_V \mathbf{f}\dot{\mathbf{u}} dV + \int_{\Omega_t} \mathbf{t}\dot{\mathbf{u}} d\Omega \right] \leq \int_0^T dt \int_V D(\dot{\boldsymbol{\epsilon}}) dV \tag{2.21}$$

2. Shakedown cannot happen when the following inequality holds

$$\int_0^T dt \left[\int_V \mathbf{f}\dot{\mathbf{u}} dV + \int_{\Omega_t} \mathbf{t}\dot{\mathbf{u}} d\Omega \right] > \int_0^T dt \int_V D(\dot{\boldsymbol{\epsilon}}) dV \tag{2.22}$$

where the plastic dissipation power $D_p(\dot{\boldsymbol{\epsilon}})$ is given by

$$D_p(\dot{\boldsymbol{\epsilon}}) = \boldsymbol{\sigma}\dot{\boldsymbol{\epsilon}} \tag{2.23}$$

Applying the principle of virtual work, the power generated by external load can be recalculated as

$$\dot{W}_E = \int_0^T dt \int_V \boldsymbol{\sigma}^E(\mathbf{x}, t)\dot{\boldsymbol{\epsilon}}^p dV \tag{2.24}$$

with $\boldsymbol{\sigma}^E(\mathbf{x}, t)$ is the elastic fictitious stress at time t in the loading domain $\mathscr{D}$.

Normalizing external work, the upper bound of shakedown load multiplier can be obtained by solving the optimization problem

$$\lambda^+ = \min \int_0^T dt \int_V D_p(\dot{\boldsymbol{\epsilon}}) dV \tag{2.25}$$

$$\text{s.t} \begin{cases} \Delta\dot{\boldsymbol{\epsilon}} = \int_0^T \dot{\boldsymbol{\epsilon}} dt \\ \Delta\dot{\boldsymbol{\epsilon}} = \Delta\nabla\dot{\mathbf{u}} \quad \text{in } V \\ \Delta\dot{\mathbf{u}} = 0 \qquad \text{on } \Omega_u \\ \dot{W}_E = 1 \end{cases} \tag{2.26}$$

2.2.2 The lower bound theorem of shakedown analysis

Shakedown occurs after several first loading cycle when the plastic strains stop ($\dot{\boldsymbol{\epsilon}}^p = 0$) at everywhere within the structure, and it is in need to introduce a fictitious residual stress field $\boldsymbol{\rho}(\mathbf{x})$ ensuring that the actual stress field $\boldsymbol{\sigma}(\mathbf{x}, t)$ does not violate

the yield criterion everywhere

$$\boldsymbol{\psi}\left[\boldsymbol{\sigma}(\mathbf{x},t)\right] = \boldsymbol{\psi}\left[\lambda\boldsymbol{\sigma}^{E}(\mathbf{x},t) + \boldsymbol{\rho}(\mathbf{x})\right] \leq 0 \tag{2.27}$$

where

$$\boldsymbol{\sigma}(\mathbf{x},t) = \lambda\boldsymbol{\sigma}^{E}(\mathbf{x},t) + \boldsymbol{\rho}(\mathbf{x}) \tag{2.28}$$

Due to the elastic stress $\boldsymbol{\sigma}^{E}(\mathbf{x},t)$ equilibrates to the external load, the residual stress field $\boldsymbol{\rho}(\mathbf{x})$ must be in self-equilibrium state

$$\nabla\boldsymbol{\rho}(\mathbf{x}) = 0 \quad \text{in } V \tag{2.29a}$$

$$\mathbf{n}\boldsymbol{\rho}(\mathbf{x}) = 0 \quad \text{on } \Omega_t \tag{2.29b}$$

The necessary and sufficient conditions for shakedown are given by Melan [14] as following theorem.

Theorem 2. Lower bound theorem of shakedown analysis

1. *Shakedown occurs if there exists a permanent residual stress field $\boldsymbol{\rho}$, statically admissible, such that*

$$\boldsymbol{\psi}\left[\lambda\boldsymbol{\sigma}^{E}(\mathbf{x},t) + \boldsymbol{\rho}(\mathbf{x})\right] < 0 \tag{2.30}$$

2. *Shakedown will not occur if no $\boldsymbol{\rho}$ exists such that*

$$\boldsymbol{\psi}\left[\lambda\boldsymbol{\sigma}^{E}(\mathbf{x},t) + \boldsymbol{\rho}(\mathbf{x})\right] \leq 0 \tag{2.31}$$

Based on above theorem, a statically admissible residual stress field needs to be determine to obtain the maximum load domain $\lambda^{-}\mathscr{D}$, in where the load multiplier λ^{-} is the lower bound of the actual factor. Now, the shakedown problem can be considered as maximizing a nonlinear optimization problem

$$\lambda = \max \lambda^{-} \tag{2.32}$$

$$\text{s.t} \begin{cases} \nabla\boldsymbol{\rho}(\mathbf{x}) = 0 & \text{in } V \\ \mathbf{n}\boldsymbol{\rho}(\mathbf{x}) = 0 & \text{on } \Omega_t \\ \boldsymbol{\psi}\left[\lambda\boldsymbol{\sigma}^{E}(\mathbf{x},t) + \boldsymbol{\rho}(\mathbf{x})\right] \leq 0 & \forall t \end{cases} \tag{2.33}$$

2.2.3 Separated and unified methods

For determining the shakedown limit of structures, there are two popular method: separated and unified methods. The first procedure assumes that the incremental collapse and alternating plasticity may occur at the same time. In this model, the kinematically admissible strain is decomposed into two parts involving alternating incremental collapse and alternating plasticity. Solving the optimization problem, the upper bound of plastic shakedown load multiplier will be obtained.

This thesis focuses on the unified model for which the static formulation introduced by Melan [14] will be employed. The obstacle caused by the time-dependent variables and integrals can be overcome using the convex-cycle theorems relating to the concept of load domain mentioned following.

2.2.4 Load domain

Shakedown analysis considers structures under n_L independent loading processes $\mathscr{P}(t)$ forming a convex polyhedral domain $\mathscr{D}(x,t)$ so-called load domain with n_L dimensions and $(m = 2^{n_L})$ vertices. The loading path $\mathscr{D}(x,t)$ can be expressed as a linear combination of loading processes as

$$\mathscr{P}(t) = \sum_{k=1}^{n_L} \mu_k(t)\mathscr{P}_k^0 \tag{2.34}$$

with $\mathscr{P}_k^0$ is the initial load; the parameter $\mu_k(t)$ can be given by

$$\mu_k(t) \in \left[\mu_k^-, \mu_k^+\right], \quad k = 1, 2, \ldots, n_L \tag{2.35}$$

Solving the optimization problems (2.26) and (2.33), in order to overcome the difficulty generated by the appearance of time-dependent variables and time-dependent integrals, Konig and Kleiber [185] introduced the convex-cycle theorems as follows

Theorem 3. *Shakedown will happen over a given load domain $\mathscr{D}$ if and only if it happens over the convex envelope of $\mathscr{D}$.*

Theorem 4. *Shakedown will happen over any load path within a given load domain $\mathscr{D}$ if it happens over a cyclic load path containing all vertices of $\mathscr{D}$.*

Figure 2.6(a) and 2.6(b) illustrate the uses of load cycle for structures subjected

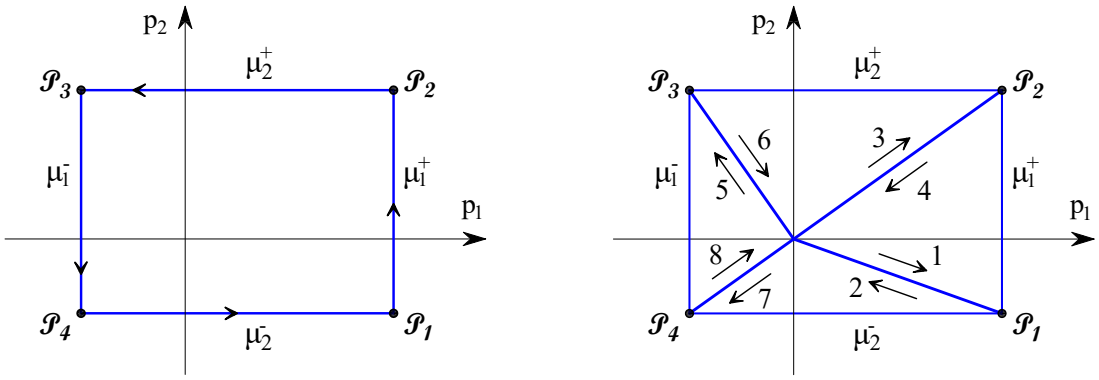

(a) Model 1 (b) Model 2

Figure 2.6: Loading cycles in shakedown analysis

to two independent loads. Above convex-cycle theorems has shown that it is sufficient to consider only the vertices of the convex polyhedral loading domain instead of time-dependent analysis. The expressions (2.26) and (2.33) for shakedown analysis can be reformulated as

1. Upper bound shakedown analysis

$$\lambda^{+} = \min \sum_{k=1}^{m} \int_{V} D_p(\dot{\boldsymbol{\epsilon}}) dV \tag{2.36}$$

$$\text{s.t} \begin{cases} \Delta\dot{\boldsymbol{\epsilon}} = \sum_{k=1}^{m} \dot{\boldsymbol{\epsilon}} \\ \Delta\dot{\boldsymbol{\epsilon}} = \Delta\nabla\dot{\mathbf{u}} \quad \text{in } V \\ \Delta\dot{\mathbf{u}} = 0 \quad \text{on } \Omega_u \\ \dot{W}_E = \sum_{k=1}^{m} \int_{V} \boldsymbol{\sigma}^E \left(\mathbf{x}, \hat{\mathscr{P}}_k(\mathbf{x})\right) \dot{\boldsymbol{\epsilon}}^p dV \end{cases} \tag{2.37}$$

2. Lower bound shakedown analysis

$$\lambda = \max \lambda^{-} \tag{2.38}$$

$$\text{s.t} \begin{cases} \nabla\boldsymbol{\rho}(\mathbf{x}) = 0 & \text{in } V \\ \mathbf{n}\boldsymbol{\rho}(\mathbf{x}) = 0 & \text{on } \Omega_t \\ \boldsymbol{\psi}\left[\lambda\boldsymbol{\sigma}^E\left(\mathbf{x}, \hat{\mathscr{P}}_k(\mathbf{x})\right) + \boldsymbol{\rho}(\mathbf{x})\right] \leq 0 & \forall k = 1, 2, \ldots, m \end{cases} \tag{2.39}$$

It is important to note that when there is only one loading point, i.e., $m = 1$,

shakedown formulations will be reduced to a limit analysis problem presented in the following section.

2.3 Limit analysis

As above mentioned, limit analysis is a special case of shakedown ones when the structures are subjected to instantaneous loads increasing gradually until the collapse appears. Similar to shakedown analysis, the limit load multiplier λ can be determined using one of two opposite formulations based on the bounding theorems.

2.3.1 Upper bound formulation of limit analysis

A kinematically admissible displacement velocity field is assumed. The upper-bound limit analysis of structures can be determined by solving the optimization problem

$$\lambda^+ = \min \int_V D_p(\dot{\boldsymbol{\epsilon}}) dV \tag{2.40}$$

$$\text{s.t} \begin{cases} \dot{\boldsymbol{\epsilon}} = \nabla \dot{\mathbf{u}} & \text{in } V \\ \dot{\mathbf{u}} = 0 & \text{on } \Omega \\ \dot{W}_E = 1 \end{cases} \tag{2.41}$$

For convenience and simplicity, from now, *displacement/strain rate or velocity* is termed *displacement/strain*, and the plasticity dissipation as well as the external work relating to displacement velocity are also performed in terms of displacement or strain. The upper bound formulation of limit analysis (2.41) can be rewritten as

$$\lambda^+ = \min \int_V D(\boldsymbol{\epsilon}) dV \tag{2.42}$$

$$\text{s.t} \begin{cases} \boldsymbol{\epsilon} = \nabla \mathbf{u} & \text{in } V \\ \mathbf{u} = 0 & \text{on } \Omega_u \\ W_E = 1 \end{cases} \tag{2.43}$$

2.3.2 Lower bound formulation of limit analysis

A statically admissible stress field $\boldsymbol{\sigma}$ is assumed. The lower bound limit load multiplier will be obtained if the yield criterion is not violated everywhere, and the static formulation of limit analysis can be expressed as

$$\lambda^{-} = \max \lambda \tag{2.44}$$

$$\text{s.t} \begin{cases} \boldsymbol{\nabla}\boldsymbol{\sigma} = 0 & \text{in } V \\ \mathbf{n}\boldsymbol{\sigma} = \mathbf{t} & \text{on } \Omega_t \\ \psi(\boldsymbol{\sigma}) \leq 0 & \text{in } V \end{cases} \tag{2.45}$$

In order to obtain the limit and shakedown load multipliers, the formulations (2.26, 2.33) and (2.43, 2.45) can be solved using various optimization tools. In this thesis, the so-called primal-dual interior point algorithm will be utilized. The problems will be cast as second order cone programming (SOCP) and solved using the commercial software package named Mosek integrated in Matlab programming.

2.4 Conic optimization programming

Conic optimization is a sub-field of convex optimization, where linear function is minimized over the intersection of an affine subspace and a convex cone. A set $\mathscr{K}$ in vector space $\mathscr{V}$ is called a cone if

$$\forall \mathbf{x} \in \mathscr{K}, \lambda > 0 \Rightarrow \lambda \mathbf{x} \in \mathscr{K} \tag{2.46}$$

where the cone is considered with the following properties

- The cone $\mathscr{K}$ is convex if and only if: $\forall \mathbf{x}, \mathbf{x}' \in \mathscr{K}, \lambda > 0, \lambda' > 0 \Rightarrow \lambda \mathbf{x} + \lambda' \mathbf{x}' \in \mathscr{K}$
- The cone $\mathscr{K}$ is non-empty and closed if: $\mathbf{x}, \mathbf{x}' \in \mathscr{K} \Rightarrow \mathbf{x} + \mathbf{x}' \in \mathscr{K}$
- The cone $\mathscr{K}$ is pointed if it contents the original point: $\mathbf{x}, -\mathbf{x} \in \mathscr{K} \Rightarrow \mathbf{x} = 0$

Recently, several relevant models of conic programming developed for treatment of convex functions [51] can be listed following

- The non-negative orthant

$$\mathscr{K} \equiv \Re^n_+ = \{\mathbf{x} \in \Re^n | x_i \geq 0, i = 1, \ldots, n\} \tag{2.47}$$

- The standard second-order cone (Lorentz or ice-cream)

$$\mathscr{K} \equiv \mathscr{L}^n_q = \{\mathbf{x} \in \Re^n | x_1 \geq \|\mathbf{x}_{2\to n}\|_{L^2}\} \tag{2.48}$$

- The rotated quadratic cone

$$\mathscr{K} \equiv \mathscr{L}^n_r = \{\mathbf{x} \in \Re^n | x_1 x_2 \geq \|\mathbf{x}_{3\to n}\|^2_{L^2}, x_1, x_2 \geq 0\} \tag{2.49}$$

- The semi-definite cone

$$\mathscr{K} \equiv \mathscr{S}^n_+ = \{\mathbf{X} \in \Re^{n\times n} | \mathbf{X} \succeq 0, \mathbf{X} = \mathbf{X}^T\} \tag{2.50}$$

  with $\succeq$ is used to the positive semi-definite matrix.

The dual form $\mathscr{K}^*$ of the cone $\mathscr{K}$ can be defined by

$$\mathbf{x}^T\mathbf{y} \geq 0, \forall \mathbf{x} \in \mathscr{K} \Leftrightarrow \mathbf{y} \in \mathscr{K}^* \tag{2.51}$$

and the cone will be self-dual if $\mathscr{K} = \mathscr{K}^*$.

Following Ciria et al. [175], BenTal and Nemirovski [51], almost yield criterion can be formulated in terms of conic programming consisting of the linear objective and conic constrains. The primal and dual formulations of conic programming can be recalled as

- Primal formulation

$$\begin{aligned} &\lambda = \min \mathbf{c}^T\mathbf{x} \\ &\text{s.t.} \begin{cases} \mathbf{A}\mathbf{x} = \mathbf{b} \\ \mathbf{x} \in \mathscr{K} = \mathscr{K}_1 \times \mathscr{K}_2 \times \ldots \times \mathscr{K}_N \end{cases} \end{aligned} \tag{2.52}$$

- Dual formulation

$$\begin{aligned} &\lambda = \max \mathbf{b}^T \mathbf{y} \\ &\text{s.t.} \begin{cases} \mathbf{A}^T \mathbf{y} + \mathbf{s} = \mathbf{c} \\ \mathbf{x} \in \mathscr{K}^* = \mathscr{K}_1^* \times \mathscr{K}_2^* \times \ldots \times \mathscr{K}_N^* \end{cases} \end{aligned} \tag{2.53}$$

where $\mathbf{x}, \mathbf{y} \in \Re^n$ are the optimization variable vectors; $\mathbf{A} \in \Re^{m \times n}, \mathbf{b} \in \Re^m, \mathbf{c} \in \Re^n$ are the parameters; $\mathbf{s} \in \Re^n$ denotes the additional variables for problems.

Several common conic programming widely used for solving the optimization problems can be can be now expressed as

- Linear programming (LP): $\mathscr{K} \equiv \Re_+^n$
- Second-order cone programming (SOCP): $\mathscr{K} \equiv \mathscr{L}_q^n$ or $\mathscr{K} \equiv \mathscr{L}_r^n$
- Semi-definite programming (SDP): $\mathscr{K} \equiv \mathscr{S}_+^n$

where LP is the particular case of SOCP, and both models can be cast as a SPD.

2.5 Homogenization theory

In homogenization analysis, material is considered under the connection between two scales involving down-scale from macro-level to micro-level (localization) and up-scale from micro-level to macro-level (globalization). For macro-to-micro translation, the macroscopic features are transformed to micro-structure as the boundary conditions. By the opposite direction, the microscopic properties are transformed to macro-structure via the average.

Let consider a heterogeneous micro-based cell $\Omega \in \mathbb{R}^2$ so-called the representative volume element (RVE) at every material point $\mathbf{x} \in V$, where $V \in \mathbb{R}^2$ denotes the heterogeneous macroscopic-continuum. The micro-structure is subjected to the body force $\mathbf{f}$, the surface load $\mathbf{t}$ on the static boundary Γ_t and fixed by the displacement field $\mathbf{u}$ on the kinematic boundary Γ_u. The material response of macro-structure is determined by solving the macro-micro transitions problems, where the RVE size plays an important role in the analysis. The RVE dimension must be significantly great to describe the material properties, but significantly small to ensure that the heterogeneity is separately identified. Actually, the size of microscopic base

cell is very small compared with those of macro-scale; therefore, the body force $\mathbf{f}$ can be neglected in the micro-scale problem.

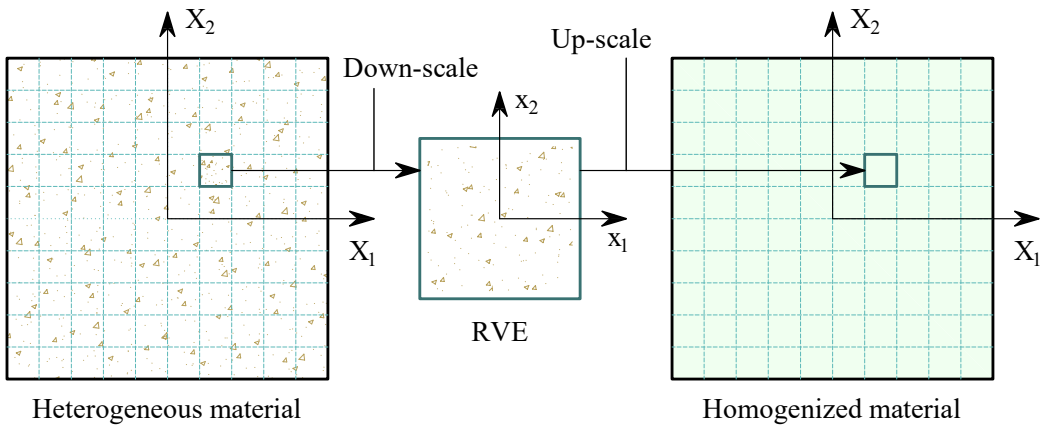

Figure 2.7: Homogenization technique: correlation between macro- and micro-scales

The micro-scale problem can be treated as the boundary value one in solid mechanics, where the overall strain $\mathbf{E}$ are transferred to micro-structure in form of kinematic boundary constrains. At microscopic scale, the local fields is decomposed into two parts: mean term and fluctuation term. Denoting $\mathbf{X}$ for the positional matrix of each material point in the computational domain, the local displacement, strain and stress are now given by

$$\mathbf{u}(\mathbf{x}) = \mathbf{E}.\mathbf{X} + \tilde{\mathbf{u}}(\mathbf{x}) \tag{2.54a}$$

$$\boldsymbol{\epsilon}(\mathbf{x}) = \mathbf{E} + \tilde{\boldsymbol{\epsilon}}(\mathbf{x}) \tag{2.54b}$$

$$\boldsymbol{\sigma}(\mathbf{x}) = \boldsymbol{\Sigma} + \tilde{\boldsymbol{\sigma}}(\mathbf{x}) \tag{2.54c}$$

where $\boldsymbol{\Sigma}$ is the overall stress; $\tilde{\mathbf{u}}(\mathbf{x})$, $\tilde{\boldsymbol{\epsilon}}(\mathbf{x})$ and $\tilde{\boldsymbol{\sigma}}(\mathbf{x})$ denote the fluctuation parts of displacement, strain and stress rate.

For the purpose of enforcing the boundary condition, this study uses the the most efficient in terms of convergence rate so-called periodic procedure, where there are the periodicity of fluctuation displacement field and anti-periodicity of traction field on RVE boundary

$$\tilde{\mathbf{u}}(\mathbf{x}^+) = \tilde{\mathbf{u}}(\mathbf{x}^-), \qquad \text{on } \Gamma_u \tag{2.55a}$$

$$\mathbf{t}(\mathbf{x}^+) = -\mathbf{t}(\mathbf{x}^-), \qquad \text{on } \Gamma_t \tag{2.55b}$$

where $\tilde{\mathbf{u}}(\mathbf{x}^+)$ and $\tilde{\mathbf{u}}(\mathbf{x}^-)$ are the fluctuation displacement field, $\mathbf{t}(\mathbf{x}^+)$ and $\mathbf{t}(\mathbf{x}^-)$ are

the traction field of positive and negative boundaries, respectively.

Note that, regarding to the periodic characteristic of the fluctuation terms, the average of $\tilde{\boldsymbol{\epsilon}}(\mathbf{x})$ and $\tilde{\boldsymbol{\sigma}}(\mathbf{x})$ over the RVE should vanish, it means

$$\langle \tilde{\boldsymbol{\epsilon}} \rangle = 0; \quad \langle \tilde{\boldsymbol{\sigma}} \rangle = 0 \tag{2.56}$$

where the operation $\langle . \rangle$ stands the volume average of fields over the RVE. Therefore, the macroscopic quantities can be calculated from the microscopic ones by the average relations

$$\mathbf{E} \equiv \langle \boldsymbol{\epsilon} \rangle = \frac{1}{|\Omega|} \int_{\Omega} \boldsymbol{\epsilon} \mathrm{d}\Omega \tag{2.57a}$$

$$\boldsymbol{\Sigma} \equiv \langle \boldsymbol{\sigma} \rangle = \frac{1}{|\Omega|} \int_{\Omega} \boldsymbol{\sigma} \mathrm{d}\Omega \tag{2.57b}$$

herein, $|\Omega|$ denotes the area of RVE.

In direct analysis, for any admissible velocity and stress field satisfying the periodic and anti-periodic conditions on boundary, the principle of macroscopic virtual work can be expressed as

$$\langle \boldsymbol{\sigma} : \boldsymbol{\epsilon} \rangle = \boldsymbol{\Sigma} : \mathbf{E} \tag{2.58}$$

2.6 The iRBF-based mesh-free method

As mentioned in the beginning of the chapter, iRBF method is the key numerical scheme for solving all problems in the thesis. The smooth function $u(\mathbf{x})$ can be approximated based on a given set of N scattered nodes and the iRBF method as

$$u^h(\mathbf{x}) = \sum_{I=1}^{N} \Phi_I(\mathbf{x}) u_I \tag{2.59}$$

where $\Phi_I(\mathbf{x})$ is the iRBF shape function; u_I denotes the nodal values. In here, the iRBF can be understand as the integrated or indirect radial basis functions. The reason for which iRBF method is called indirect procedure is the strategy to construct the shape function clarified following.

2.6.1 iRBF shape function

In this thesis, the RBF functions will be employed to construct the second-order derivative of shape function, then the first-order and the original functions will be calculated using the integrals as

$$u^h_{,\alpha\beta}(\mathbf{x}) = \sum_{I=1}^{N} g_I(\mathbf{x}) a_I = \mathbf{R}_2(\mathbf{x})\mathbf{a} \tag{2.60}$$

$$u^h_{,\alpha}(\mathbf{x}) = \int \sum_{I=1}^{N} g_I(\mathbf{x}) a_I dx_\beta + C_1 = \sum_{I=1}^{N+n_1} R_{1I}(\mathbf{x}) a_I = \mathbf{R}_1(\mathbf{x})\mathbf{a} \tag{2.61}$$

$$u^h(\mathbf{x}) = \iint \sum_{I=1}^{N} g_I(\mathbf{x}) a_I dx_\beta dx_\alpha + C_1 x_j + C_2 = \sum_{I=1}^{N+n_2} R_{0I}(\mathbf{x}) a_I = \mathbf{R}_0(\mathbf{x})\mathbf{a} \tag{2.62}$$

where C_1 and C_2 are the integral constants; n_1 and n_2 represent number of integral constants ($n_2 = 2n_1$); $\mathbf{a}$ is the vector consisting the unknowns.

$$\mathbf{R}_2(\mathbf{x}) = [g_1(\mathbf{x}),\ g_2(\mathbf{x}),\ ...,\ g_N(\mathbf{x}),\ \underbrace{0,\ ...,\ 0}_{n_2}] \tag{2.63a}$$

$$\mathbf{R}_1(\mathbf{x}) = [R_{11}(\mathbf{x}),\ R_{12}(\mathbf{x}),\ ...,\ R_{1(N+n_1)}(\mathbf{x}),\ \underbrace{0,\ ...,\ 0}_{n_1}] \tag{2.63b}$$

$$\mathbf{R}_0(\mathbf{x}) = [R_{01}(\mathbf{x}),\ R_{02}(\mathbf{x}),\ ...,\ R_{0(N+n_2)}(\mathbf{x})] \tag{2.63c}$$

with $R_{0i},\ R_{1i}$ can be found in [152, 153].

This thesis uses the multiquadric (MQ) basis function well-known as the best iRBF function in terms of accuracy

$$g_I(\mathbf{x}) = \sqrt{r_I^2(\mathbf{x}) + (\alpha_s d_I)^2} \tag{2.64}$$

where $r_I(\mathbf{x})$ is the radius of node I and other ones in its influent domain; d_I is the minimum distance measured form node I to its neighbours; $\alpha_s > 0$ is the dimensionless factor used to control the shape parameter $\alpha_s d_I$.

Estimating the function at the set of N scattered points, Equation (2.62) can be

rewritten in terms of matrix form as

$$\mathbf{u} = \mathbf{R}_0 \mathbf{a} \tag{2.65}$$

where

$$\mathbf{R}_0 = \begin{bmatrix} \cdots & \cdots & \cdots & \cdots \\ R_{01}(\mathbf{x}_k) & R_{02}(\mathbf{x}_k) & \cdots & R_{0(N+n_2)}(\mathbf{x}_k) \\ \cdots & \cdots & \cdots & \cdots \end{bmatrix} \tag{2.66}$$

As a result, vector $\mathbf{a}$ can be expressed via the nodal values $\mathbf{u} = [u_1\ u_2\ ...\ u_N]$ as

$$\mathbf{a} = \mathbf{R}_0^{-1}\mathbf{u} = \hat{\mathbf{\Psi}}_{Ik}\mathbf{u} \tag{2.67}$$

Substituting $\mathbf{a}$ into Equations (2.60) - (2.62), the approximate function and its derivatives are recalculated as

$$u^h(\mathbf{x}) = \mathbf{R}_0(\mathbf{x})\hat{\mathbf{\Psi}}_{Ik}\mathbf{u} = \mathbf{\Phi}\mathbf{u} \tag{2.68a}$$

$$u^h_{,\alpha}(\mathbf{x}) = \mathbf{R}_1(\mathbf{x})\hat{\mathbf{\Psi}}_{Ik}\mathbf{u} = \mathbf{\Phi}_{,\alpha}\mathbf{u} \tag{2.68b}$$

$$u^h_{,\alpha\beta}(\mathbf{x}) = \mathbf{R}_2(\mathbf{x})\hat{\mathbf{\Psi}}_{Ik}\mathbf{u} = \mathbf{\Phi}_{,\alpha\beta}\mathbf{u} \tag{2.68c}$$

where the shape function and its derivatives can be defined by

$$\Phi_s(\mathbf{x}) = \sum_{I=1}^{N} R_{0I}(\mathbf{x})\hat{\psi}_{Is} \tag{2.69a}$$

$$\Phi_{s,\alpha}(\mathbf{x}) = \sum_{I=1}^{N} R_{1I}(\mathbf{x})\hat{\psi}_{Is} \tag{2.69b}$$

$$\Phi_{s,\alpha\beta}(\mathbf{x}) = \sum_{I=1}^{N} g_I(\mathbf{x})\hat{\psi}_{Is} \tag{2.69c}$$

with $\hat{\psi}_{Is}$ is the element (I, s) within matrix $\mathbf{R}_0^{-1}$.

The iRBF method overcomes an important obstacle of almost meshless methods in enforcing the essential boundary condition caused by the lack of Kronecker-delta property. Moreover, the high-order shape function obtained owing to the integration also helps to improve the computational aspect of numerical approach.

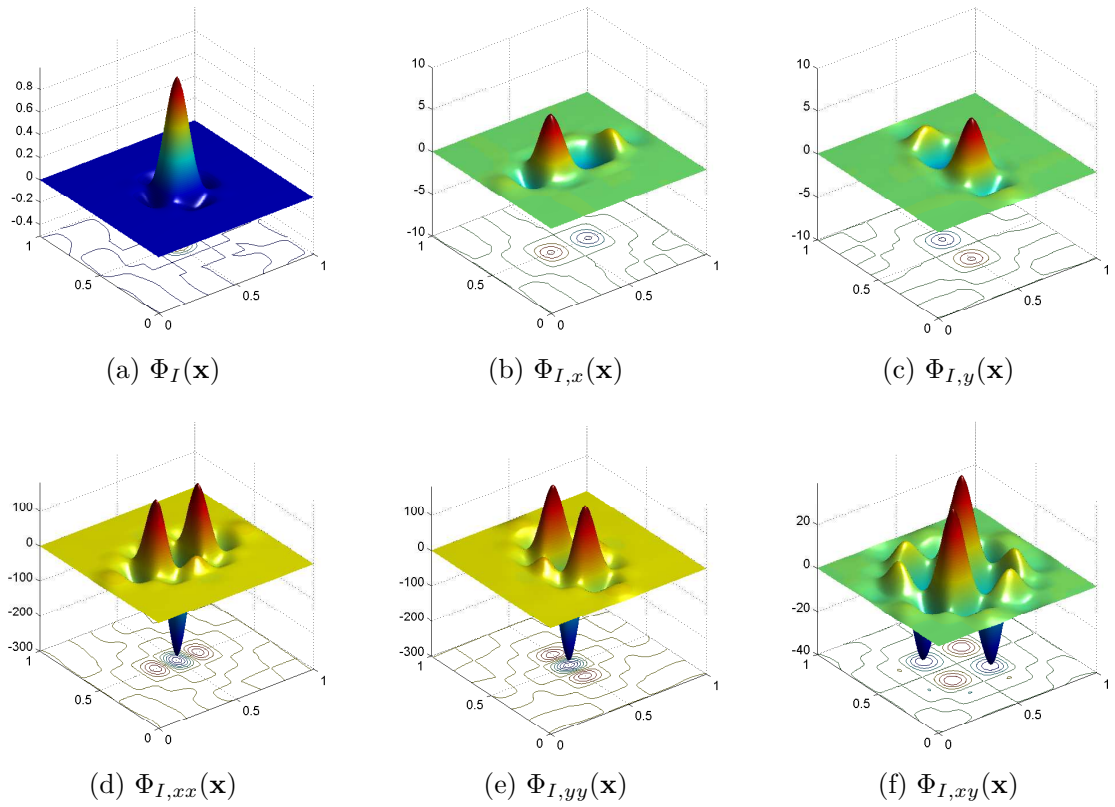

(a) $\Phi_I(\mathbf{x})$ (b) $\Phi_{I,x}(\mathbf{x})$ (c) $\Phi_{I,y}(\mathbf{x})$

(d) $\Phi_{I,xx}(\mathbf{x})$ (e) $\Phi_{I,yy}(\mathbf{x})$ (f) $\Phi_{I,xy}(\mathbf{x})$

Figure 2.8: The iRBF shape function and its derivatives

2.6.2 The integrating constants in iRBF approximation

In indirect RBF formulation, the approximate function $u^h(\mathbf{x})$ is calculated by the multiple integration; therefore, after each step, the new constants C_1 and C_2 appear. In this thesis, the integrating constants will be computed using the similar way to those carried out for the approximate function $u^h(\mathbf{x})$, it means the multiple integrals will be utilized as

$$C^h_{,jk}(\mathbf{x}) = \sum_{I=1}^{N} g_I(\mathbf{x}) \tag{2.70a}$$

$$C^h_{,j}(\mathbf{x}) = \int \sum_{I=1}^{N} g_I(\mathbf{x}) dx_k + \hat{C}_1 \tag{2.70b}$$

$$C^h(\mathbf{x}) = \iint \sum_{I=1}^{N} g_I(\mathbf{x}) dx_k dx_j + \hat{C}_1 x_j + \hat{C}_2 \tag{2.70c}$$

Herein, two new constant $\hat{C}_1$ and $\hat{C}_2$ will occur, and strictly, those must be calculated. However, thank to the constants C_1 and C_2 have been approximated,

for simplify, $\hat{C}_1$ and $\hat{C}_2$ can be ignored without effect on the approximation of the iRBF shape function.

It should be note that, in RPIM approximation, the radial basis cannot produce the linear polynomials exactly; consequently, the polynomials must be added into the basis functions to ensure the consistency of shape function. In other words, that makes sure the reproduction of the approximated field, and hence, helps to pass the standard patch tests, more details can be found in [156]. In this study, with the use of integrals when constructing shape functions, the constants C_1 and C_2 are generated evidently, making the iRBF approximation passes the patch tests naturally. However, it's worth noting that the patch test is neither sufficient nor necessary for convergence of numerical solutions [186], and many finite elements are widely used in FEM packages without passing this test [156].

2.6.3 The influence domain and integration technique

In order to evaluate the efficiency of a numerical method, it is necessary to consider not only the accuracy, stability and convergence of solutions but also the the computational cost. In mesh-free method, that depends on the influence or support domain and the technique to handle the integration.

The influence or support domain is defined as an area where a node or a point exerts an influence upon, but it is necessary to distinguish clearly between support and influence domains in meshless methods. The concept of support domain is used for the purpose of interpolating a value at a point. That domain is usually a small local field including a number of nodes in the problem domain. As an alternative way to select nodes for interpolation, the influence domain is defined for each node in the problem domain. In mesh-free methods, the influence domain can be global or local, and the density of the nodes depends on the accuracy requirement of the analysis and the resources available. The global domain enclosing all nodes in the problem domain ensures the continuity and ability to approximate and interpolate functions; hence the highly accuracy solutions can be obtained. However, using lots of nodes, the matrix of shape function and constrains in the problem will become densely increasing the expense of computation. In the opposite direction, the compact domain makes sure the local property and reduces the computational cost significantly, but it requires enough nodes to avoid the inaccuracy and singularity when approximating the shape function and interpolating nodal values. There are

several technique to determine the influence domain in mesh-free methods. The shapes of the domain mostly used are circular or rectangular. Since this thesis uses the radial basis function, the circular domain will be utilized as shown in Figure 2.9(a). The size of this domain can be operated using formulae (1.1) presented in previous chapter.

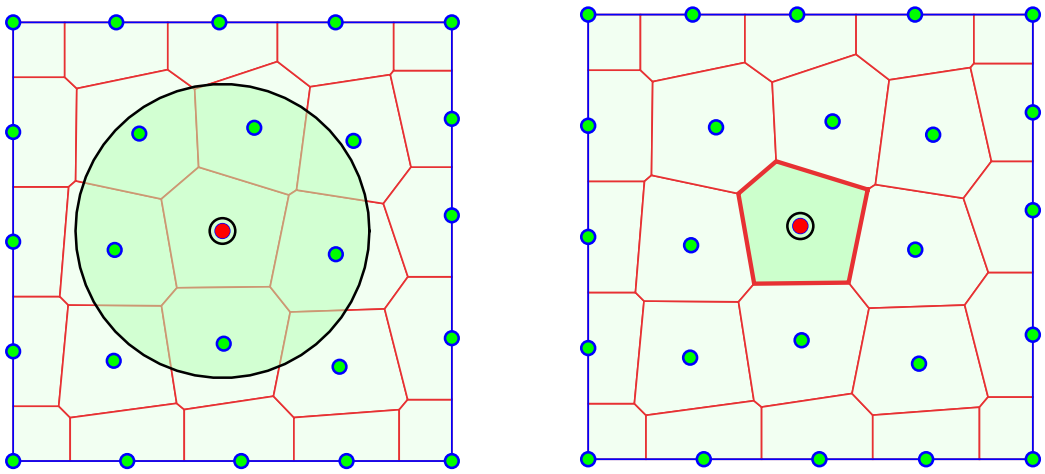

(a) The influence domain (b) The representative domain

Figure 2.9: The influence domain and representative domain of nodes

In several mesh-free methods, the background cells can be utilized to create the Gauss points where the computation will be implemented on. However, as discussed in previous chapters, this work does not ensure the truly meshless feature. In addition, a very fine mesh generating a number of Gauss points is required to obtained the good solutions, and hence the cost increases. Several meshless procedures in strong form use the collocation method, the constrains will be enforced and satisfied directly at scattered nodes. Consequently, the expense for the computation can be reduced significantly. Beside the advantage owing to the simplicity in implementation, the well-known drawback of strong form methods is the lack of stability and accuracy. In this thesis, a weak form using the stability conforming nodal integration (SCNI) technique [166] is employed, all constrains will be directly imposed at nodes instead of Gauss points. This scheme not only keeps the size of problems in a minimum but also ensures to obtain the solutions with high accuracy, stability and convergence.

Using SCNI technique, each node will has a integration area so-called representative domain Ω_J. For convenience, this domain can be determined using Voronoi

diagram as illustrated in Figure 2.9(b). The smoothed version of strain rate at node $\tilde{\epsilon}_{ij}^{h}(\mathbf{x}_J)$ can be calculated by

$$\tilde{\epsilon}_{ij}^{h}(\mathbf{x}_J) = \int_{\Omega_J} \epsilon_{ij}(\mathbf{x}) \varphi(\mathbf{x}, \mathbf{x} - \mathbf{x}_J) d\Omega \tag{2.71}$$

where φ is the smoothed function satisfying the condition

$$\varphi > 0 \quad \text{and} \quad \int_{\Omega_J} \varphi d\Omega = 1 \tag{2.72}$$

For simplicity, assuming that the function φ is a constant over the representative domain

$$\varphi(\mathbf{x}, \mathbf{x} - \mathbf{x}_J) = \begin{cases} \dfrac{1}{A_J} & \text{if } \mathbf{x} \in \Omega_J, \\ 0 & \text{if } \mathbf{x} \notin \Omega_J. \end{cases} \tag{2.73}$$

where A_J is the area of domain Ω_J.

Substituting φ in (2.73) into (2.71), then applying the Green's theorem to transfer the integral over domain to the line integral, the smoothed strain rate can be rewritten as

$$\begin{aligned} \tilde{\epsilon}_{ij}^{h}(\mathbf{x}_J) &= \frac{1}{A_J} \int_{\Omega_J} \frac{1}{2} \left(u_{i,j}^{h} + u_{j,i}^{h} \right) d\Omega \\ &= \frac{1}{2A_J} \oint_{\Gamma_J} \left(u_i^h n_j + u_j^h n_i \right) d\Gamma \end{aligned} \tag{2.74}$$

where Γ_J is the boundary of the representative domain; u_i and u_j are the displacement components; n is the outward normal of edges bounding domain Ω_J as Figure 2.10.

In the numerical implementation, the smoothed strain $\tilde{\epsilon}(\mathbf{x}_J)$ can be expressed via the relation to the displacements according to the compatible condition as follow

$$\tilde{\epsilon}(\mathbf{x}_J) = \tilde{\mathbf{B}}\mathbf{d} \tag{2.75}$$

where $\mathbf{d}$ is the displacement vector; $\tilde{\mathbf{B}}$ is the displacement-strain matrix including

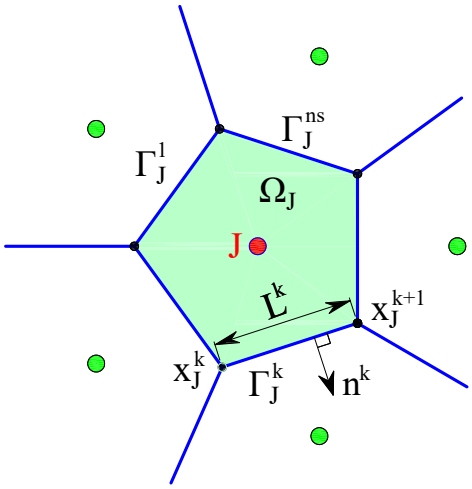

Figure 2.10: The SCNI technique in a representative domain

the smoothed derivatives of shape function

$$\begin{aligned}\tilde{\Phi}_{I,\alpha}(\mathbf{x}_J) &= \frac{1}{A_J}\oint_{\Gamma_J}\Phi_I(\mathbf{x}_J)n_\alpha(\mathbf{x})d\Omega \\ &= \frac{1}{2A_J}\sum_{k=1}^{ns}\left(n_\alpha^k L^k + n_\alpha^{k+1}L^{k+1}\right)\Phi_I(\mathbf{x}_J^{k+1})\end{aligned} \tag{2.76}$$

where ns is number of edges; $\Phi_I(\mathbf{x}_J^k)$ and $\Phi_I(\mathbf{x}_J^{k+1})$ are the shape function relating to two end of the edge Γ^k of Voronoi; L^k and n^k are the length and the normal of edge Γ^k.

In several problems, the high-order derivatives of shape function may be in need due to the variables can be the high-order derivatives of displacement, for example in bending plate problem, the curvature variables $\kappa(\mathbf{x})$ are the second-order derivative of the deflection $w(\mathbf{x})$. Similarly, the smoothed version of second-order derivatives of shape function can be calculated from the first-order ones as

$$\begin{aligned}\tilde{\Phi}_{I,\alpha\beta}(\mathbf{x}_J) &= \frac{1}{2A_J}\oint_{\Gamma_J}\left(\Phi_{I,\alpha}(\mathbf{x}_J)n_\beta(\mathbf{x}) + \Phi_{I,\beta}(\mathbf{x}_J)n_\alpha(\mathbf{x})\right)d\Omega \\ &= \frac{1}{4A_J}\sum_{k=1}^{ns}\left(n_\beta^k L^k + n_\beta^{k+1}L^{k+1}\right)\Phi_{I,\alpha}(\mathbf{x}_J^{k+1}) \\ &+ \frac{1}{4A_J}\sum_{k=1}^{ns}\left(n_\alpha^k L^k + n_\alpha^{k+1}L^{k+1}\right)\Phi_{I,\beta}(\mathbf{x}_J^{k+1})\end{aligned} \tag{2.77}$$

with $\Phi_{I,\alpha}(\mathbf{x})$ and $\Phi_{I,\beta}(\mathbf{x})$ are the first-order derivatives of shape function $\Phi_I(\mathbf{x})$ relating to variables α and β.

Chapter 3

Displacement and equilibrium mesh-free formulation based on integrated radial basis functions for dual yield design [1]

3.1 Introduction

This chapter presents an application of iRBF-based mesh-free method for plane structures at limit state using both of kinematic and static formulations. A lower bound on the actual limit load of a structure or body can be achieved by using the static theorem and approximated stress fields, while the upper bound is obtained as a result of combining displacement-based model and kinematic theorem [93]. In the static yield design formulation, the assumed stress fields are often expressed in terms of nodal stress values. In the framework of equilibrium finite elements, these approximated fields are also required to satisfy a priori equilibrium conditions within elements and at their interfaces [36, 58, 93, 187, 188]. Due to these additional conditions, construction of such fields is often difficult. Compared with the equilibrium models, the displacement formulation is more popular. This may be because of the facts that the internal compatibility condition can be satisfied straightaway in the assembly scheme, and that essential (kinematic) boundary conditions can be enforced directly.

Unlike FEM, mesh-free methods does not encounter the obstacle of enforcing the equilibrium conditions thank to their independence to elements, and hence the displacement as well as equilibrium formulations can be used easily. The EFG method, one of the most widely used mesh-free methods, has been applied successfully to

[1] based on P. L. H. Ho, C. V. Le, and T. Tran-Cong, "Displacement and equilibrium mesh-free formulation based on integrated radial basis functions for dual yield design," *Eng. Anal. Bound. Elem.*, vol. 71, pp. 92–100, Oct. 2016.

the framework of yield design problems [90, 92–95], showing that the method is, in general, well suited for yield design problems and that accurate solutions can be obtained with a minimal computational cost. However, a typical limitation of the EFG method is that its shape functions do not hold Kronecker delta property, leading to difficulty in enforcing essential boundary conditions. An other mesh-free procedure so-called NEM has been applied for limit analysis in [88, 89]. Possessing a weak form of Kronecker-delta property at the boundary, NEM shows more advantage than EFG in imposing the boundary conditions. Using the stricter Kronecker-delta property compared with NEM, RPIM has been also extent to this area in [96].

The aim of this study is to investigate the performance of the integrated radial basis function-based mesh-free method in the framework of yield design problems. The iRBF approach will be employed to approximate both displacement and stress fields. Multiquadric iRBF method generally results in a high order approximation of the displacement fields, and hence volumetric locking phenomena in the kinematic yield design formulation can be prevented. Moreover, the stress fields constructed based on iRBF are smooth over the entire problem domain, and consequently there is no need to enforce continuity conditions at interfaces within the problem domain. With the use of iRBF-approximated stress fields the strong-form of equilibrium equations can be satisfied in a point-wise manner using a collocation method. In addition, the iRBF-based approximation possesses the Kronecker delta property as in RPIM, but the order of iRBF shape function is higher than RPIM ones when using similar basis function. As a result, kinematic and static boundary conditions can be imposed as easily as in the finite element method. Finally, the kinematic and static formulations based on iRBF discretization are formulated as a conic optimization problem, ensuring that they can be solved using available efficient solvers.

3.2 Kinematic and static iRBF discretizations

Consider an elastic-plastic body of area $\Omega \in \mathbb{R}^2$, with fixed boundary Γ_u and free portion Γ_t such that $\Gamma_u \cup \Gamma_t = \Gamma$, $\Gamma_u \cap \Gamma_t = \varnothing$, and is subjected to a body force $\mathbf{f}$ in Ω and surface traction $\mathbf{t}$ on Γ_t. The structure is investigated in both kinematically and statically admissible spaces. The iRBF-based mesh-free method will be utilized to approximate the statically admissible stress field as well as the kinematically displacement velocity field. As presented in previous chapter, for simplify, the

displacement velocity field will be briefly called displacement field.

3.2.1 iRBF discretization for kinematic formulation

For the upper bound analysis at limit state, the displacement field can be approximated via the nodal values as

$$u^h(\mathbf{x}) = \begin{bmatrix} u \\ v \end{bmatrix} = \sum_{I=1}^{N} \Phi_I(\mathbf{x}) \begin{bmatrix} u_I \\ v_I \end{bmatrix} \tag{3.1}$$

where, $\Phi_I(\mathbf{x})$ denotes the iRBF shape function.

The strain rate are calculated by

$$\boldsymbol{\epsilon} = \begin{bmatrix} \epsilon_{xx} \\ \epsilon_{yy} \\ \gamma_{xy} \end{bmatrix} = \begin{bmatrix} \sum_{I=1}^{N} \Phi_{I,x}(\mathbf{x}) & 0 \\ 0 & \sum_{I=1}^{N} \Phi_{I,y}(\mathbf{x}) \\ \sum_{I=1}^{N} \Phi_{I,y}(\mathbf{x}) & \sum_{I=1}^{N} \Phi_{I,x}(\mathbf{x}) \end{bmatrix} \begin{bmatrix} u_I \\ v_I \end{bmatrix} = \mathbf{B}(\mathbf{x})\mathbf{d} \tag{3.2}$$

where $\mathbf{d}$ is the nodal displacement vector; $\mathbf{B}$ is called displacement-strain matrix and given by

$$\mathbf{d}^T = [u_1, u_2, ..., u_n, v_1, v_2, ..., v_n] \tag{3.3a}$$

$$\mathbf{B} = \begin{bmatrix} \mathbf{B}_{xx} \\ \mathbf{B}_{yy} \\ \mathbf{B}_{xy} \end{bmatrix} = \begin{bmatrix} \Phi_{1,x} & \Phi_{2,x} & ... & \Phi_{N,x} & 0 & 0 & ... & 0 \\ 0 & 0 & ... & 0 & \Phi_{1,y} & \Phi_{2,y} & ... & \Phi_{N,y} \\ \Phi_{1,y} & \Phi_{2,y} & ... & \Phi_{N,y} & \Phi_{1,x} & \Phi_{2,x} & ... & \Phi_{N,x} \end{bmatrix} \tag{3.3b}$$

For von Mises yield criterion, the dissipation power can be formulated as

$$D_p(\boldsymbol{\epsilon}) = \int_\Omega \sigma_p \sqrt{\boldsymbol{\epsilon}^T \boldsymbol{\Theta} \boldsymbol{\epsilon}} = \sum_{I=1}^{N} \sigma_p A_I \sqrt{(\mathbf{B}_I \mathbf{d})^T \boldsymbol{\Theta} \mathbf{B}_I \mathbf{d}} \tag{3.4}$$

where σ_p is the yield stress of materials; A_I is area of the representative domain

I^{th}, e.g. Voronoi cells; N denotes number of nodes in problem domain and

$$\mathbf{\Theta} = \frac{1}{3}\begin{bmatrix} 4 & 2 & 0 \\ 2 & 4 & 0 \\ 0 & 0 & 1 \end{bmatrix} \quad \text{for plane stress problem} \tag{3.5}$$

or

$$\mathbf{\Theta} = \begin{bmatrix} 1 & -1 & 0 \\ -1 & 1 & 0 \\ 0 & 0 & 1 \end{bmatrix} \quad \text{for plane strain problem.} \tag{3.6}$$

Using SOCP, a sum of norm can be employed to calculate the internal dissipation work as

$$D_p = \sum_{I=1}^{N} \sigma_p A_I \|\rho_I\| \tag{3.7}$$

with ρ_I denotes the additional variables defined by

$$\rho_I = \begin{cases} \begin{bmatrix} \rho_1 \\ \rho_2 \\ \rho_3 \end{bmatrix} = \frac{1}{\sqrt{3}} \begin{bmatrix} 2 & 0 & 0 \\ 1 & \sqrt{3} & 0 \\ 0 & 0 & 1 \end{bmatrix} \mathbf{B}_I \mathbf{d} & \text{for plane stress;} \\ \begin{bmatrix} \rho_1 \\ \rho_2 \end{bmatrix} = \begin{bmatrix} \mathbf{B}_{xxI}\mathbf{d} - \mathbf{B}_{yyI}\mathbf{d} \\ 2\mathbf{B}_{xyI}\mathbf{d} \end{bmatrix} & \text{for plane strain.} \end{cases} \tag{3.8}$$

Now, the optimization can be rewritten as follow

$$\lambda^+ = \min \sum_{I=1}^{N} \sigma_p A_I \|\boldsymbol{\rho}_I\| \tag{3.9}$$

$$\text{s.t} \quad \begin{cases} \mathbf{d} = 0 \text{ on } \Gamma_u \\ F(\mathbf{d}) = 1 \end{cases} \tag{3.10}$$

Introducing additional variables $t_1, t_2, ..., t_N$, problem (3.10) can be reformulated

in form of second-order cone programming as

$$\lambda^{+} = \min \sum_{I=1}^{N} \sigma_p A_I t_I \tag{3.11}$$

$$\text{s.t} \begin{cases} \mathbf{d} = 0 \text{ on } \Gamma_u \\ F(\mathbf{d}) = 1 \\ \|\rho_I\| \leq t_I, \ I = 1, 2, ..., N \end{cases} \tag{3.12}$$

Note that for plane strain problems, incompressibility conditions, $\Delta^T \epsilon = 0$ with $\Delta^T = [1, 1, 0]$, must be introduced. If low-order displacement approximations are used, volumetric locking phenomena in the kinematic formulations associated with the von Mises may occur due to these incompressibility conditions. However, here the iRBF method results in high-order displacement fields, and hence volumetric locking problem can be prevented. Moreover, it is evident that the size of optimization problem (3.12) depends on the number of integration points to be used. In this study, the nodal integration technique is used, and hence the size of the resulting optimization problem is kept to be minimum.

3.2.2 iRBF discretization for static formulation

While in the upper bound formulation the displacement fields are approximated, here the stress fields need to be approximated. With the use of the iRBF method, approximations of these stress fields can be presented as

$$\boldsymbol{\sigma}^h(\mathbf{x}) = \begin{bmatrix} \sigma_{xx}^h \\ \sigma_{yy}^h \\ \sigma_{xy}^h \end{bmatrix} = \sum_{I=1}^{N} \Phi_I(\mathbf{x}) \begin{bmatrix} \sigma_{xxI} \\ \sigma_{yyI} \\ \sigma_{xyI} \end{bmatrix} = \mathbf{Cs} \tag{3.13}$$

where

$$\mathbf{s}^T = [\sigma_{xx1}, \cdots, \sigma_{xxN}, \sigma_{yy1}, \cdots, \sigma_{yyN}, \sigma_{xy1}, \cdots, \sigma_{xyN}] \tag{3.14a}$$

$$\mathbf{C} = \begin{bmatrix} \mathbf{C_{xx}} \\ \mathbf{C_{yy}} \\ \mathbf{C_{xy}} \end{bmatrix} = \begin{bmatrix} \Phi_1 & \cdots & \Phi_N & 0 & \cdots & 0 & 0 & \cdots & 0 \\ 0 & \cdots & 0 & \Phi_1 & \cdots & \Phi_N & 0 & \cdots & 0 \\ 0 & \cdots & 0 & 0 & \cdots & 0 & \Phi_1 & \cdots & \Phi_N \end{bmatrix} \tag{3.14b}$$

These approximated stress fields must be ensured to be statically admissible, meaning that equilibrium and continuity conditions within elements and on their boundary must be satisfied. While the strong form of equilibrium equations can be treated using collocation method, its equivalent weak form (involving integrals) is often handled using the weighted residual method. The strong-form method is simple and fast, and hence the collocation method using the iRBF will be considered in this study. The equilibrium equations can be imposed at N nodes, and are expressed as

$$\begin{cases} \mathbf{A}_1\boldsymbol{\sigma}_1 + \mathbf{A}_2\boldsymbol{\sigma}_3 = 0 \\ \mathbf{A}_1\boldsymbol{\sigma}_3 + \mathbf{A}_2\boldsymbol{\sigma}_2 = 0 \end{cases} \tag{3.15}$$

with

$$\mathbf{A}_1 = \begin{bmatrix} \cdots & \cdots & \cdots & \cdots \\ \Phi_{1,x}(\mathbf{x}_k) & \Phi_{2,x}(\mathbf{x}_k) & \cdots & \Phi_{N,x}(\mathbf{x}_k) \\ \cdots & \cdots & \cdots & \cdots \end{bmatrix}_{N\times N} \tag{3.16a}$$

$$\mathbf{A}_2 = \begin{bmatrix} \cdots & \cdots & \cdots & \cdots \\ \Phi_{1,y}(\mathbf{x}_k) & \Phi_{2,y}(\mathbf{x}_k) & \cdots & \Phi_{N,y}(\mathbf{x}_k) \\ \cdots & \cdots & \cdots & \cdots \end{bmatrix}_{N\times N} \tag{3.16b}$$

and

$$\boldsymbol{\sigma}_1 = [\sigma_{xx1},\ \sigma_{xx2},\ \cdots\ \sigma_{xxN}]^T \tag{3.17a}$$

$$\boldsymbol{\sigma}_2 = [\sigma_{yy1},\ \sigma_{yy2},\ \cdots\ \sigma_{yyN}]^T \tag{3.17b}$$

$$\boldsymbol{\sigma}_3 = [\sigma_{xy1},\ \sigma_{xy2},\ \cdots\ \sigma_{xyN}]^T \tag{3.17c}$$

Additionally, the approximated stress fields must belong to a convex domain, $\mathscr{B}$. In other words, these stress fields must satisfy the following second-order cone constraints obtaining from the von Mises criterion

$$\sigma^h(\mathbf{x}) \in \mathscr{B} \tag{3.18}$$

with

$$\mathscr{B} \equiv \left\{ \boldsymbol{\rho} \in \mathbb{R}^3 \;\middle|\; \rho_1 \geq \|\rho_{2\to 4}\|_L^2 = \sqrt{\rho_2^2 + \rho_3^2 + \rho_4^2} \right\} \quad \text{for plane stress} \tag{3.19a}$$

$$\mathscr{B} \equiv \left\{ \boldsymbol{\rho} \in \mathbb{R}^3 \;\middle|\; \rho_1 \geq \|\rho_{2\to 3}\|_L^2 = \sqrt{\rho_2^2 + \rho_3^2} \right\} \quad \text{for plane strain} \tag{3.19b}$$

where

$$\begin{aligned} &\rho_1 = \sigma_p \\ &\rho_{2\to 4} = \begin{bmatrix} \rho_2 \\ \rho_3 \\ \rho_4 \end{bmatrix} = \frac{1}{2} \begin{bmatrix} 2 & 0 & 0 \\ -1 & \sqrt{3} & 0 \\ 0 & 0 & 2\sqrt{3} \end{bmatrix} \mathbf{Cs} \quad \text{for plane stress} \\ &\rho_{2\to 3} = \begin{bmatrix} \rho_2 \\ \rho_3 \end{bmatrix} = \frac{1}{2} \begin{bmatrix} \mathbf{C}_{xx} - \mathbf{C}_{yy} \\ 2\mathbf{C}_{xy} \end{bmatrix} \mathbf{s} \quad \text{for plane strain} \end{aligned} \tag{3.20}$$

Hence the static yield design formulation can now be expressed as

$$\lambda = \max \lambda^- \tag{3.21}$$

$$\text{s.t} \begin{cases} \mathbf{A}_1\sigma_{\mathbf{1}} + \mathbf{A}_2\sigma_{\mathbf{2}} & \text{in } \Omega \\ \mathbf{A}_1\sigma_{\mathbf{3}} + \mathbf{A}_2\sigma_{\mathbf{2}} & \text{in } \Omega \\ \boldsymbol{\rho}^k \in \mathscr{L}^k & k = 1, 2, ..., N_p \end{cases} \tag{3.22}$$

and accompanied by appropriate boundary conditions.

It should be emphasized that in the present static formulation equilibrium equations and yield criterion are enforced at nodes only, and therefore the strict property of the lower bound λ^- is not guaranteed. However, using a fine nodal distribution one can hope to achieve a reliable approximated lower bound on the actual limit load multiplier. Moreover, by enforcing the equilibrium equations and yield criterion at nodes only the number of constraints in optimization problem (3.22) is kept to be minimum, and hence the presented static method is computationally inexpensive.

The whole numerical implementations of both upper and lower bound approaches are illustrated by flow chart shown in Figure 1.1.

3.3 Numerical examples

The described procedures are tested by their application to solve various problems for which, in most cases, exact and numerical solutions are available. Upper and lower bound solutions based on direct radial basis function (dRBF) are also carried out for comparison purpose. Optimization problems (3.12) and (3.22) are implemented in the Matlab environment. Mosek optimization solver version 6.0 is used to solve the conic optimization problem obtained (using a 2.8 GHz Intel Core i5 PC running Window 7).

3.3.1 Prandtl problem

The first example is the classical punch problem presented in [189], as shown in Figure 3.1. Due to symmetry, a rectangular region of dimensions B = 5 and H = 2 is considered. Appropriate displacement and stress boundary conditions are enforced as shown in Figure 3.2. For a load of $2\tau_0$, the analytical limit multiplier is $\lambda = 2 + \pi = 5.142$.

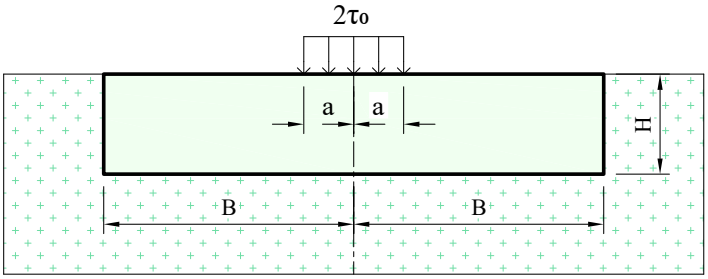

Figure 3.1: Prandtl problem

Approximations of upper and lower bounds on the actual limit load for both dRBF and iRBF methods with various nodal discretizations are reported in Table 3.1. From these results, it can be seen that for both kinematic and static formulations the iRBF-based method can provide more accurate solutions than the dRBF-based method. Convergence analysis and relative errors in collapse multipliers versus number of variables are also shown in Figures 3.3(a) and 3.3(b), respectively. It should be stressed that the mean values of upper and lower approximations obtained using the iRBF-based numerical procedures are in excellent agreement with the analytical solutions for all nodal discretizations, as shown in Figure 3.3, with less than 0.4% even for coarse nodal distribution. Furthermore, as mentioned, the

present procedure cannot theoretically provide strict lower bound solutions, it is evident that all approximated lower bound results are below the exact value.

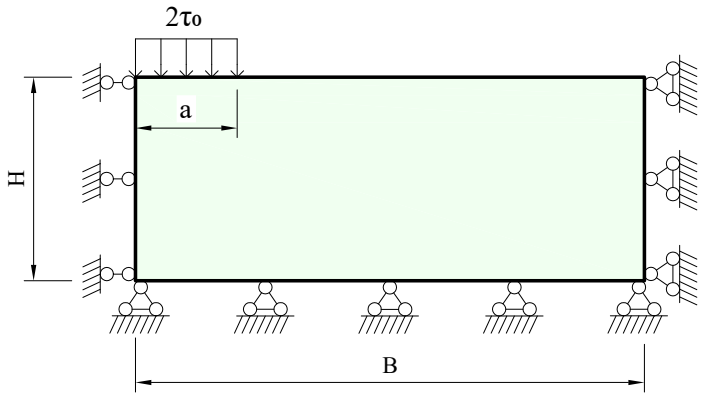

(a) Computational domain

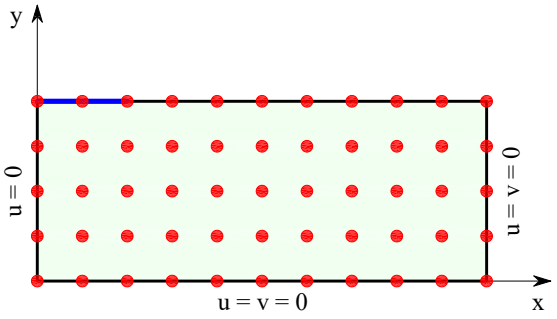

(b) Displacement boundary condition

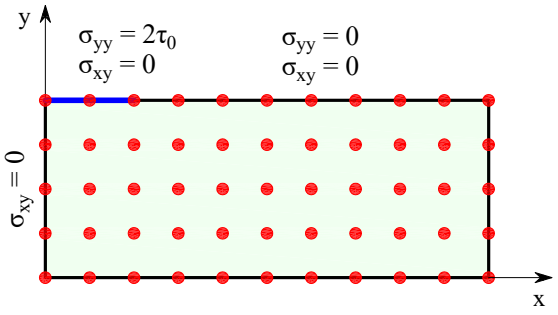

(c) Stress boundary condition

Figure 3.2: Prandtl problem: approximation displacement and stress boundary conditions

Note that in the kinematic formulation, volumetric (or isochoric) locking often occurs when adding the incompressibility condition to the low-order displacement based yield design problem. The volumetric locking behavior of the Prandtl yield design problem has been studied in [78, 95]. In these papers, it has been demonstrated that when smoothed strains were used, the volumetric locking problem can be eliminated. Here, we have shown that the iRBF method used in combination with direct nodal integration can remove such the volumetric locking behavior and also result in stable and accurate solutions.

In Table 3.2 the solutions obtained using the present methods with 2560 nodes are compared with those obtained previously by different yield design approaches using FEM, smoothed finite element (SFEM) and EFG simulations. In general, the present solutions are close to results in the literature. Considering upper solutions,

Table 3.1: Prandtl problem: upper and lower bound of collapse multiplier

Nodes	dRBF				iRBF			
	Upper bound		Lower-bound		Upper bound		Lower-bound	
	λ^+	e (%)	λ^-	e (%)	λ^+	e (%)	λ^-	e (%)
40	6.857	33.35	2.761	46.31	6.036	17.39	4.218	17.97
160	5.548	7.90	4.244	17.46	5.279	2.66	4.960	3.54
360	5.289	2.86	4.800	6.65	5.209	1.30	5.061	1.58
640	5.211	1.34	5.042	1.95	5.191	0.95	5.108	0.66
1000	5.189	0.91	5.125	0.33	5.180	0.74	5.134	0.16

e (%) - relative error

Table 3.2: Prandtl problem: comparison with previous solutions

Author	Approach	Collapse load multiplier	
		λ^+	λ^-
Present method, *iRBF*	Kinematic, static	5.146	5.140
Present method, *dRBF*	Kinematic, static	5.159	5.133
Makrodimopoulos and Martin [190], *FEM*	Kinematic, static	5.148	5.141
Vicente da Silva and Antao [191], *FEM*	Kinematic	5.264	-
Sloan and Kleeman [192], *FEM*	Kinematic	5.210	-
Le et al. [78], *CS-FEM*	Kinematic	5.143	-
Le et al. [95], *EFG*	Kinematic	5.147	-
Capsoni and Corradi [63], *FEM*	Mixed formulation	5.240	

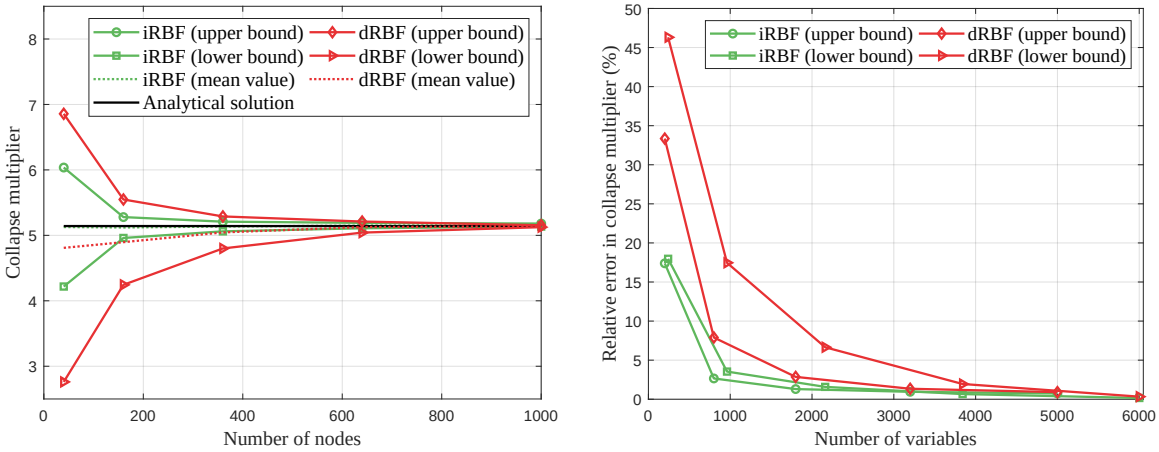

(a) Bounds on the collapse multiplier

(b) Relative error in collapse multipliers

Figure 3.3: Bounds on the collapse multiplier versus the number of nodes and variables

the result obtained using the iRBF method is slightly lower than the one obtained using the EFG mesh-free method with the same nodal discretization [95].

3.3.2 Square plates with cutouts subjected to tension load

Next, two thin square plates with a central square cutout and a thin crack subjected to a uniform tension load, as shown in Figure 3.4, are considered. These problems have been investigated numerically by finite elements [193, 194], symmetric Galerkin boundary elements [195], and mesh-free methods [88, 90]. Owing to the symmetry, only the top- right quarter of plates is modeled, as shown in Figure 3.5. Uniform nodal distribution is used to discretize the computational domain, see Figure 3.6.

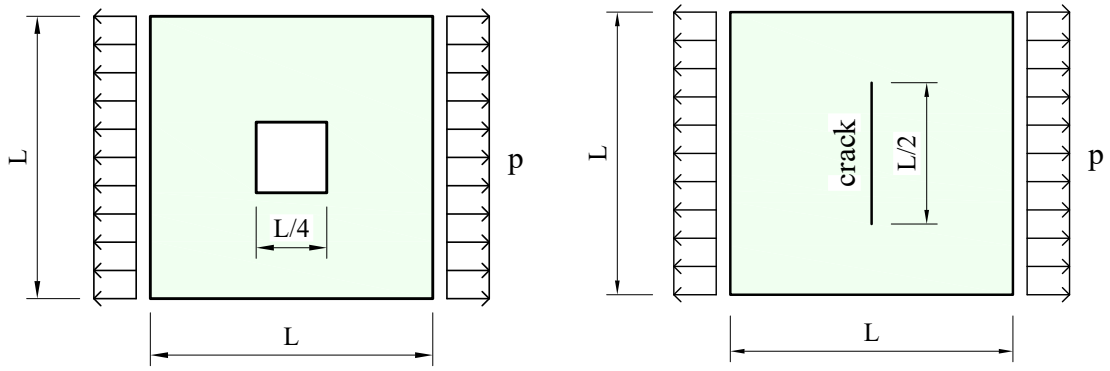

(a) Square cutout (b) Thin crack

Figure 3.4: Thin square plates

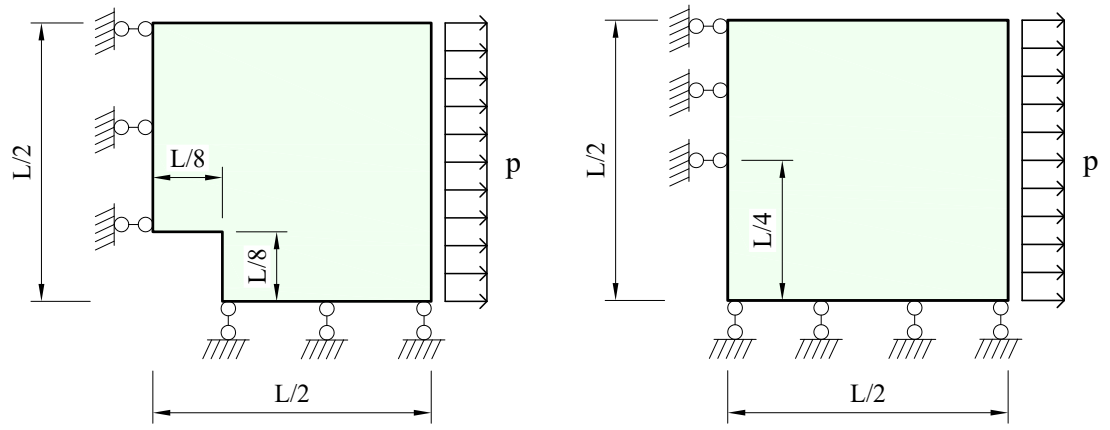

(a) Square cutout (b) Thin crack

Figure 3.5: The upper-right quater of plates

Limit load multipliers obtained using uniform nodal distributions are reported in Tables 3.3 and 3.4. Collapse load multiplier versus the number of nodes is also shown in Figure 3.7. Again, it can be observed that the iRBF-based method can provide more accurate solutions than the dRBF-based method, particularly for the static approach.

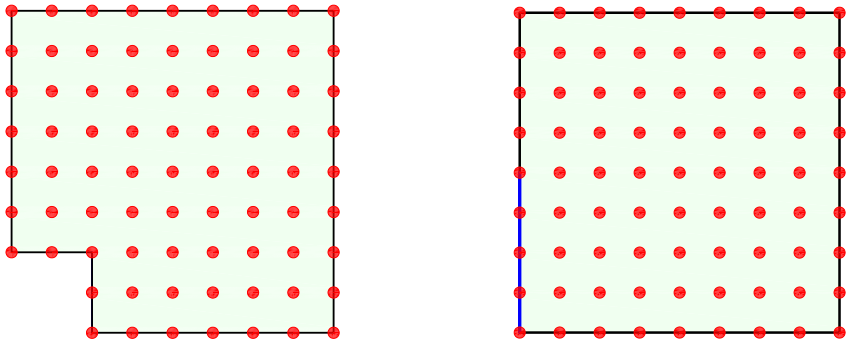

(a) Square cutout (b) Thin plate

Figure 3.6: Uniform nodal discretization

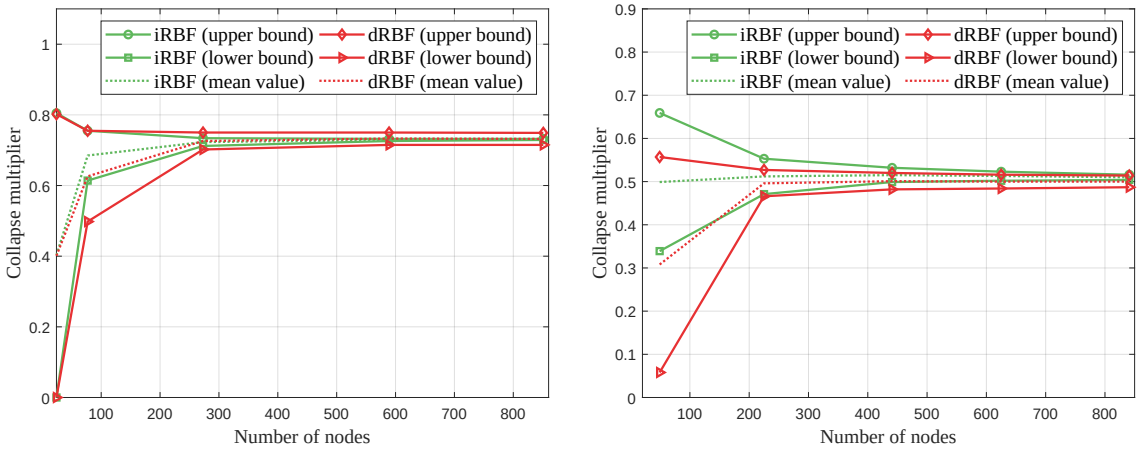

(a) Square cutout (b) Thin plate

Figure 3.7: Convergence of limit load factor for the plates

Table 3.5 shows that the results obtained by using RBF methods are in good agreement with previously reported numerical solutions. Considering upper bound limit factor, the present results are close to Zhou and Liu's solutions, with the maximum error of only 2.79%. It is important to note that the estimated lower bounds reported in [90, 195] are higher than the present lower bound solutions, and surpasses the upper bound of the present iRBF method for the plate with square cutout. This can be explained by the fact that in [90, 195] the strong form

of the equilibrium equations was transformed into the so-called weak form, and to be satisfied locally in an average sense using approximated virtual displacement fields. Therefore, the static method in [90, 195] may result in a higher value than the actual limit multiplier. In contrast, it is clear that all the present lower bound solutions obtained are below the upper bounds reported in Table 3.5.

Table 3.3: Collapse multipliers for the square plate with a central square cutout

	dRBF		iRBF	
Number of nodes	Upper bound	Lower bound	Upper bound	Lower bound
273	0.750	0.702	0.734	0.712
589	0.750	0.715	0.732	0.726
851	0.749	0.715	0.732	0.729

Table 3.4: Collapse multipliers for the square plate with a central thin crack

	dRBF		iRBF	
Number of nodes	Upper bound	Lower bound	Upper bound	Lower bound
441	0.520	0.482	0.532	0.499
625	0.516	0.484	0.523	0.502
841	0.514	0.487	0.516	0.504

Table 3.5: Plates with cutouts problem: comparison with previous solutions

Author	Approach	Square cutout		Thin crack	
		λ^+	λ^-	λ^+	λ^-
Present method, *iRBF*	Kinematic, static	0.732	0.729	0.516	0.504
Present method, *dRBF*	Kinematic, static	0.749	0.715	0.514	0.487
Pixin et al. [194], *FEM*	Kinematic	0.764	-	0.534	-
Zhou and Liu [88], *NEM-Sibson*	Kinematic	0.753	-	0.515	-
Zhou and Liu [88], *NEM-Laplace*	Kinematic	0.752	-	0.513	-
Belytschko and Hodge [193], *FEM*	Static	-	0.693	-	0.498
Zhang et al. [195], *FEM*	Static	-	0.747	-	0.514
Chen et al. [90], *EFG*	Static	-	0.736	-	0.513

3.3.3 Notched tensile specimen

Finally, a double notched specimen consists of a rectangular specimen with two thin cracks under in-plane tensile stresses t_0 as shown in Figure 3.8 (W = L = 2a = 1), is also considered. This problem exhibits volumetric locking phenomena

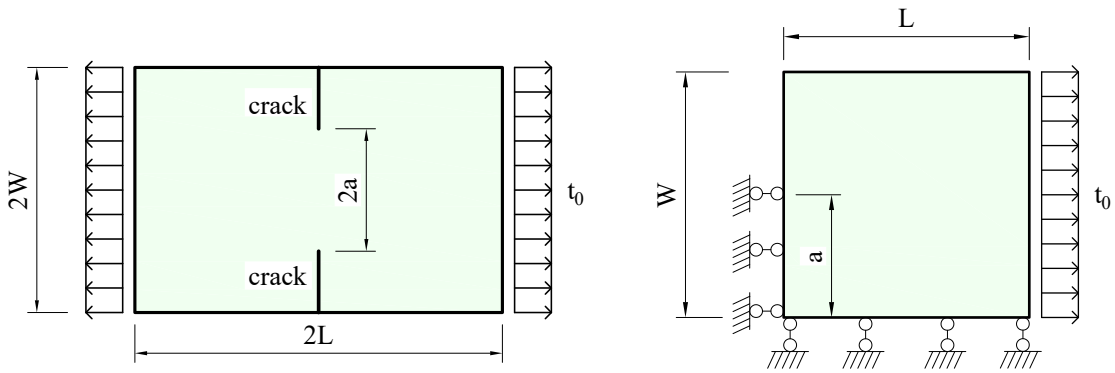

(a) Geometry and loading (b) Computational model

Figure 3.8: Double notch specimen

[196] and became a popular benchmark test for plastic yield design procedures. The locking problem was handled using various techniques proposed in the literature, including higher-order displacement-based finite element method [197], mixed finite elements [44, 63, 198] and discontinuous elements [59, 192, 199], mesh-free methods [95], smoothed finite elements [78, 79].

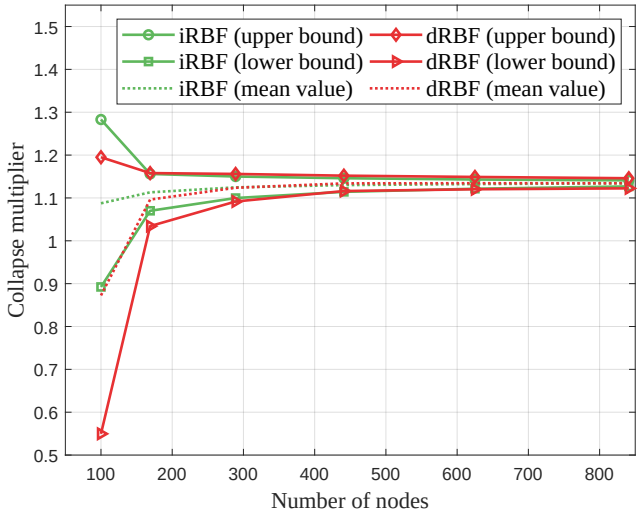

Figure 3.9: Convergence study for the double notched specimen problem

Owing to the symmetry, only the upper-right quarter of the double notched problem is discretized. Several uniform nodal distributions are employed. Computed solutions and convergence analysis are presented in Table 3.6 and Figure 3.9. Table 3.6 compares the present solutions with those obtained previously. The mean values of the dRBF and iRBF results are 1.1343 and 1.1342, respectively. It can be observed that these mean values are very close to the benchmark solution obtained using

Table 3.6: The double notched specimen: comparison with previous solutions

Author	Approaoch	Collapse multiplier λ	
		λ^+	λ^-
Present method, *iRBF*	Kinematic, static	1.141	1.127
Present method, *dRBF*	Kinematic, static	1.146	1.122
Ciria et al. [175], *FEM-uniform mesh*	Kinematic, static	1.149	1.131
Ciria et al. [175], *FEM-adaptive mesh*	Kinematic, static	1.139	1.132
Le et al. [78], *CS-FEM*	Kinematic	1.137	-
Le et al. [95], *EFG*	Kinematic	1.137	-
Tin-Loi and Ngo [197], *FEM*	Static	-	1.166
Krabbenhoft and Damkilde [200], *FEM*	Static	-	1.132
Christiansen and Andersen [198], *FEM*	Mixed formulation	1.136	

mixed formulation by Christiansen and Andersen [198].

3.4 Conclusions

The present contribution has presented displacement and equilibrium mesh-free formulation based on integrated radial basis functions (iRBF) for dual yield design problems. In the kinematic formulation, the high-order approximation of the displacement fields using the integrated radial basis functions can prevent volumetric locking. Moreover, direct nodal integration of the iRBF approximation not only results in inexpensive computational cost, but also overcomes the instability problems. In the static formulation, with the use of iRBF approximation of the stress fields in combination with the collocation method, equilibrium equations and yield conditions only need to be enforced at the nodes, leading to the reduction in computational effort. It has been shown in several examples that the mean values of the iRBF upper and lower bounds are accurate, and can be considered as the actual collapse load multiplier for most practical engineering problems, for which exact solution is unknown.

Chapter 4

Limit state analysis of reinforced concrete slabs using an integrated radial basis function based mesh-free method [1]

4.1 Introduction

This chapter presents an application of iRBF method for upper bound limit analysis of structures. This study aims to estimate the limit load as well as collapse mechanics of reinforced concrete slabs. Dealing with that structures, yield line or discontinuity layout optimization (DLO) methods can be employed. The element based yield line methods [201–204] have the intrinsic advantage of providing accurate solutions for many practical engineering problems. However, the solutions of the element based yield line analysis are highly affected by the initial mesh topology because the yield-lines are restricted to be formed only at the edges of elements. Alternatively, discontinuity layout optimization, a generally applicable numerical limit analysis procedure that can be used to automatically identify the critical yield-line pattern, has been proposed in [205, 206]. However, owing to their advantages in treating problems of arbitrary geometries, complicated boundary conditions and complex loads, limit analysis procedures based on numerical discretization techniques has been found to be more popular [58, 64, 93, 207–209] in solving real-world engineering problems.

In the kinematic formulation, these unknown variables are often approximated in terms of nodal displacements and rotations. In order to minimize the total number of the problem degrees of freedom, and hence reduce computational effort, elements

[1] based on P. L. H. Ho, C. V. Le, and T. Tran-Cong, "Limit state analysis of reinforced concrete slabs using an integrated radial basis function based mesh-free method," *Appl. Math. Model.*, vol. 53, pp. 1–11, Jan. 2018.

without rotational degree of freedom, namely rotation-free elements, have been proposed by several researchers [210–213]. Taking advantages of such a rotation-free formulation, various rotation-free mesh-free based models have been proposed for thin plate structures [214–216]. Recently, a rotation-free formulation, that uses moving least squares approximation technique, has been developed for collapse analysis of reinforced concrete slabs [209]. It has been shown that the method can provide accurate collapse load multipliers with a relatively small number of degrees of freedom. Its main disadvantage, on the other hand, is the need to specially treat the kinematic boundary conditions due to the fact that the moving least squares approximation does not hold the so-called Kronecker delta property. Mesh-free method based on radial basis functions and point interpolation [217] may be used to overcome such the difficulty.

In this study, a novel rotational-free mesh-free formulation for limit state analysis of reinforced concrete slabs is developed. Note that the formulation for limit analysis of reinforced concrete slabs is very much different from those of plane problems, i.e., the formulation to determine the internal dissipation, the yield criterion used, and boundary conditions. The transverse velocity field is approximated by using the integrated radial basis functions (iRBF), particularly the multiquadric basis, and there is no rotational degree of freedom involved in the approximation. The resultant shape functions satisfy the Kronecker delta property, and hence displacement boundary conditions can be enforced in a way similar to one in the finite element method. The obtained discrete kinematic problem for limit state analysis of reinforced concrete slabs governed by Nielsen's yield criterion is handled using available highly efficient solvers. Several reinforced concrete slabs of arbitrary geometries and different boundary conditions are examined, demonstrating that the proposed numerical procedure can provide accurate collapse load multipliers, and showing that yield-patterns in terms of plastic dissipation distribution can be automatically identified.

4.2 Kinematic formulation using the iRBF method for reinforced concrete slab

Consider a thin reinforced concrete slab of area Ω, with kinematic boundary Γ_u. In the kinematic formulation, the approximation of the velocity field can be

expressed in terms of nodal velocities within the computational domain as follows

$$u^h(\mathbf{x}) = \sum_{I=1}^{N} \Phi_I(\mathbf{x}) u_I \tag{4.1}$$

The related rotations and curvatures are directly computed by differentiating the approximated velocity function as

$$\theta_\alpha^h := u_\alpha^h(\mathbf{x}) = \sum_{I=1}^{N} \Phi_{I,\alpha}(\mathbf{x}) u_I \tag{4.2a}$$

$$\kappa_{\alpha\beta}^h := u_{\alpha\beta}^h(\mathbf{x}) = \sum_{I=1}^{N} \Phi_{I,\alpha\beta}(\mathbf{x}) u_I \tag{4.2b}$$

where $\Phi_I(\mathbf{x})$, $\Phi_{I,\alpha}(\mathbf{x})$ and $\Phi_{I,\alpha\beta}(\mathbf{x})$ are iRBF shape function and its derivatives described above.

For bending plate, the plastic dissipation function can be computed as

$$D_p(\boldsymbol{\kappa}) = \int_\Omega \mathbf{m}^T \boldsymbol{\kappa} d\Omega \tag{4.3}$$

where $\mathbf{m} = [m_{xx}\ m_{yy}\ m_{xy}]$ presents moments on the yield surface associated with the plastic curvature rates $\boldsymbol{\kappa}$, which relates to the transverse velocity via the standard relations $\boldsymbol{\kappa}^T = [\kappa_{xx}\ \kappa_{yy}\ 2\kappa_{xy}] = \nabla^2 \mathbf{u}$, in which the differential operator ∇^2 is defined as

$$\nabla^2 = \begin{bmatrix} \dfrac{\partial^2}{\partial x^2} & \dfrac{\partial^2}{\partial y^2} & 2\dfrac{\partial^2}{\partial x \partial x} \end{bmatrix} \tag{4.4}$$

By means of numerical nodal integration, the plastic dissipation function can be expressed as

$$D_p(\boldsymbol{\kappa}) = \sum_{j=1}^{N} a_j (m_{px}^+ \kappa_x^+ + m_{py}^+ \kappa_y^+ + m_{px}^- \kappa_x^- + m_{py}^- \kappa_y^-)_j \tag{4.5}$$

where a_j is the area of nodal representative domain j, i.e., a Voronoi cell; $\left(\kappa^+,\ \kappa^-\right)$ are the related curvatures; $\left(m_p^+, m_p^-\right)$ present the positive and negative yield moments per unit length in $x-$ and $y-$directions, which can be calculated as follows

$$m_p = A_s f_Y d \left(1 - \frac{\phi}{2}\right) \tag{4.6}$$

where A_s and f_Y denote the area and yield strength of reinforcement; dimension of d is illustrated in Figure 4.1; and the reinforcement degree ϕ is given by

$$\phi = \frac{A_s f_Y}{d f_c} \tag{4.7}$$

where f_c is compressive strength of concrete.

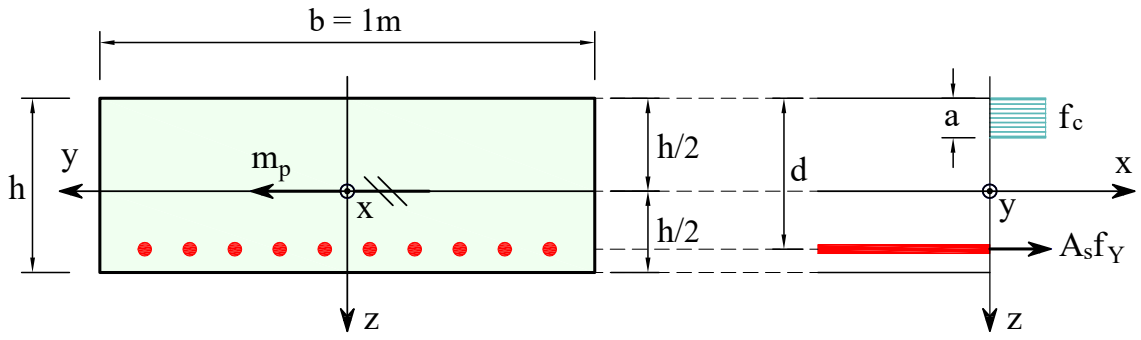

Figure 4.1: Slab element subjected to pure bending in the reinforcement direction

For reinforced concrete slabs, the commonly used yield criterion is the Nielsen's one, which can be expressed by two rotated quadratic cones

$$\mathbf{b}_i + \mathbf{Q}_i \mathbf{m} \in \mathscr{K}_r^3, \quad i = 1, 2 \tag{4.8}$$

where

$$\mathbf{Q}_1 = \begin{bmatrix} -1 & 0 & 0 \\ 0 & -1 & 0 \\ 0 & 0 & \sqrt{2} \end{bmatrix}; \qquad \mathbf{Q}_2 = \begin{bmatrix} 1 & 0 & 0 \\ 0 & 1 & 0 \\ 0 & 0 & \sqrt{2} \end{bmatrix} \tag{4.9}$$

and

$$\mathbf{b}_1^T = \left[m_{px}^+, m_{py}^+, 0 \right]; \qquad \mathbf{b}_2^T = \left[m_{px}^-, m_{py}^-, 0 \right] \tag{4.10}$$

Finally, the upper bound limit analysis of the reinforced concrete slabs can be formulated in the form of a conic optimization problem as follows conic optimization problem as follows

$$\lambda^+ = \min \sum_{j=1}^{N} a_j (m_{px}^+ \kappa_x^+ + m_{py}^+ \kappa_y^+ + m_{px}^- \kappa_x^- + m_{py}^- \kappa_y^-)_j \tag{4.11}$$

$$\text{s.t} \begin{cases} (\kappa_x^+, \kappa_y^+, \kappa_{xy}^+)_j \in \mathscr{K}_r^{+(3)}, & \forall j \in \{1, 2, \ldots, N\} \\ (\kappa_x^-, \kappa_y^-, \kappa_{xy}^-)_j \in \mathscr{K}_r^{-(3)}, & \forall j \in \{1, 2, \ldots, N\} \\ \sum_{i=1}^{N} \Phi_{I,xx}(\mathbf{x})(\mathbf{x}_j) u_I = (\kappa_x^- - \kappa_x^+)_j, & \forall j \in \{1, 2, \ldots, N\} \\ \sum_{i=1}^{N} \Phi_{I,yy}(\mathbf{x})(\mathbf{x}_j) u_I = (\kappa_y^- - \kappa_y^+)_j, & \forall j \in \{1, 2, \ldots, N\} \\ \sum_{i=1}^{N} \Phi_{I,xy}(\mathbf{x})(\mathbf{x}_j) u_I = \sqrt{2}(\kappa_{xy}^+ + \kappa_{xy}^-)_j, & \forall j \in \{1, 2, \ldots, N\} \\ \mathbf{A}\mathbf{u} = \mathbf{b} \end{cases} \tag{4.12}$$

where $\mathbf{A}$ and $\mathbf{b}$ are obtained by imposing the unitary external work and the kinematic boundary conditions, respectively and given by

$$\mathbf{A}_{eq} = \begin{bmatrix} \sum_{j=1}^{N} a_j \phi_1(\mathbf{x}_j) & \sum_{j=1}^{N} a_j \phi_2(\mathbf{x}_j) & \ldots & \sum_{j=1}^{N} a_j \phi_N(\mathbf{x}_j) \\ \phi_1(\mathbf{x}_1^b) & \phi_2(\mathbf{x}_1^b) & \ldots & \phi_N(\mathbf{x}_1^b) \\ \ldots & \ldots & \ddots & \ldots \\ \phi_1(\mathbf{x}_d^b) & \phi_2(\mathbf{x}_d^b) & \ldots & \phi_N(\mathbf{x}_d^b) \\ \phi_{1,x}(\mathbf{x}_1^b) & \phi_{2,x}(\mathbf{x}_1^b) & \ldots & \phi_{N,x}(\mathbf{x}_1^b) \\ \ldots & \ldots & \ddots & \ldots \\ \phi_{1,x}(\mathbf{x}_{rx}^b) & \phi_{2,x}(\mathbf{x}_{rx}^b) & \ldots & \phi_{N,x}(\mathbf{x}_{rx}^b) \\ \phi_{1,y}(\mathbf{x}_1^b) & \phi_{2,y}(\mathbf{x}_1^b) & \ldots & \phi_{N,y}(\mathbf{x}_1^b) \\ \ldots & \ldots & \ddots & \ldots \\ \phi_{1,y}(\mathbf{x}_{ry}^b) & \phi_{2,y}(\mathbf{x}_{ry}^b) & \ldots & \phi_{N,y}(\mathbf{x}_{ry}^b) \end{bmatrix} \tag{4.13}$$

and

$$\mathbf{b}_{eq} = \begin{bmatrix} 1 & \overbrace{0 \ \ldots \ 0}^{d} & \overbrace{0 \ \ldots \ 0}^{r_x} & \overbrace{0 \ \ldots \ 0}^{r_y} \end{bmatrix} \tag{4.14}$$

where $(d,\ r_x,\ r_y)$ are number of boundary nodes having velocity, x and y-rotation conditions, respectively.

As above-presented, the rotations and curvatures are directly determined from the approximated transverse velocity. As a result, there is only one variable at each

node, and hence the size of the resultant optimization problem, (4.12) , is kept to be minimum. Moreover, all equations in problem (4.12) are straightforwardly satisfied at discretized nodes within the computational domain. Problem (4.12) consists of N variables for nodal velocity and $3 \times N$ variables for each rotated cone. Therefore, the total variables in problem (4.12) is $N_{var} = N + 2 \times 3 \times N = 7 \times N$.

The numerical implementation of the upper bound limit approach is a part of flow chart shown in Figure 1.1.

4.3 Numerical examples

This section investigates a number of benchmark problems, for which analytical and/or numerical solutions are available for comparison. For all examples, input data are: thickness $t = 1$; unit plastic moment of resistance $m_p = 1$; and slabs are subjected to the unit uniform pressure load $q = 1$. The solutions are obtained using Mosek optimization solver version 6.0 on a 2.8 GHz Intel Core i5 PC running Window 7.

4.3.1 Rectangular slabs

Rectangular slabs with either simply supported (SSSS) or clamped (CCCC), $(\cdot)$ corresponds to left, bottom, right and top edges respectively, boundary conditions on all edges are considered first. It is assumed that the slabs are isotropic with positive and negative yield moments($m_p^+ = m_p^- = m_p$) in both directions. Due to the symmetry, only the upper-right quarter of plate is modeled, as shown in Figure 4.2.

The influence of the shape parameter α_s on the limit load factor of a simply supported square slab is studied first. The relationship between the computed limit load factors and the parameter α_s, is illustrated in Figure 4.3. It can be seen that for all nodal distribution solutions obtained when setting $\alpha = 2$ are lower (better) than those of smaller α_s, $\alpha_s = 0.00001$ or $\alpha_s = 1$. Note that when α_s is taken to be larger than 2, a lower (i.e., improved) computed limit load factor may sometimes be obtained, however the computational cost increases. Therefore, in order to compromise between accuracy and computational cost α_s is taken as 2 for all problems considered henceforth.

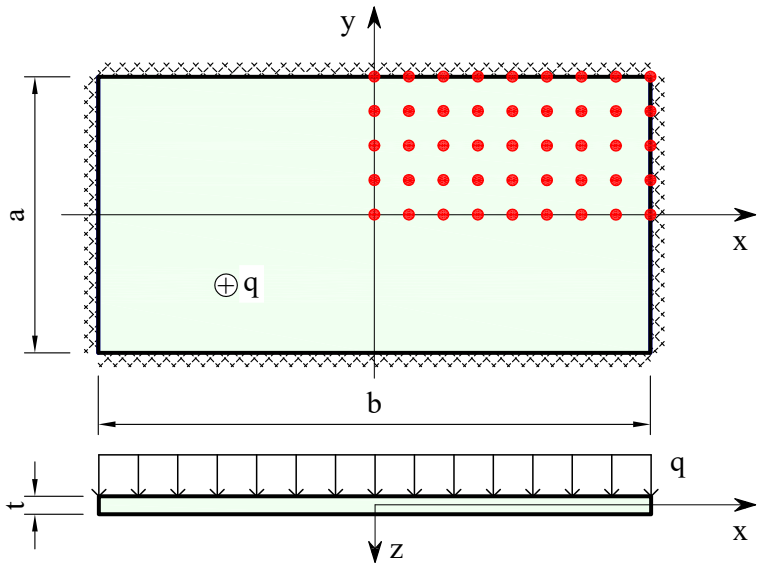

Figure 4.2: Rectangular slab: geometry, loading, boundary conditions and nodal discretization

Various ratios of b/a are investigated, and Table 4.1 summarizes computed numerical solutions using a regular nodal distribution of 35×35 nodes, corresponding to 8575 variables in the resultant optimization problem. Analytical solutions for a fully simply supported boundary condition slab are given as

$$\lambda = \begin{cases} \dfrac{24}{\left[\sqrt{3+\left(\dfrac{a}{b}\right)^2}-\dfrac{a}{b}\right]^2} \times \dfrac{m_p}{qab}, & \text{Ingerslev [218];} \\ 8\left[1+\dfrac{a}{b}+\dfrac{b}{a}\right] \times \dfrac{m_p}{qab}, & \text{Johansen [219].} \end{cases} \tag{4.15}$$

Table 4.1: Rectangular slabs with various ratios b/a: limit load factors

$\frac{b}{a}$	Present method		Reference [209]		SSSS-Reference [218]	
	SSSS	CCCC	SSSS	CCCC	Johansen	Ingerslev
1.0	24.00	44.83	24.18	43.61	24.00	24.00
1.5	25.62	50.00	25.92	47.20	25.33	25.45
2.0	28.48	56.13	28.45	52.50	28.00	28.28
2.5	31.86	63.46	32.00	59.62	31.20	31.61
3.0	35.53	71.30	35.82	66.50	34.67	35.18
3.5	39.48	81.76	39.07	72.48	38.29	38.89

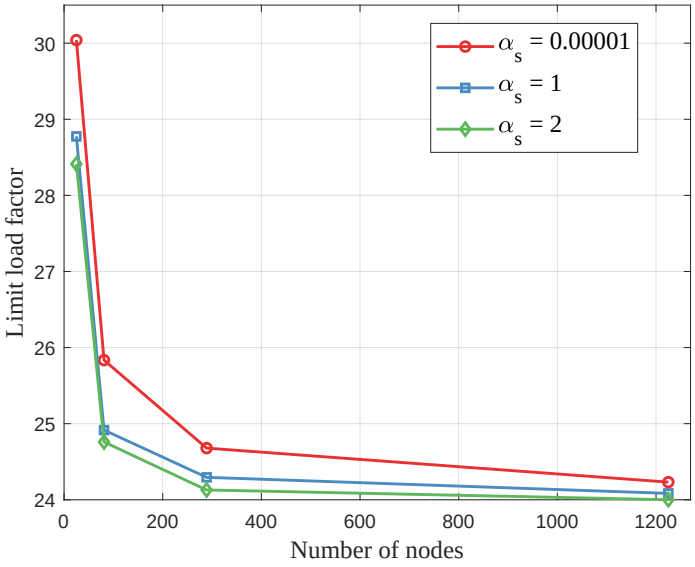

Figure 4.3: Simply supported square slab: normalized limit load factor λ^+ versus the parameter α_s

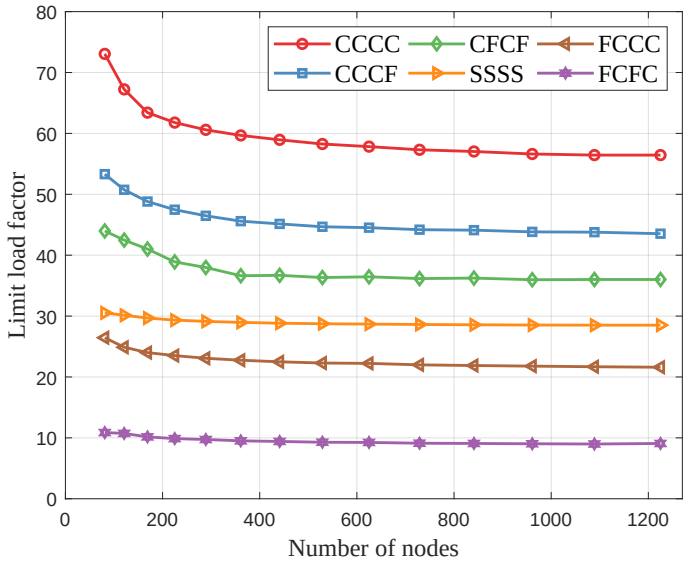

Figure 4.4: Limit load factors λ^+ (m_p/qab) of rectangular slabs $(b/a = 2)$ with different boundary conditions: CCCC (56.13), CCCF (48.53), CFCF (36.01), SSSS (28.48), FCCC (21.61), FCFC (9.08)

Rectangular slabs with other boundary conditions including free (F), simply supported (S) and clamped (C) edges are also considered. Limit load factors and convergence analysis for the case when $b/a = 2$ are illustrated in Figure 4.4.

To illustrate the performance of the iRBF based limit state analysis procedure,

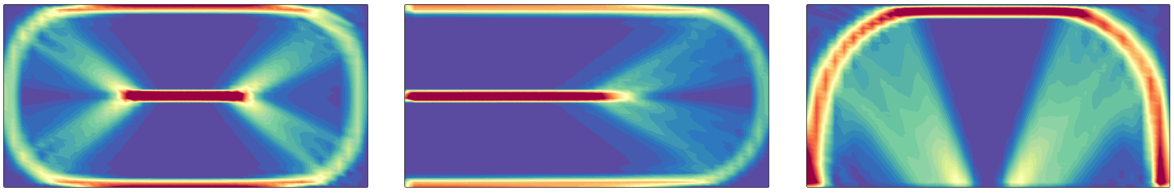

(a) CCCC (b) CCCF (c) FCCC

(d) SSSS (e) CFCF (f) FCFC

Figure 4.5: Rectangular slabs ($b = 2a$) with various boundary conditions: plastic dissipation distribution

the present solutions and associated computational aspects, including relative errors and number of variables, for simply supported and clamped square plates ($a = b = L$) are compared with those obtained using the CS-HCT [208] and EFG methods [209], see Table 4.2. It can be observed that the proposed method can provide more accurate solutions with less computational effort (in terms of number of variables) than other selected approaches, particularly for simply supported slab. For simply supported slab, a solution of $24.00 m_p/qL^2$ is obtained by using the iRBF method with 8575 variables, which is better than results of $24.07 m_p/qL^2$ obtained by CS-HCT method [208] using 136188 variables, and of $24.18 m_p/qL^2$ presented in [209] using 8575 variables in the EFG formulation.

Table 4.2: Results of simply supported and clamped square slabs

Author	Present method		EFG [209]		CS-HCT [208]	
	SSSS	CCCC	SSSS	CCCC	SSSS	CCCC
λ^+	24.00	44.83	24.18	43.61	24.07	44.81
e (%)	0.00	4.62	0.75	1.80	0.29	4.57
t (s)	14	14	-	30	-	826
N_{var}	8575	8575	8575	8575	136188	136188

e: relative errors; t: CPU-Time; N_{var}: number of variables

In Table 4.3, the iRBF solutions are also compared with previously published upper and lower bounds using displacement discontinuous finite elements [64], equilibrium mesh-free method [93] and equilibrium finite elements [58, 207] . It is evident

Table 4.3: Square slabs: limit load multipliers in comparison with other methods

Author	Simple supported		Clamped	
	λ^+	λ^-	λ^+	λ^-
Present method	24.00	-	44.83	-
Le et al. [208], *CS-HCT*	24.07	-	44.81	-
Le et al. [209], *EFG*	24.14	-	43.61	-
Bleyer et al. [64], *FEM-T6b*	24.00	-	44.03	-
Bleyer et al. [64], *FEM-H3*	24.43	-	43.45	-
Le et al. [93], *FEM*	-	23.96	-	42.83
Krabbenhoft [58], *FEM*	-	-	-	42.82
Maunder et al. [207], *FEM*	-	-	-	42.00

that these solutions are, in general, in good agreement. Note that in approaches proposed by others, there is at least 3 variables per node, and hence the size of corresponding formulation may be larger than that of the present method. The yield patterns in terms of plastic dissipation distribution for rectangular slabs with different boundary conditions are also plotted in Figure 4.5.

4.3.2 Regular polygonal slabs

Next, regular polygonal slabs with n-sides ($n = 3, 4, 5, 6, +\infty$) are examined. Nodal distribution and computational domains of all slabs are shown in Figure 4.6. For square and circular slabs, only the upper-right quarters are modeled, while for triangular, pentagonal and hexagonal slabs the whole domains are discretized. All slabs are assumed to be isotropic with equal magnitudes of hogging and sagging yield moments $m_p^+ = m_p^- = m_p$ in both directions. Let R denotes the radius of incircle of regular polygons. Both simply supported and clamped boundary conditions are investigated.

Computed limit load multipliers and associated dissipation distribution for polygonal slabs are reported in Figure 4.7. Table 4.4 compares the present results for clamped slabs with analytical solutions and recent selected upper bounds obtained us- ing CS-HCT and EFG based numerical procedures. For all cases, the EFG based approach can provide lower (better) upper bound solutions than the present iRBF method. This may be explained by the fact that the plastic dissipation along clamped boundaries can be accurately produced by the high-order shape functions obtained by the moving least squares approximation technique, that uses

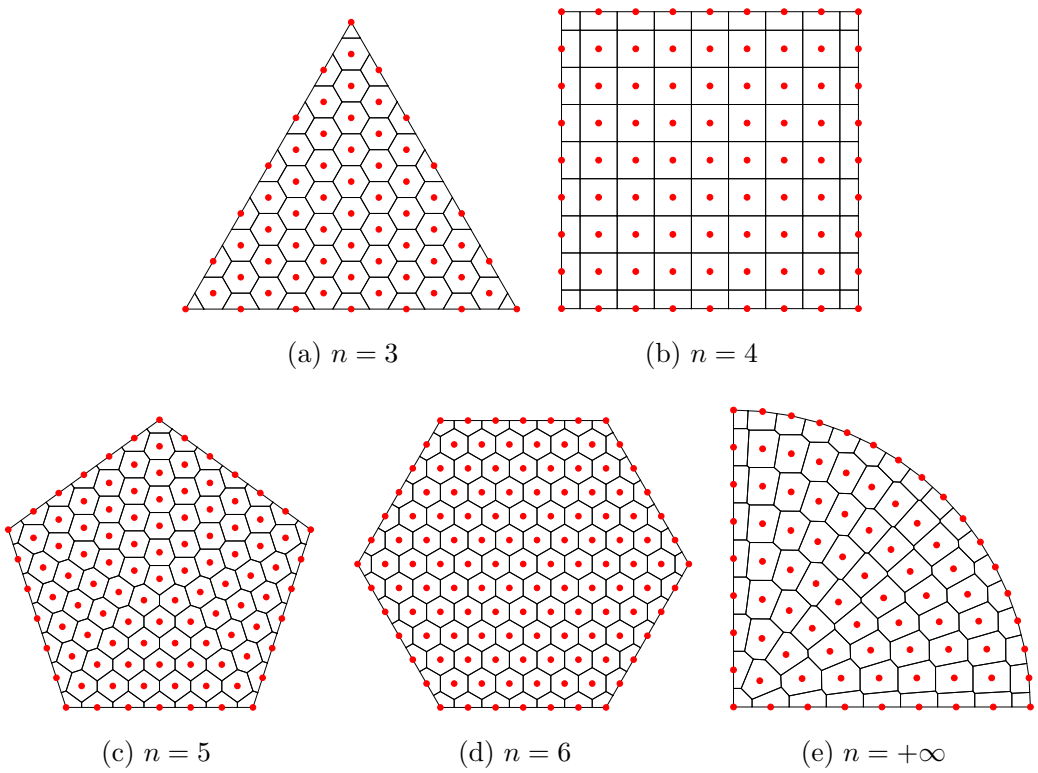

(a) $n = 3$ (b) $n = 4$

(c) $n = 5$ (d) $n = 6$ (e) $n = +\infty$

Figure 4.6: Nodal distribution and computational domains of polygonal slabs: (a) triangle; (b) square; (c) pentagon; (d) hexagon; (e) circle

an isotropic quartic spline weight function. However, the advantages of the iRBF method over the EFG approach are that the iRBF shape functions hold the Kronecker delta property, and hence there is no need of any special treatment when enforcing boundary conditions as encountered in the EFG method; and that the computation of iRBF shape functions is less expensive in terms of CPU time than that of EFG's ones, i.e., for a mesh of 15×15 nodes, the iRBF method takes approximately $0.5s$, compared with about $5.8s$ when using the EFG method.

Table 4.4: Clamped regular polygonal slabs: limit load factors in comparison with other solutions (m_p/qR^2)

Author	Geometry of slabs				
	Triangle	Square	Pentagon	Hexagon	Circle
Present method	10.42	11.21	12.13	12.86	12.40
Le et al. [208], *CS-HCT*	10.67	11.15	12.21	-	13.09
Le et al. [209], *EFG*	9.98	10.90	11.54	-	12.31
Fox [220], *analytical method*	9.61	10.71	11.19	11.44	-
Johansen [219], *analytical method*	-	-	-	-	12.00

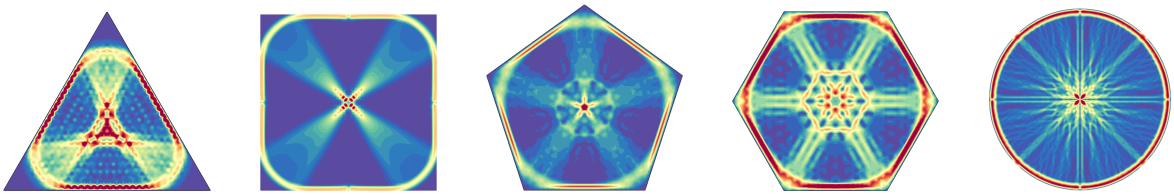

(a) $\lambda^+ = 10.42$ (b) $\lambda^+ = 11.21$ (c) $\lambda^+ = 12.13$ (d) $\lambda^+ = 12.86$ (e) $\lambda^+ = 12.40$

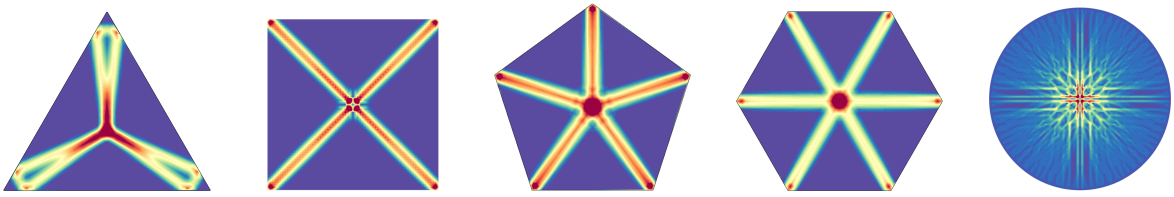

(f) $\lambda^+ = 5.63$ (g) $\lambda^+ = 6.00$ (h) $\lambda^+ = 6.21$ (i) $\lambda^+ = 6.36$ (j) $\lambda^+ = 5.97$

Figure 4.7: Plastic dissipation distribution and collapse load multipliers (m_p/qR^2) of polygonal slabs: (a, b, c, d, e)-clamped; (f, g, h, i, j)-simply supported

4.3.3 Arbitrary geometric slab with a rectangular hole

The last example comprises an arbitrary geometric slab with an eccentric rectangular cutout, as shown in Figure 4.8, which has been examined previously using equilibrium finite elements [200], curvature smoothing HCT elements [208] and the displacement mesh-free method [209]. The problem is solved using a nodal distribution of 1151 nodes, corresponding to 8051 variables in the resultant optimization problem.

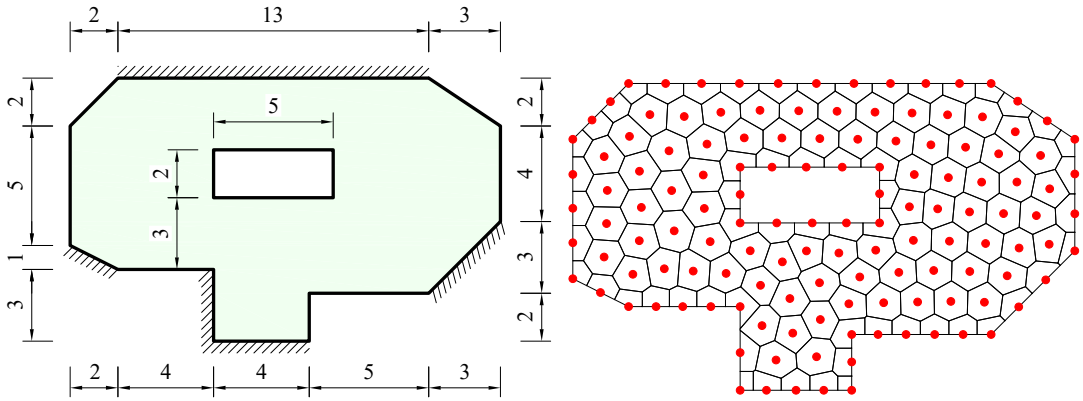

(a) Geometry, dimension and boundary condition (b) Nodal discretization

Figure 4.8: Arbitrary shape slabs: geometry (all dimensions are in meter) and discretization

For isotropic slab with equal positive and negative yield moments ($m_p^+ = m_p^- = m_p$), the collapse load factor obtained is $0.1421 \times m_p$, which is in good agreement with results of $0.148 \times m_p$ in [200], of $0.1420 \times m_p$ in [208] and of $0.1424 \times m_p$ in [209]. Table 4.5 summarizes limit load multipliers of slabs with various ratios of m_p^+/m_p^-, illustrating the influence of negative yield moment on the bearing capacity of slabs. The present results are competitive with those reported in [208, 209]. Moreover, it is interesting to point out that, here, for all cases involving simply supported boundary conditions the present iRBF method can result in lower (better) solutions than the EFG approach. Orthotropic slab with the ratio of yield moments in $x-$ and $y-$directions $m_{px}/m_{py} = 0.5$ is also considered. The computed result of $0.086 \times m_p$ is in excellent agreement with a solution of $0.086 \times m_p$ reported in [208, 209]. In general, the present method is more efficient than those of [208, 209].

Plastic dissipation distribution and collapse mechanism for the case of isotropic reinforcement are also shown in Figure 4.9. It can be observed that the failure mechanism obtained by present method is in good agreement compared with one in [205] using DLO approach.

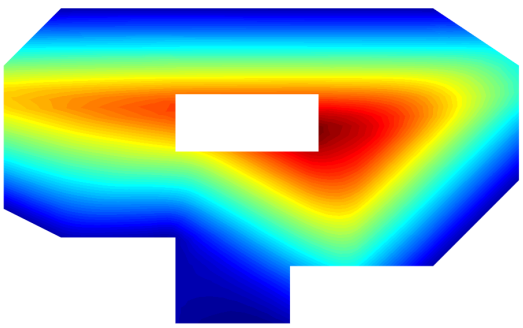

(a) Displacement contour

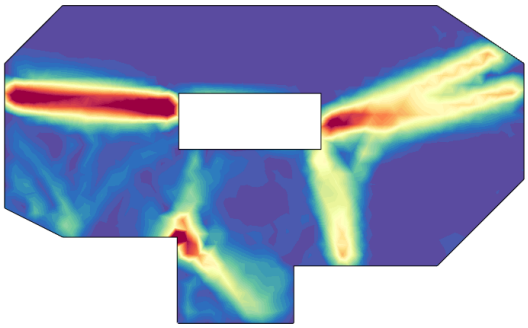

(b) Dissipation distribution

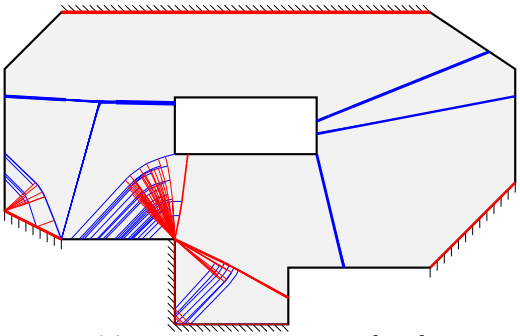

(c) Failure mechanism [205]

Figure 4.9: Arbitrary geometric slab with an eccentric rectangular cutout ($m_p^+ = m_p^- = m_p$): displacement contour and dissipation distribution at collapse state

Table 4.5: Collapse load of an arbitrary shape slab ($\times m_p^-$)

$\frac{m_p^+}{m_p^-}$	1	$\frac{1}{2}$	$\frac{1}{4}$	$\frac{1}{8}$
Present method ($N_{var} = 8057$)	0.1421	0.1295	0.1217	0.1167
Le et al. [208], *CS-HCT* ($N_{var} = 38139$)	0.1420	0.1298	0.1233	0.1217
Le et al. [209], *EFG* ($N_{var} = 8057$)	0.1424	0.1299	0.1226	0.1181

4.4 Conclusions

A novel rotation-free mesh-free method based on integrated radial basis functions has been developed for limit state analysis of reinforced concrete slabs. The transverse velocity is approximated without using rotational degrees of freedom, and therefore the total number of variables in the resultant optimization problem is kept to a minimum, i.e., equal to the number of discretized nodes in the problem domain. The proposed formulation is tested by applying it to various Nielsen's reinforced concrete slabs of arbitrary geometries. It has been demonstrated that the present method, consisting of high-order shape functions obtained by integrating radial basis functions, can provide accurate collapse load multipliers. Moreover, the high-order and smooth iRBF approximation is capable of capturing yield patterns of arbitrary geometric slabs. The present optimization strategy based on conic programming enables solutions of practical sized reinforced concrete slabs to be obtained rapidly. It should be noted that in the mesh-free based numerical procedures for limit state analysis of structures nodes may be moved, discarded or introduced conveniently. Hence the implementation of an h-adaptive scheme is facilitated, and will be the subject of future research.

Chapter 5

A stabilized iRBF mesh-free method for quasi-lower bound shakedown analysis of structures [1]

5.1 Introduction

In chapters 3 and 4, the iRBF-based mesh-free method is extent to the limit analysis of structures, where it is assumed that loading increases gradually until the collapse appears. In fact, engineering structures are usually subjected to repeat, cyclic or time-dependent loads. Under a repeated cycle of loading, the structures may be fail due to some collapse modes, e.g. rotating plasticity, a general mode of alternating plasticity (lower cycle fatigue) [32], incremental plasticity (ratcheting) or instantaneous plasticity. Direct analysis, a perfect alternative scheme for step-by-step method, has been successfully applied for this field. Limit analysis for the case of proportional loading and shakedown analysis in case of variable repeated loading, have been found to be more efficient [19, 73, 77, 221–223]. In direct shakedown analysis, the load limits can be determined without a need of loading history, and hence the method can be applied to a wide range of problems in engineering practices.

The implementation of computational shakedown analysis generally involves two main steps: (*i*) approximate the problem fields using a discretization method, and (*ii*) solve the resulting optimization to obtain the solution. In the literature, various numerical approaches have been developed for both kinematic and static shakedown analysis, for instance, mesh-based methods [67, 80, 82, 224–226], boundary element method [86, 87] and mesh-free approaches [90, 91]. When the variable fields

[1] based on P. L. H. Ho and C. V Le, "A stabilized iRBF mesh-free method for quasi-lower bound shakedown analysis of structures," *Comput. Struct.*, vol. 228, p. 106157, 2020.

are approximated and bound theorems is applied, shakedown analysis becomes an optimization problem which can be solved using iterative algorithm [86, 90] or primal-dual interior-point method [73, 80]. However, in treating large-scale optimization problem, the second-order cone programming has been proved to be more powerful [32, 77].

The objective of this study is to extend the iRBF mesh-free method to quasi-static shakedown analysis of 2D and 3D structures. In the quasi-static formulation, the stress field is decomposed into two parts involving a fictitious elastic stress and a self-equilibrated residual stress. The fictitious elastic stresses are calculated using the usual Galerkin procedure. The virtual strains are approximated by the (stabilized) iRBF shape functions, and equilibrium equations for the self-equilibrated residual stress field are enforced in a weak form. It is worth noting that the present formulation is different from the one presented in chapter 3, where total stress fields are approximated and a strong form of equilibrium equations are used. The yield conditions for two and three dimensional problems are formulated as conic constraints. All constrains of the resulting optimization problem are imposed at a finite number of discretized nodes, instead of Gaussian points, and hence the size of the obtained optimization problem is kept to a minimum. The combination of iRBF mesh-free method and conic programming enables the shakedown solutions to be obtained rapidly, and consequently the load domains consisting of a large number of points can be approximated efficiently. The performance of proposed procedure will be illustrated by investigating various benchmark problems in plane stress, plane strain and three-dimensions conditions.

5.2 iRBF discretization for static shakedown formulation

Consider an elastic-perfectly plastic structure of volume V subjected to variable repeated loads. Let $\boldsymbol{\sigma}^E$ denote the fictitious elastic stress belonging to a bounded time-independent global loading domain $\mathscr{P} = \{\boldsymbol{\sigma}^E \mid \boldsymbol{\sigma}^E(\mathbf{x}, t) \in \mathscr{P}_x,\ \mathbf{x} \in V,\ t \in [0, T]\}$, where $\mathscr{P}_x$ is the local loading domain at a point $\mathbf{x} \in V$. The static/lower bound shakedown theorem states that if there exits a residual stress $\boldsymbol{\rho}$, which is time-independent and self-equilibrium, so that the total stress, $\boldsymbol{\sigma} = \boldsymbol{\sigma}^E + \boldsymbol{\rho}$, does not violate the yield condition at any point in the structure for all possible load combination. Let λ be the shakedown safety factor, the lower bound on the actual shakedown safety factor of a structure, λ_s, can be determined by solving the

following optimization problem

$$\lambda_s = \max_{\boldsymbol{\rho}\in\mathscr{R}} \{\lambda \mid \psi(\lambda\boldsymbol{\sigma}^E + \boldsymbol{\rho},\, \sigma_p) \leq 0\ ,\ \forall \boldsymbol{\sigma}^E \in \mathscr{P}\} \tag{5.1}$$

where $\mathscr{R}$ is the set of admissible bounded residual stress field, σ_p is the yield stress, and ψ is the yield function of ductile materials.

In terms of numerical implementation, the fictitious residual stress field can be approximated via a reflection of nodal values in the problem domain using the iRBF method as follows

$$\boldsymbol{\rho}^h(\mathbf{x}) = \sum_{i=1}^{N} \Phi_i(\mathbf{x})\rho_i \tag{5.2}$$

where $\Phi_i(\mathbf{x})$ is the iRBF shape function; the residual stresses at nodes are denoted by a vector consisting $(\rho_{xx},\ \rho_{yy},\ \rho_{xy})$ for 2D and $(\rho_{xx},\ \rho_{yy},\ \rho_{zz},\ \rho_{xy},\ \rho_{xz},\ \rho_{yz})$ for 3D discretizations.

In the equilibrium shakedown analysis formulation, the residual stress fields is required to be equilibrated at every point in the problem domain. This results in difficulties in a numerical solution strategy due to the fact that equilibrium equations are often accessed at integration points. A way out of such the difficulties is to transform the strong form of the equilibrium equations into its weak form by using the principle of virtual work as follows

$$\int_{\mathscr{V}} \delta\boldsymbol{\epsilon}^T(\mathbf{x})\boldsymbol{\rho}(\mathbf{x})\mathrm{d}\mathscr{V} = 0 \tag{5.3}$$

where $\delta\boldsymbol{\epsilon}(\mathbf{x})$ denotes any virtual strain which satisfies the kinematic boundary conditions. The virtual strain field $\delta\boldsymbol{\epsilon}(\mathbf{x})$ can be approximated using the iRBF method as

$$\delta\boldsymbol{\epsilon}(\mathbf{x}) = \mathbf{B}(\mathbf{x})\delta\mathbf{d} \tag{5.4}$$

where $\delta\mathbf{d}$ denotes the nodal displacement vector and $\mathbf{B}(\mathbf{x})$ is the strain-displacement matrices defined for 2D problems as

$$\mathbf{B}(\mathbf{x}) = \begin{bmatrix} \phi_{1,x} & 0 & \phi_{2,x} & 0 & \cdots & \phi_{N,x} & 0 \\ 0 & \phi_{1,y} & 0 & \phi_{2,y} & \cdots & 0 & \phi_{N,y} \\ \phi_{1,y} & \phi_{1,x} & \phi_{2,y} & \phi_{2,x} & \cdots & \phi_{N,y} & \phi_{N,x} \end{bmatrix} \tag{5.5}$$

and for 3D problems as

$$\mathbf{B}(\mathbf{x}) = \begin{bmatrix} \phi_{1,x} & 0 & 0 & \phi_{2,x} & 0 & 0 & \cdots & \phi_{N,x} & 0 & 0 \\ 0 & \phi_{1,y} & 0 & 0 & \phi_{2,y} & 0 & \cdots & 0 & \phi_{N,y} & 0 \\ 0 & 0 & \phi_{1,z} & 0 & 0 & \phi_{2,z} & \cdots & 0 & 0 & \phi_{N,z} \\ \phi_{1,y} & \phi_{1,x} & 0 & \phi_{2,y} & \phi_{2,x} & 0 & \cdots & \phi_{N,y} & \phi_{N,x} & 0 \\ 0 & \phi_{1,z} & \phi_{1,y} & 0 & \phi_{2,z} & \phi_{2,y} & \cdots & 0 & \phi_{N,z} & \phi_{N,y} \\ \phi_{1,z} & 0 & \phi_{1,x} & \phi_{2,z} & 0 & \phi_{2,x} & \cdots & \phi_{N,z} & 0 & \phi_{N,x} \end{bmatrix} \tag{5.6}$$

With the use of the iRBF approximated virtual strain field, the weak form (5.3) can be rewritten as

$$\int_{\mathscr{V}} [\mathbf{B}(\mathbf{x})\delta\mathbf{d}]^T \boldsymbol{\rho}(\mathbf{x}) \mathrm{d}\mathscr{V} = \delta\mathbf{d}^T \int_{\mathscr{V}} \mathbf{B}^T(\mathbf{x}) \boldsymbol{\rho}(\mathbf{x}) \mathrm{d}\mathscr{V} = 0 \tag{5.7}$$

Equation (5.7) must hold for all $\delta\mathbf{d}$, hence ones can obtain

$$\int_{\mathscr{V}} \mathbf{B}^T(\mathbf{x}) \boldsymbol{\rho}(\mathbf{x}) \mathrm{d}\mathscr{V} = \sum_{k=1}^{N} \mathscr{V}_k \mathbf{B}_k^T \boldsymbol{\rho}_k = \mathbf{C}_{eq} \boldsymbol{\rho} = 0 \tag{5.8}$$

where $\mathscr{V}_k$ is the volume of a representative Voronoi domain of node k, $\mathbf{C}_{eq}$ is a constant equilibrium matrix, in which the essential boundary conditions are taken into account by eliminating the corresponding degrees of freedom of nodes on the kinematic boundaries. Therefore, the number of rows of $\mathbf{C}_{eq}$ is reduced to $(sdof - N_{BC})$, where $sdof$ denotes the number of total degrees of freedom of the system, and N_{BC} is the number of degrees of freedom of nodes on the kinematic boundaries.

In the next step, the mathematical algorithms will be extent to handle the optimization problem. Using the primal-dual interior-point algorithms, the von Mises criterion will be employed and formulated for 2D problems as follows

$$\boldsymbol{\psi}(\boldsymbol{\sigma}) = \sqrt{\sigma_{xx}^2 + \sigma_{yy}^2 - \sigma_{xx}\sigma_{yy} + 3\sigma_{xy}^2} - \sigma_y \qquad \text{for plane stress} \tag{5.9a}$$

$$\boldsymbol{\psi}(\boldsymbol{\sigma}) = \sqrt{\frac{1}{4}(\sigma_{xx} - \sigma_{yy})^2 + \sigma_{xy}^2} - \sigma_y \qquad \text{for plane strain} \tag{5.9b}$$

and for 3D problems as

$$\boldsymbol{\psi}(\boldsymbol{\sigma}) = (\sigma_{xx} - \sigma_{yy})^2 + (\sigma_{xx} - \sigma_{zz})^2 + (\sigma_{yy} - \sigma_{zz})^2 + 6(\sigma_{xy}^2 + \sigma_{xz}^2 + \sigma_{yz}^2) - 2\sigma_p^2 \tag{5.10}$$

Introducing auxiliary variables $\mathbf{r}$ defined by

$$r_1 = \sigma_p; \quad \mathbf{r}_{2\to 4} = \mathbf{J}_1\boldsymbol{\sigma} = \mathbf{J}_1(\lambda\boldsymbol{\sigma}^E + \boldsymbol{\rho}) \qquad \text{for plane stress} \tag{5.11a}$$

$$r_1 = \sigma_p; \quad r_{2\to 3} = \mathbf{J}_2\boldsymbol{\sigma} = \mathbf{J}_2(\lambda\boldsymbol{\sigma}^E + \boldsymbol{\rho}) \qquad \text{for plane strain} \tag{5.11b}$$

$$r_1 = \sqrt{2}\sigma_p; \quad \mathbf{r}_{2\to 7} = \mathbf{J}_3\boldsymbol{\sigma} = \mathbf{J}_3(\lambda\boldsymbol{\sigma}^E + \boldsymbol{\rho}) \qquad \text{for 3D} \tag{5.11c}$$

where

$$\mathbf{J}_1 = \frac{1}{2}\begin{bmatrix} 2 & -1 & 0 \\ 0 & \sqrt{3} & 0 \\ 0 & 0 & 2\sqrt{3} \end{bmatrix}; \quad \mathbf{J}_2 = \frac{1}{2}\begin{bmatrix} 1 & -1 & 0 \\ 0 & 0 & 1 \end{bmatrix} \tag{5.12}$$

and

$$\boldsymbol{J}_3 = \frac{1}{\sqrt{2}\sigma_0}\begin{bmatrix} \frac{1}{2} & -1 & \frac{1}{2} & 0 & 0 & 0 \\ -\frac{\sqrt{3}}{2} & 0 & \frac{\sqrt{3}}{2} & 0 & 0 & 0 \\ 0 & 0 & 0 & \sqrt{3} & 0 & 0 \\ 0 & 0 & 0 & 0 & \sqrt{3} & 0 \\ 0 & 0 & 0 & 0 & 0 & \sqrt{3} \\ \frac{\sqrt{2}}{2} & \frac{\sqrt{2}}{2} & \frac{\sqrt{2}}{2} & 0 & 0 & 0 \end{bmatrix} \tag{5.13}$$

The von Mises failure criterion $\psi(\lambda\boldsymbol{\sigma}^E + \boldsymbol{\rho})$ can be now rewritten in terms of standard conic constraints as

$$\mathscr{L} = \left\{\mathbf{r} \in \mathbb{R}^4 \;\middle|\; r_1 \geq \|\mathbf{r}_{2\to 4}\|_{L^2} = \sqrt{r_2^2 + r_3^2 + r_4^2}\right\} \quad \text{for plane stress} \tag{5.14a}$$

$$\mathscr{L} = \left\{\mathbf{r} \in \mathbb{R}^3 \;\middle|\; r_1 \geq \|\mathbf{r}_{2\to 3}\|_{L^2} = \sqrt{r_2^2 + r_3^2}\right\} \quad \text{for plane strain} \tag{5.14b}$$

$$\mathscr{L} = \left\{\mathbf{r} \in \mathbb{R}^6 \;\middle|\; r_1 \geq \|\mathbf{r}_{2\to 6}\|_{L^2} = \sqrt{r_2^2 + r_3^2 + r_4^2 + r_5^2 + r_6^2}\right\} \quad \text{for 3D} \tag{5.14c}$$

Finally, the equilibrium formulation of a direct analysis problem can be expressed as follows

$$\begin{aligned} \lambda_s \;&=\; \max\ \lambda \\ &\text{s.t} \begin{cases} \mathbf{C}_{eq}\boldsymbol{\rho} = 0 \\ \mathbf{r}_{kt} \in \mathscr{L}_{kt}, \quad k = 1, 2, \ldots, N;\ t = 1, 2, \ldots, M \end{cases} \end{aligned} \tag{5.15}$$

where $\mathbf{r}_{kt}$ is the additional vector defined at the discretized nodes k^{th} for the loading

vertex t^{th}, $M = 2^{n_L}$ is the number of vertices of the convex polyhedral load domain, in which n_L is the number of independent loading processes. It is important to note that the safety load multipliers λ_s obtained from problem (5.15) are quasi-lower-bound on the actual solutions. This is because the fact that equilibrium equations and yield condition in the present formulation are enforced and satisfied at a finite number of nodes in the computational domain.

The whole numerical implementation of quasi-lower bound limit and shakedown formulation for structural analysis is summarized in Figure 5.1.

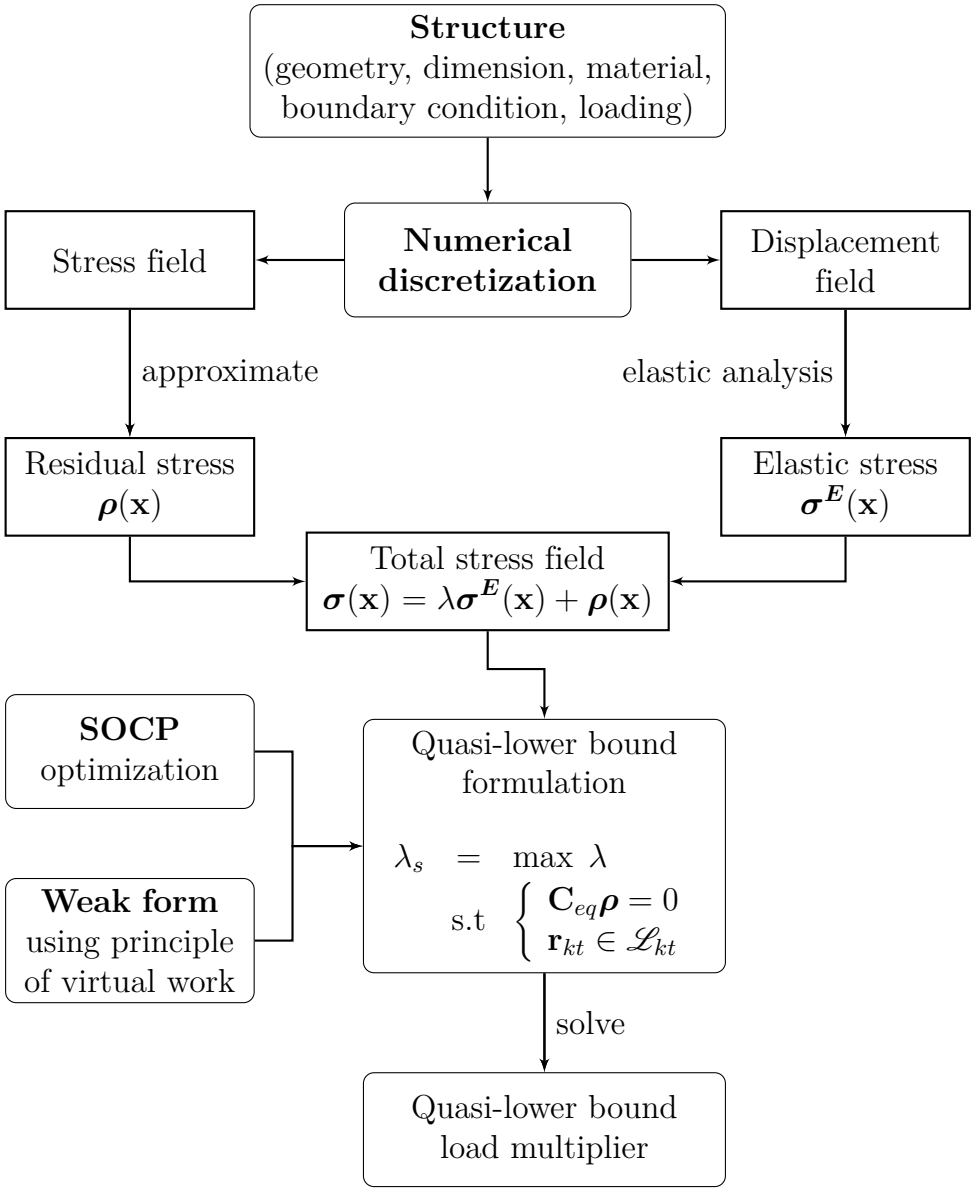

Figure 5.1: Quasi-static shakedown analysis.

5.3 Numerical examples

In this section, various examples in two-and three-dimensions are examined to illustrate the performance of proposed method. The resulting optimization problems are solved using the commercial software package Mosek on a 2.8 GHz Intel Core i7 PC running Window 10. The number of variables N_{var} in the resulting optimization problem is equal to $3\times N+1+4\times 2^{n_L}$ for plane stress, $3\times N+1+3\times 2^{n_L}$ for plane strain and $6\times N+1+6\times 2^{n_L}$ for 3D problems. For comparison purpose, numerical solutions based on the radial point interpolation method (RPIM) are also reported.

5.3.1 Punch problem under proportional load

In order to study computational aspects of the present iRBF-based quasi-static direct analysis procedure, the punch problem consisting of a semi-infinite rigid-plastic von Mises medium under a punch load of $2\tau_0$ ($n_L = 1$) is considered. Note that the problem has been investigated in [227] using both kinematic and static formulation based on the iRBF mesh-free method. The problem is solved using various nodal distribution in the computational domain of $B = 5$, $H = 2$ and $a = 1$ as shown in Figure 5.3.

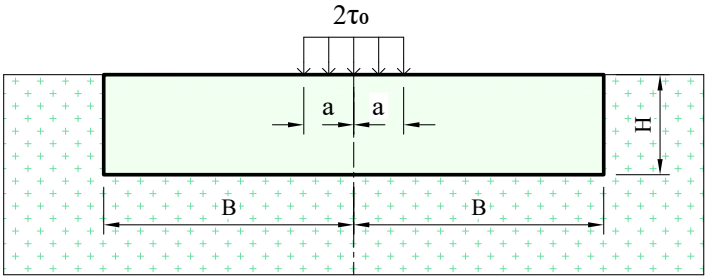

Figure 5.2: Prandtl's punch problem

Figure 5.4 compares the present computed solutions with results using the iRBF static method presented in [227]. It can be observed that present solutions converge from above while results in [227] approach to the exact collapse load factor from below. Both methods are based on equilibrium formulation, but convergence behaviour is different. This may be explained by the fact that in the present formulation the virtual displacement fields are approximated and equilibrium equations are satisfied in a weak form, whereas in [227] stress fields are approximated and the strong form of equilibrium conditions are enforced using collocation technique.

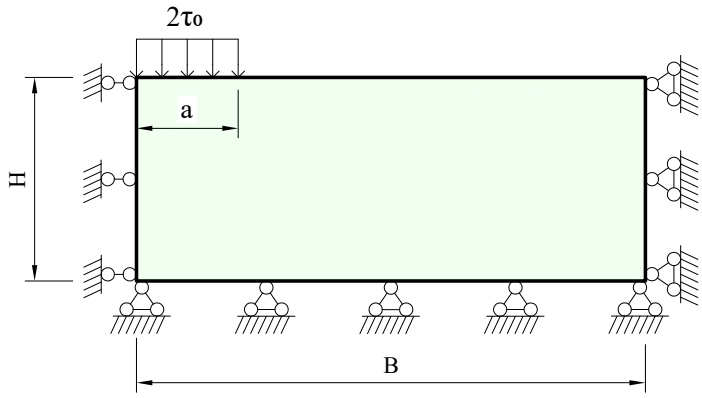

Figure 5.3: Prandtl's punch problem: computational model

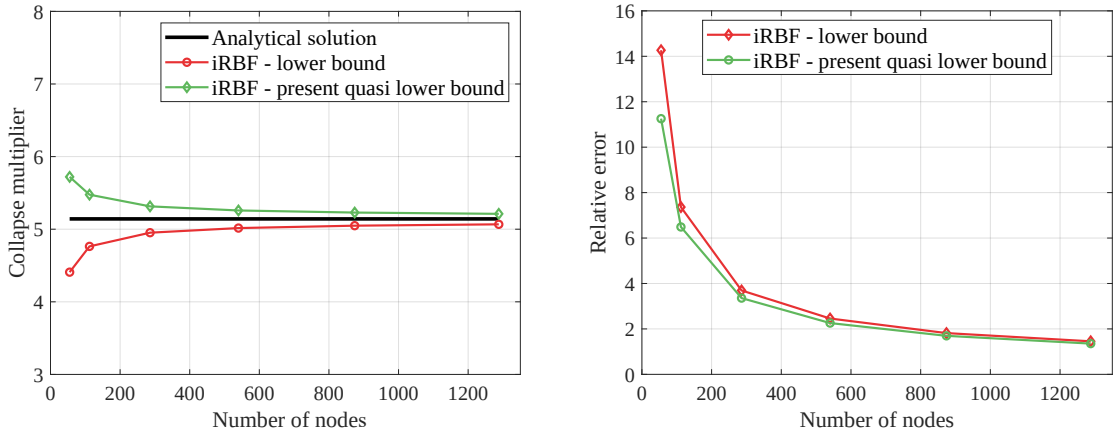

(a) Numerical solutions

(b) Relative errors

Figure 5.4: The punch problem: computational analysis

It is also interesting to point out that both methods results in the same number of variables in its optimization problem when using the same nodal distribution, but the present method can provide more accurate solutions (smaller relative errors).

Table 5.1: Computational results of iRBF and RPIM methods

Approach	Collapse load factor				Exact solution
	λ_s	e (%)	t (s)	$\mathcal{N}_{var}$	
iRBF, *quasi lower bound*	5.186	0.86	79.34	12355	
RPIM, *quasi lower bound*	5.208	1.29	122.72	12355	5.142
RPIM, *lower bound* in [227]	5.087	1.07	214.41	12355	

t is the CPU optimization time, e is the relative errors in collapse load factor

Table 5.1 reports computed collapse load factors, relative errors, computational

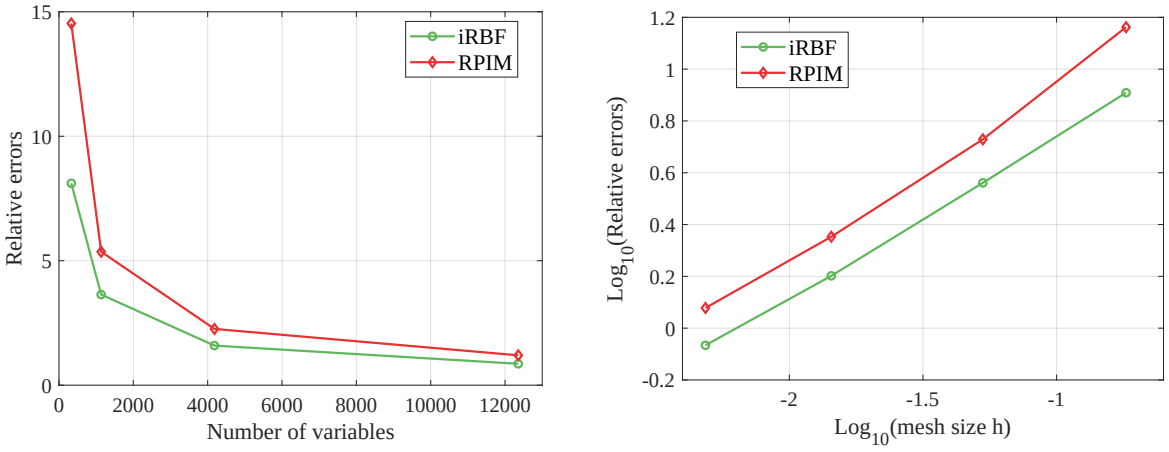

(a) Relative errors (b) Convergence rate

Figure 5.5: The punch problem: iRBF versus RPIM

(a) Elastic stress field

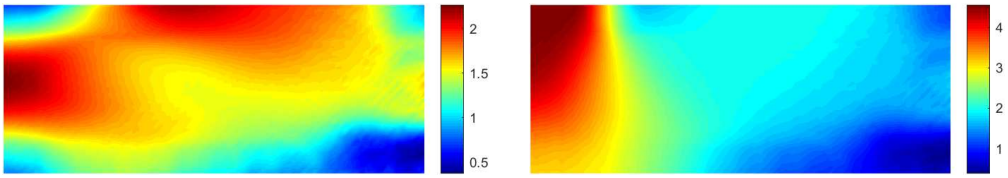

(b) Residual stress field (c) Limit stress field

Figure 5.6: Prandtl's punch problem: distribution of elastic, residual and limit stress fields

CPU time using both iRBF and RPIM based numerical procedures with a nodal distribution of 2059 nodes (using 2D model). Convergence analysis of the two methods is also illustrated in Figure 5.5. It can be observed that for all nodal distribution the iRBF method results in more accurate collapse load factors than the RPIM method, while the computational CPU time taken to solve the iRBF optimization problem is smaller that that of the RPIM method. In short, the present method is more advantaged than the RPIM approach and the iRBF based static method presented in [227] in terms of computational efficiency and solution accuracy. The distribution of elastic, residual stresses and stress field at limit state is also shown in Figure 5.6.

5.3.2 Thin plate with a central hole subjected to variable tension loads

Next, consider a square plate with a circular hole at its center, see Figure 5.7, and subjected to a biaxial tension loads varying independently as

$$0 \leq p_1 \leq p_{01} \ , \quad 0 \leq p_2 \leq p_{02} \tag{5.16}$$

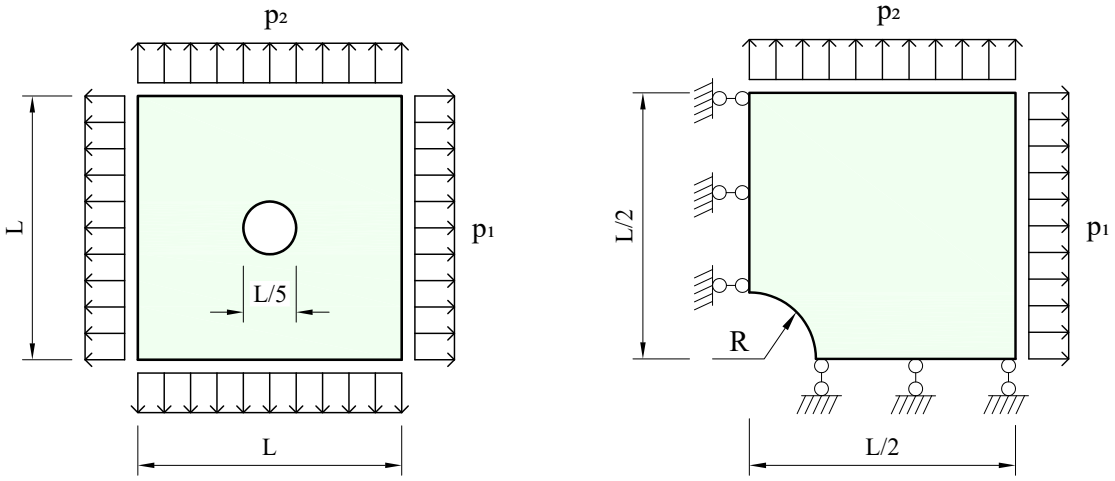

(a) Geometry and loading (b) Computational model

Figure 5.7: Square plate with a central circular hole: geometry (thickness $t = 0.4R$), loading and computational domain

The problem has been extensively investigated in the literature using different numerical procedures, for example static formulation [82, 90, 193, 197, 221, 224, 225, 228, 229], kinematic formulation [68, 78, 80, 96, 191], mixed formulation [226]. The plate is solved employing only upper-right quarter, see 5.7, and using the following data: $E = 2.1 \times 10^5$ MPa, $\nu = 0.3$ and $\sigma_p = 200$ MPa. The two- and three-dimension nodal discretization and associated Voronoi diagrams are respectively plotted in Figures 5.8(a) and 5.8(b).

Tables 5.2 and 5.3 report computed limit and shakedown load factors using the proposed numerical procedure, together with those obtained using different methods in the literature [80, 86, 87, 90, 96, 226], for three different loading cases. In general, good agreement of these solutions is observed. However, the present method posses more advantages in terms of discretization technique and optimization algorithm, compared with previously proposed approaches. The iRBF method results in high-

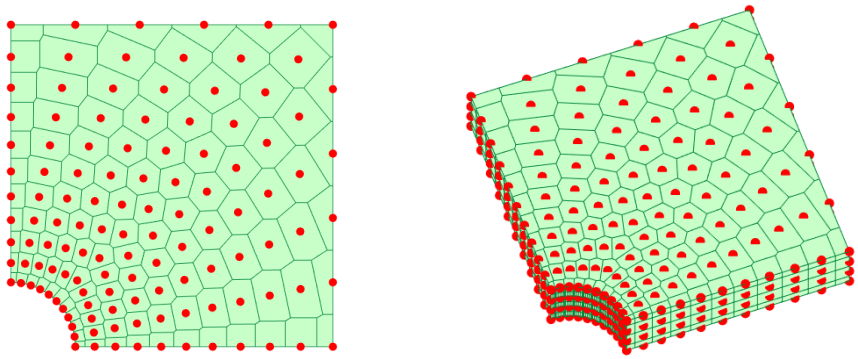

(a) 2D model (b) 3D model

Figure 5.8: Square plate with a central circular hole: the nodal distribution and Voronoi diagrams

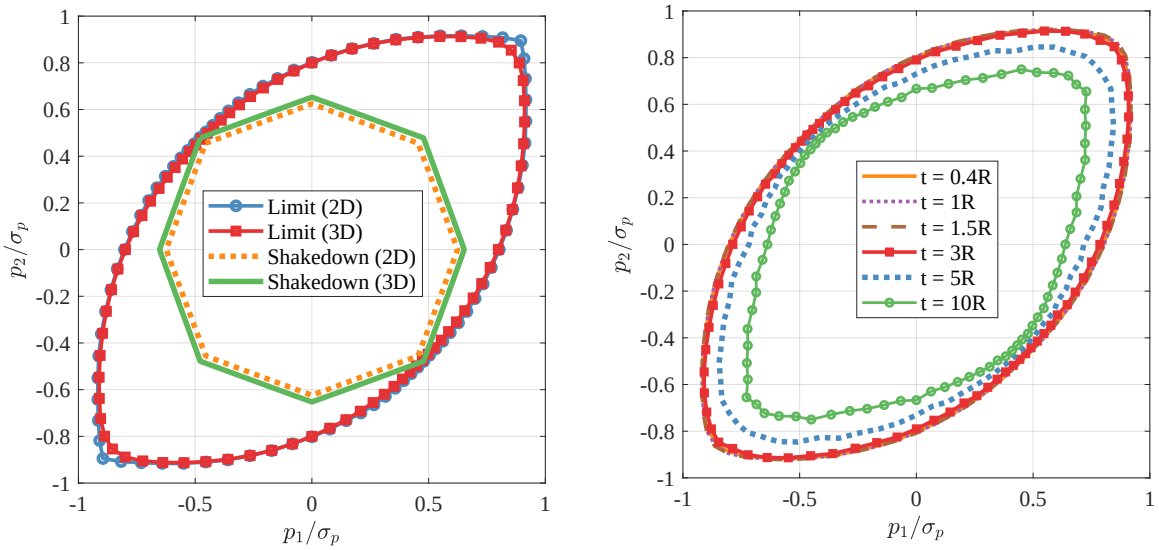

(a) Load domains ($t = 0.4R$) (b) Limit load domains for various thickness

Figure 5.9: Plate with hole: loading domain

order shape functions than finite elements [226], smoothed finite elements [80], and boundary elements [86, 87], and hence more accurate solutions can be obtained when using the same mesh. Note that in [96], the radial point interpolation mesh-free method (RPIM) is used in the kinematic formulation, but as shown in the first example the method does not perform as well as the iRBF method. In [90], the EFG mesh-free method is used in the framework of static theorem, providing accurate solutions. However, the EFG shape functions do not hold Kronecker's delta properties, and hence attention must be paid to enforce boundary conditions.

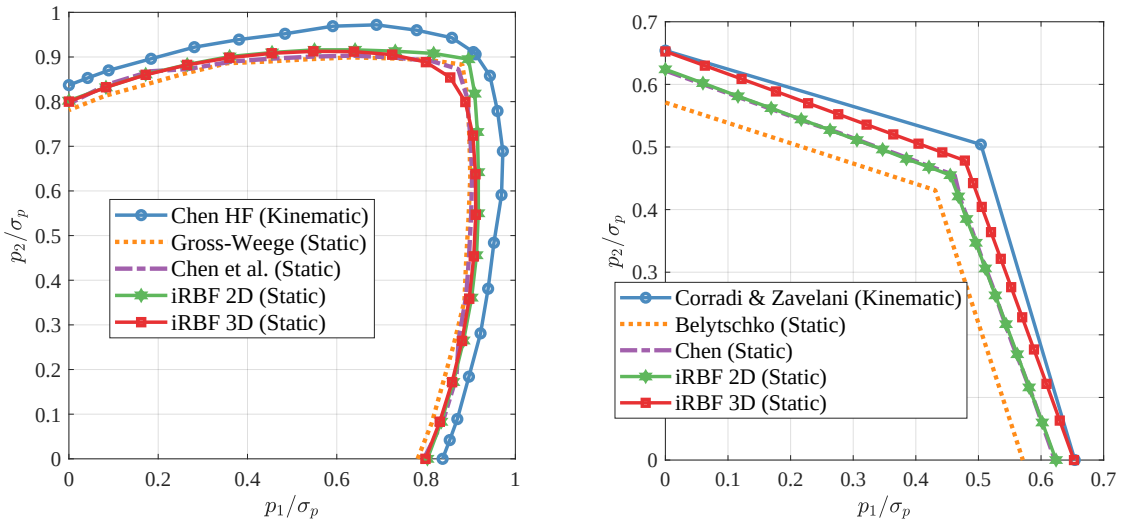

(a) Limit load factor

(b) Shakedown load factor

Figure 5.10: Plate with hole: load domains in comparison with other numerical methods

This is not the case for the iRBF method, in which boundary conditions can be enforced in a way similar to ones in the finite element method. Regarding the optimization algorithm, the second-order cone programming used in the present numerical procedure is able to solve large-scale problems with up to thousands of variables in a couple of minutes, enabling the efficient computation of a large number of points to describe a load domain. Stress fields for various load cases are plotted in Figures 5.11–5.13. Limit load domains for various plate thickness are also shown in Figure 5.9(b).

Graphics of proportional plastic limit curve and shakedown limit curve for all range of (5.16) are plotted in the plane of load coordinates $p_1/\sigma_p, p_2/\sigma_p$ as in Figure 5.9(a). Figure 5.10 shows the limit and shakedown load domains using the iRBF based static method and other numerical approaches. It is evident that iRBF solutions are in good agreement with those obtained using static theorem [90, 193, 221] and kinematic formulation [166, 228].

Table 5.2: Plate with hole: comparison of limit load multipliers

Authors	Loading cases		
	$p_1 = p_2$	$p_1 = 2p_2$	$p_2 = 0$
Present iRBF 2D, *quasi-static*	0.871	0.902	0.8001
Present iRBF 3D, *quasi-static*	0.858	0.909	0.8002
Ho et al. [82], *CS-FEM, quasi-static*	0.896	0.911	0.8007
Gross-Weege[221], *FEM, static*	0.882	0.891	0.792
Liu et al. [86], *EFG, static*	0.903	0.915	0.795
Chen et al. [90], *EFG, static*	0.874	0.899	0.798
Tin-Loi and Ngo [197], *FEM, static*	0.895	0.912	0.803
Vicente da Silva and Antao [191], *FEM, kinematic*	0.899	0.915	0.807
Le et al. [78], *CS-FEM, kinematic*	0.895	0.911	0.801
Zouain et al. [226], *FEM, mixed*	0.894	0.911	0.903
Gaydon and McCrum [230], *analytical solution*	-	-	0.800

Table 5.3: Plate with hole: comparison of shakedown load multipliers

Authors	Loading cases		
	$p_1 = p_2$	$p_1 = 2p_2$	$p_2 = 0$
Present iRBF 2D, *quasi-static*	0.478	0.551	0.650
Present iRBF 3D, *quasi-static*	0.474	0.546	0.645
Ho et al. [82], *quasi-static*	0.449	0.536	0.617
Gross-Weege [221], *static*	0.446	0.524	0.614
Genna [225], *static*	0.478	0.566	0.653
Liu et al. [87], *static*	0.477	0.549	0.647
Carvelli et al. [68], *kinematic*	0.518	0.607	0.696
Corradi and Zavelani [228], *kinematic*	0.504	0.579	0.654
Krabbenhoft [229], *kinematic*	0.430	0.499	0.595
Zouain et al. [226], *mixed*	0.429	0.500	0.594
Garcea et al. [231], *mixed*	0.438	0.508	0.604
Tran et al. [80], *dual algorithms*	0.444	0.514	0.610

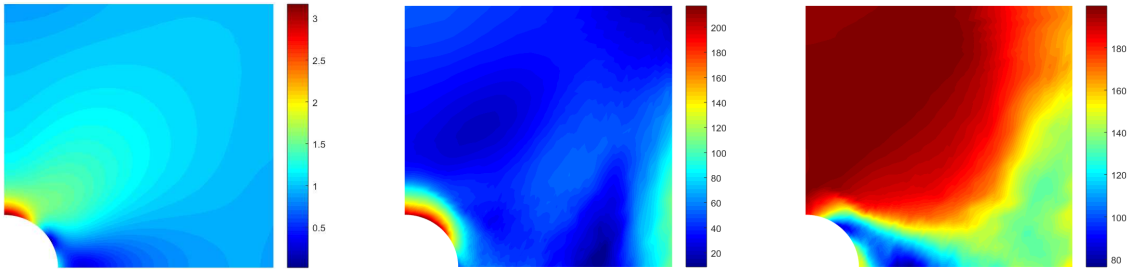

(a) Elastic stress field (b) Residual stress field (c) Limit stress field

Figure 5.11: Plate with hole: stress fields in case of $[p_1, p_2] = [1, 0]$

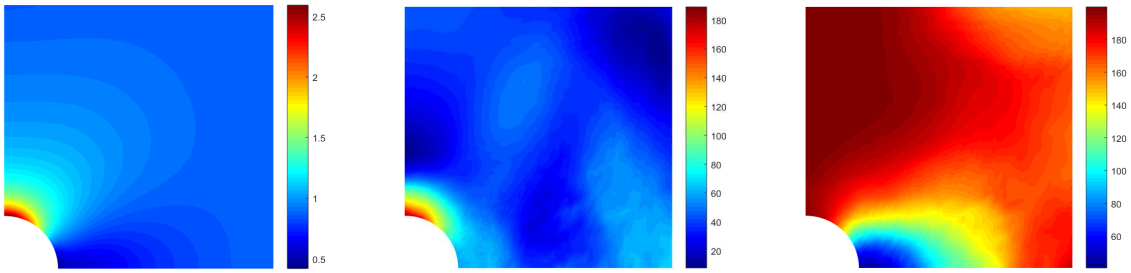

(a) Elastic stress field (b) Residual stress field (c) Limit stress field

Figure 5.12: Plate with hole: stress fields in case of $[p_1, p_2] = [1, 0.5]$

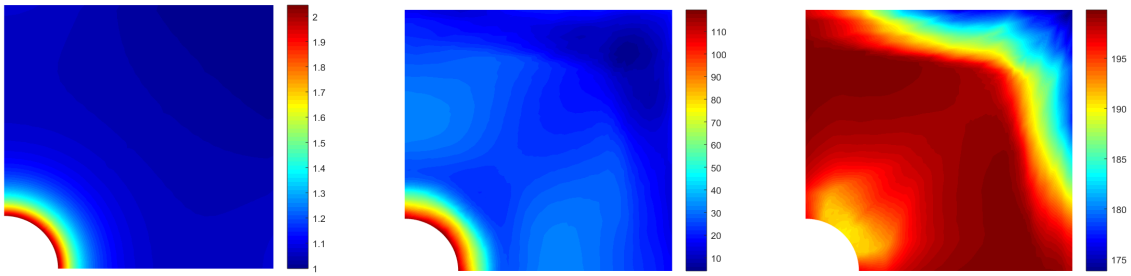

(a) Elastic stress field (b) Residual stress field (c) Limit stress field

Figure 5.13: Plate with hole: stress fields in case of $[p_1, p_2] = [1, 1]$

5.3.3 Grooved plate subjected to tension and in-plane bending loads

A grooved plate subjected to in-plane tension load p_N and bending load p_M is also considered. The variable loads are defined by

$$0 \leq p_N \leq \sigma_p; \quad 0 \leq p_M \leq \sigma_p \tag{5.17}$$

Geometry, loading, boundary conditions and computational nodal distribution

are shown in Figure 5.15. Geometry and material properties are given as: $R = 250$ mm, $L = 4R$, $E = 2.1 \times 10^5$ MPa, $\nu = 0.3$, $\sigma_p = 116.2$ MPa.

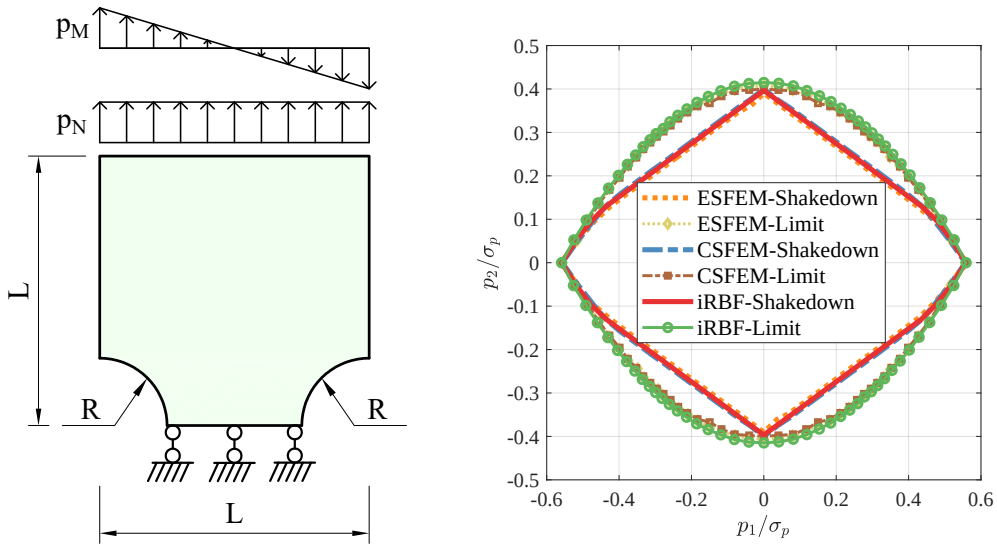

(a) Computational model (b) Limit and shakedown load domains

Figure 5.14: Grooved square plate subjected to tension and in-plane bending loads

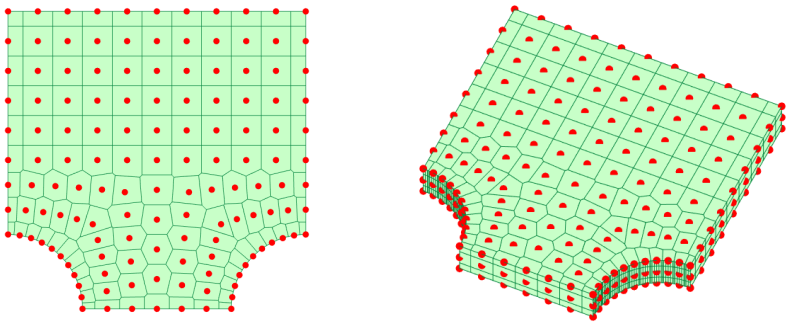

(a) Nodal mesh 2D (b) Nodal mesh 3D ($t = 0.4R$)

Figure 5.15: Grooved square plate: computational nodal distribution

Limit and shakedown interaction diagram is illustrated in the plane of load coordinates $p_N/\sigma_p, p_M/\sigma_p$ as in Figure 5.14(b). Table 5.4 reports computed limit and shakedown load multipliers for two loading cases: *(i)* pure tension ($p_N \neq 0,\ p_M = 0$); *(ii)* both tension and bending ($p_N \neq 0,\ p_M \neq 0$). It is evident that the iRBF solutions agree well with published results using different discretization methods. Stress fields for various load cases are plotted in Figures 5.16 and 5.17.

Table 5.4: Grooved plate: present solutions in comparison with other results

Authors	Limit load factor		Shakedown load factor
	$p_N \neq 0$	$p_N \neq 0$	$0 \leq p_N \leq \sigma_p$
	$p_M = 0$	$p_M \neq 0$	$0 \leq p_M \leq \sigma_p$
Present iRBF 2D	0.524	0.25832	0.22024
Present iRBF 3D	0.571	0.26418	0.22065
Ho et al. [82], *CS-FEM*	0.557	0.29394	0.24807
Tran et al. [80], *ES-FEM*	0.562	0.27811	0.23603
Nguyen-Xuan et al. [81], *ES-FEM*	0.559	0.29660	0.22477
Tran [232], *ES-FEM*	0.572	0.30498	0.23603
Vu [233], *FEM*	0.557	-	0.23494
Prager and Hodge [234], *FEM*	0.500	-	-
Casciaro [235], *FEM*	0.568	-	-
Yan [236], *numerical*	0.558	-	-
Yan [236], *analytical*	0.500 - 0.577	-	-

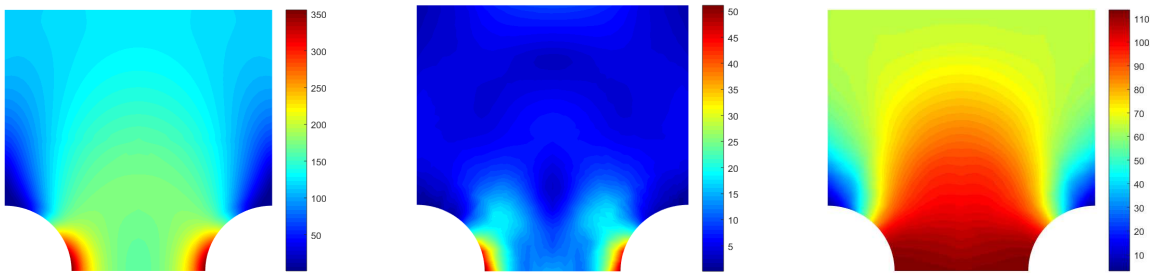

(a) Elastic stress field (b) Residual stress field (c) Limit stress field

Figure 5.16: Grooved plate: stress fields in case of $[p_N, p_M] = [\sigma_p, 0]$

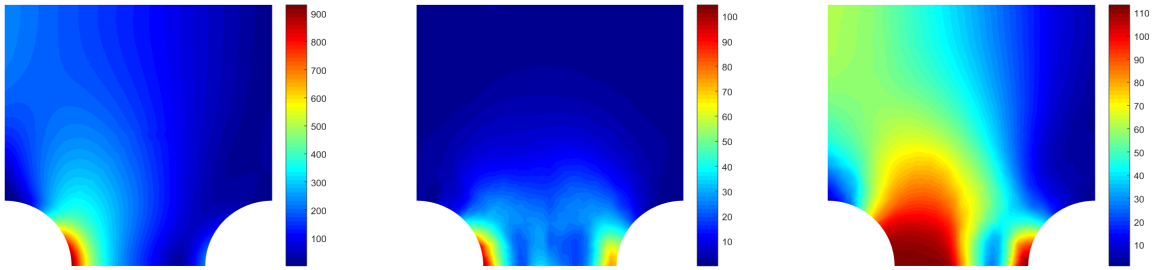

(a) Elastic stress field (b) Residual stress field (c) Limit stress field

Figure 5.17: Grooved plate: stress fields in case of $[p_N, p_M] = [\sigma_p, \sigma_p]$

5.3.4 A symmetric continuous beam

This example deals with a symmetric continuous beam subjected to two independently variable loads $p_1 \in [1.2,\ 2]$ and $p_2 \in [0,\ 1]$, as presented in Figure 5.18(a). The material properties are assumed as: $E = 1.8 \times 10^5$ MPa, $\nu = 0.3$, $\sigma_p = 100$ MPa. Tables 5.5 and 5.6 compares the iRBF results with published solutions using finite elements [231], cell-based smoothed finite elements [82], node-based strain smoothing method [81] and the EFG mesh-free method [90].

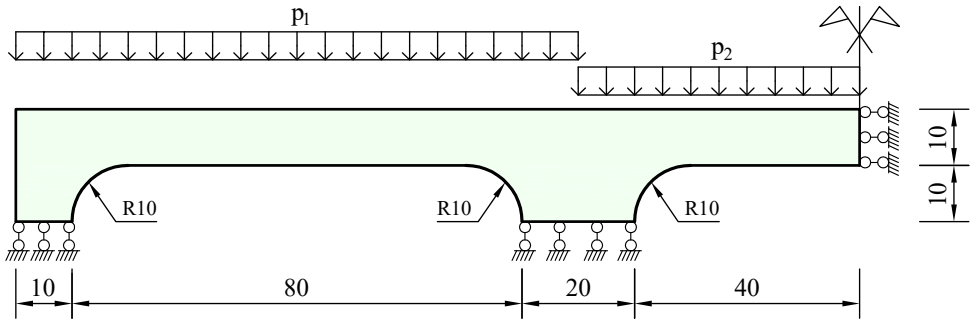

(a) Computational model

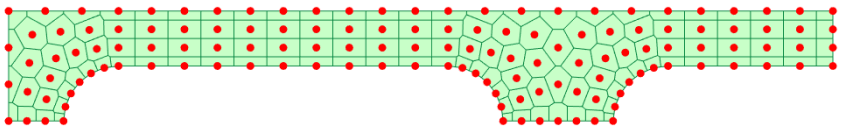

(b) Nodal mesh & Voronoi 2D

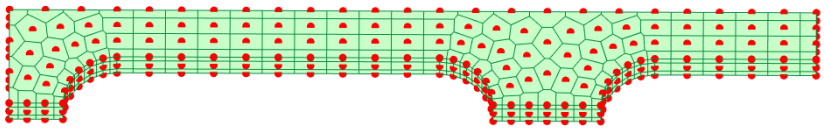

(c) Nodal mesh & Voronoi 3D

Figure 5.18: Symmetric continuous beam subjected to two independent load

Table 5.5: Symmetric continuous beam: limit load factors

Authors	Loading cases			
	$p_1 = 2.0$ $p_2 = 0.0$	$p_1 = 0.0$ $p_2 = 1.0$	$p_1 = 1.2$ $p_2 = 1.0$	$p_1 = 2.0$ $p_2 = 1.0$
Present iRBF 2D	3.225	8.836	5.530	3.309
Present iRBF 3D	3.337	8.671	5.472	3.282
Ho et al. [82], *CS-FEM*	3.301	8.748	5.504	3.302
Garcea et al. [231], *FEM*	3.280	8.718	5.467	3.280
Nguyen-Xuan et al. [81], *ES-FEM*	3.297	8.722	5.493	3.296

Table 5.6: Symmetric continuous beam: shakedown load factors

Authors	Loading cases		
	$1.2 \leq p_1 \leq 2$ $0 \leq p_2 \leq 1$	$0 \leq p_1 \leq 2$ $0.6 \leq p_2 \leq 1$	$0 \leq p_1 \leq 2$ $0 \leq p_2 \leq 1$
Present iRBF 2D	3.217	2.333	2.308
Present iRBF 3D	3.228	2.357	2.276
Ho et al. [82], *CS-FEM*	3.362	2.228	2.205
Chen et al. [90], *EFG*	3.297	2.174	2.152
Garcea et al. [231], *FEM*	3.244	-	-
Nguyen-Xuan et al. [81], *ES-FEM*	3.259	2.036	2.016

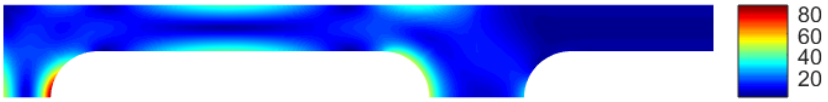

(a) Elastic stress field

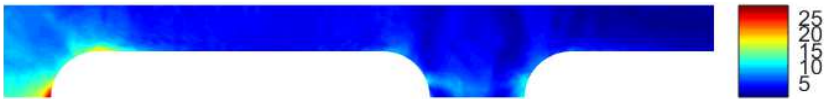

(b) Residual stress field

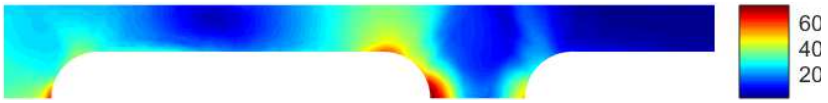

(c) Limit stress field

Figure 5.19: Symmetric continuous beam: stress fields in case of $[p_1, p_2] = [2, 0]$

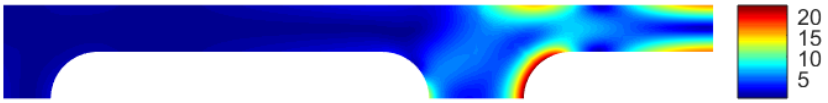

(a) Elastic stress field

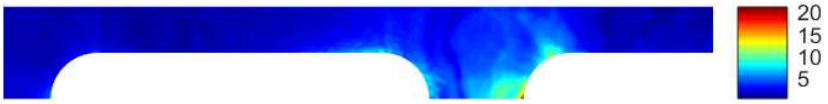

(b) Residual stress field

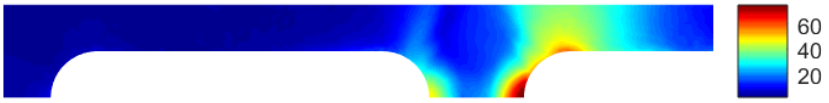

(c) Limit stress field

Figure 5.20: Symmetric continuous beam: stress fields in case of $[p_1, p_2] = [0, 1]$

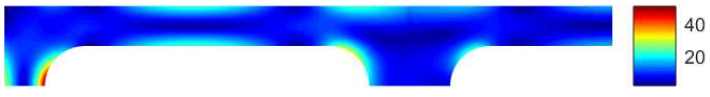

(a) Elastic stress field

(b) Residual stress field

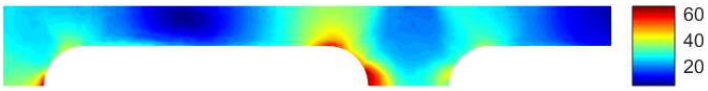

(c) Limit stress field

Figure 5.21: Symmetric continuous beam: stress fields in case of $[p_1, p_2] = [1.2, 1]$

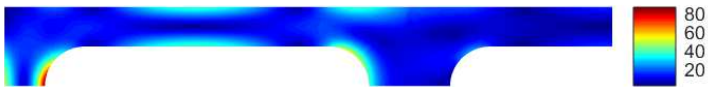

(a) Elastic stress field

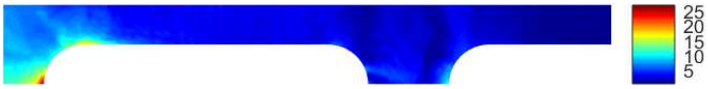

(b) Residual stress field

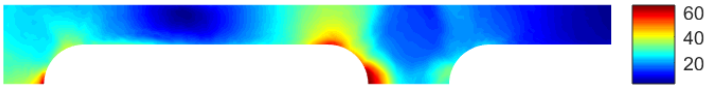

(c) Limit stress field

Figure 5.22: Symmetric continuous beam: stress fields in case of $[p_1, p_2] = [2, 1]$

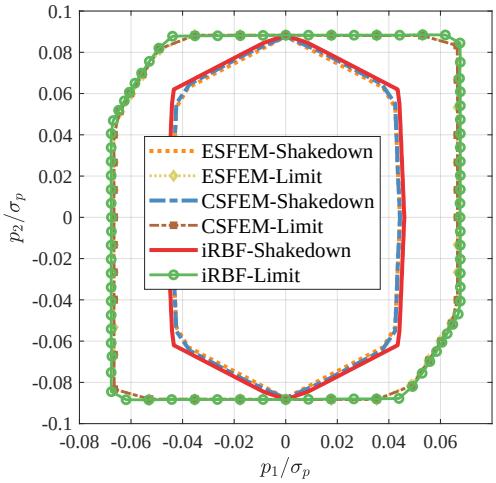

Figure 5.23: Continuous beam: iRBF load domains compared with other methods

The approximated limit and shakedown load domains for all load range $p_N \in [-1,\ 1]$ and $p_M \in [-1,\ 1]$ are compared with those using smoothed finite elements [82] in Figure 5.23. Stress fields for various load cases are also plotted in Figures 5.19 – 5.22.

5.3.5 A simple frame with different boundary conditions

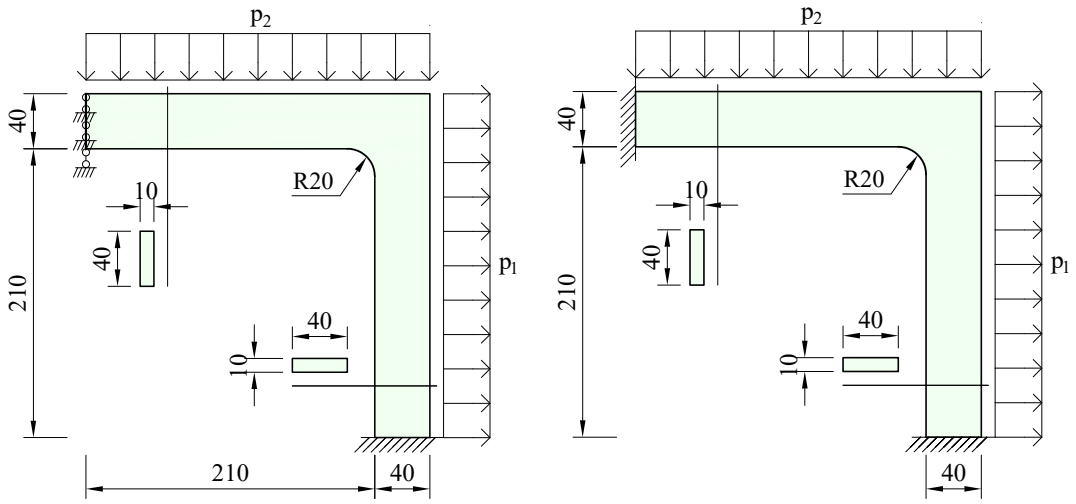

(a) Model A (b) Model B

Figure 5.24: A simple frame: geometry, loading, boundary conditions

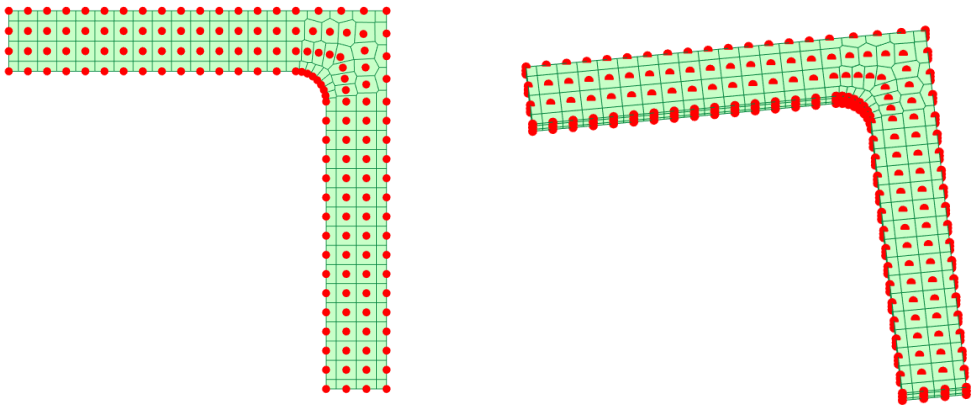

(a) Nodal discretization 2D (b) Nodal discretization 3D

Figure 5.25: A simple frame: nodal mesh

The last example is the simple frames with different boundary conditions, see Figure 5.24 (all dimensions in cm). The problem are investigated in [82, 231] under plane stress condition. Data for analysis is given as: $E = 2 \times 10^5$ MPa, $\nu = 0.3$,

Table 5.7: A simple frame (model A): limit and shakedown load multipliers

Authors	Limit analysis			Shakedown analysis
	$p_1 = 0.4$	$p_1 = 1.0$	$p_1 = 1.0$	$0.4 \leq p_1 \leq 1.0$
	$p_2 = 3.0$	$p_2 = 1.2$	$p_2 = 3.0$	$1.2 \leq p_2 \leq 3.0$
Present iRBF 2D	3.153	2.979	2.728	2.649
Present iRBF 3D	3.261	3.073	2.818	2.676
Ho et al. [82], *CS-FEM*	2.981	2.820	2.634	2.452
Garcea et al. [231], *FEM*	2.831	2.975	2.645	2.473

Table 5.8: A simple frame (model B): limit and shakedown load multipliers

Authors	Limit analysis			Shakedown analysis
	$p_1 = 0.4$	$p_1 = 1.0$	$p_1 = 1.0$	$0.4 \leq p_1 \leq 1.0$
	$p_2 = 3.0$	$p_2 = 1.2$	$p_2 = 3.0$	$1.2 \leq p_2 \leq 3.0$
Present iRBF 2D	4.152	8.095	3.874	3.964
Present iRBF 3D	4.209	8.077	4.150	4.172
Ho et al. [82], *CS-FEM*	4.186	7.810	3.931	3.817
Garcea et al. [231], *FEM*	4.207	7.804	3.949	3.925

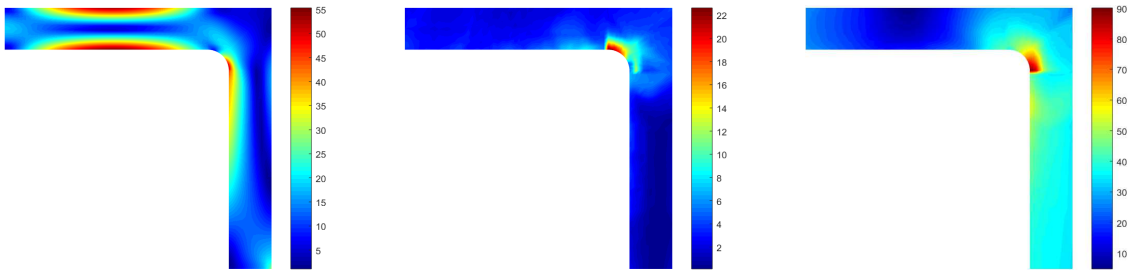

(a) Elastic stress field (b) Residual stress field (c) Limit stress field

Figure 5.26: Simple frame (model A): stress fields in case of $[p_1, p_2] = [3, 0.4]$

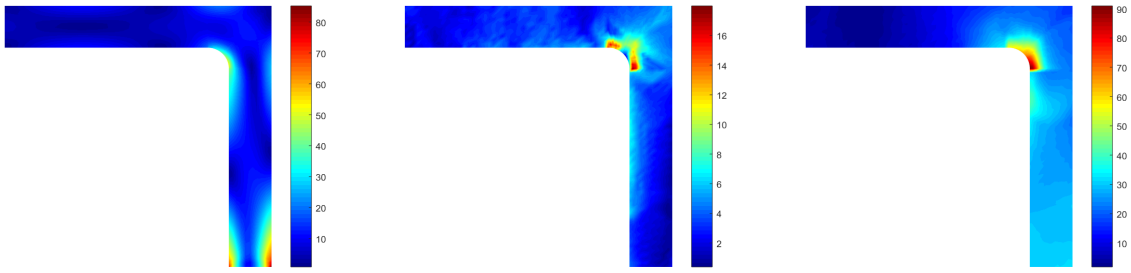

(a) Elastic stress field (b) Residual stress field (c) Limit stress field

Figure 5.27: Simple frame (model A): stress fields in case of $[p_1, p_2] = [1.2, 1]$

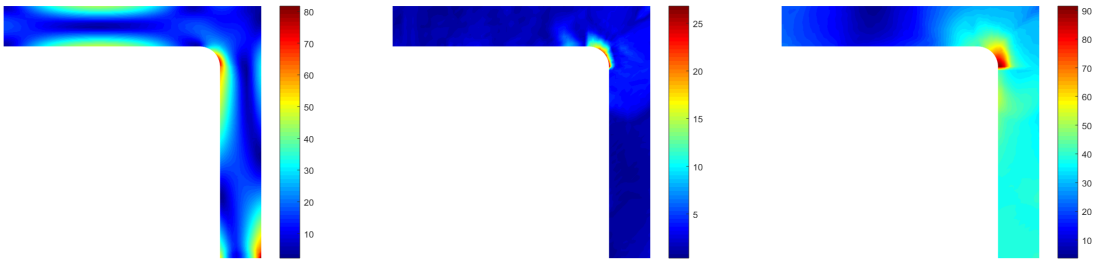

(a) Elastic stress field (b) Residual stress field (c) Limit stress field

Figure 5.28: Simple frame (model A): stress fields in case of $[p_1, p_2] = [3, 1]$

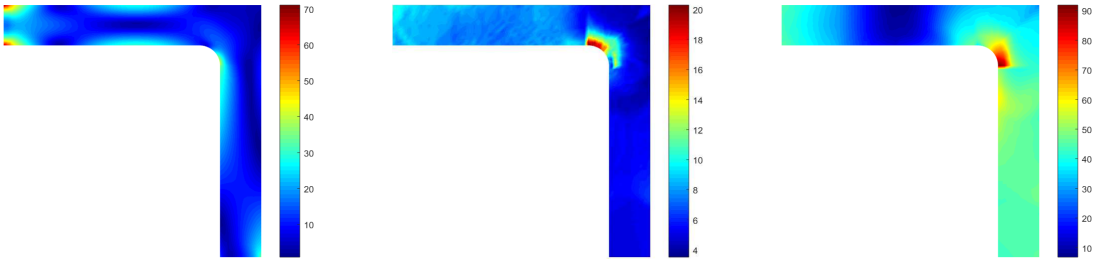

(a) Elastic stress field (b) Residual stress field (c) Limit stress field

Figure 5.29: Simple frame (model B): stress fields in case of $[p_1, p_2] = [3, 0.4]$

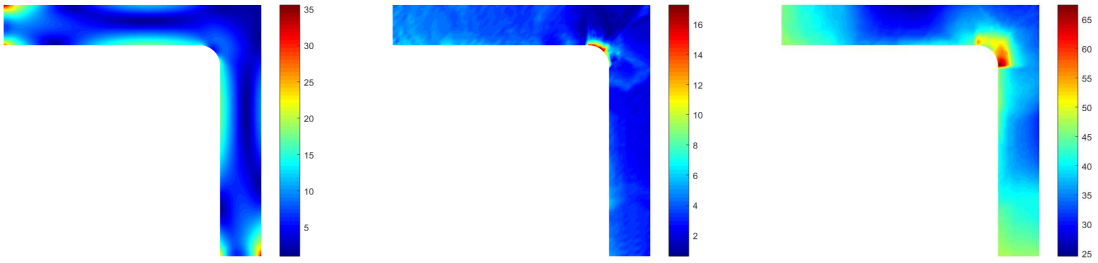

(a) Elastic stress field (b) Residual stress field (c) Limit stress field

Figure 5.30: Simple frame (model B): stress fields in case of $[p_1, p_2] = [1.2, 1]$

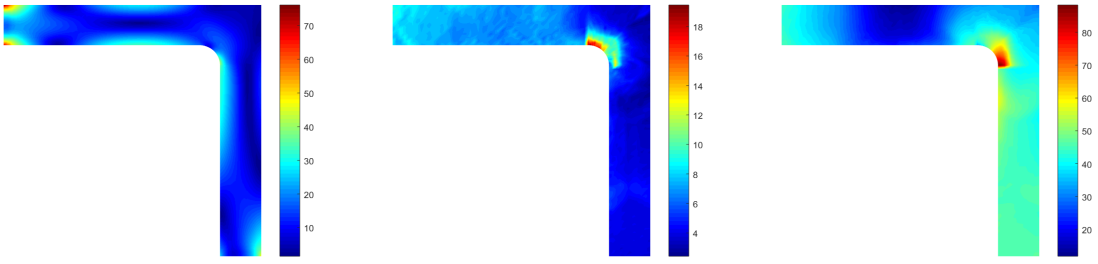

(a) Elastic stress field (b) Residual stress field (c) Limit stress field

Figure 5.31: Simple frame (model B): stress fields in case of $[p_1, p_2] = [3, 1]$

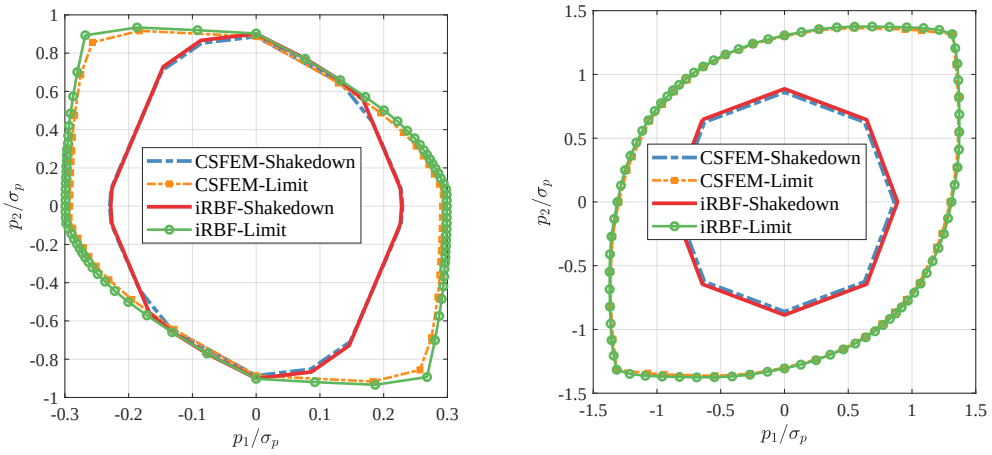

(a) Model A (b) Model B

Figure 5.32: Simple frame: iRBF load domains compared with other method

$\sigma_p = 10$ MPa and the thick of frame $t = 10$ cm. The frames are subjected to biaxial load with the loading domain defined as

$$0.4 \leq p_1 \leq 1; \quad 1.2 \leq p_2 \leq 3 \tag{5.18}$$

Numerical solutions obtained using the present iRBF-based equilibrium formulation are reported in Table 5.7 and 5.8. The approximated limit and shakedown load domains for different models are compared with those using smoothed finite elements [82] in Figure 5.32, showing excellent agreement. Stress fields for various load cases are also plotted in Figures 5.26 – 5.31.

5.4 Conclusions

A quasi-static approach based on integrated radial basis function mesh-free method and conic programming is proposed for direct analysis of structures. Instead of approximating stress fields, in the present formulation the virtual displacement fields are approximated by stabilized iRBF shape functions, and equilibrium condition for residual stress are satisfied in its weak form by using the virtual work principle. With the use of stabilized iRBF shape functions, equilibrium equations and yield conditions are enforced at discretized nodes, keeping the size of the resulting optimization problem to be minimum. Numerical examples show that the present requires less optimization CPU time comparing with other shakedown al-

gorithms in the literature, and has a faster convergence behavior in comparison with the RPIM approach. The proposed approach is capable of providing solutions rapidly, and hence load domains of 2D and 3D structures can be approximated efficiently. Moreover, the present method is able to capture stress fields at limit state for various problems.

Chapter 6

Kinematic yield design computational homogenization of micro-structures using the stabilized iRBF mesh-free method [1]

6.1 Introduction

The applications of iRBF-based meshless method for direct analysis of different structures subjected to various loading conditions have been presented in chapters 3, 4 and 5. In current chapter, the stabilized iRBF formulation previously developed in chapter 5 will be employed for limit analysis of microstructures.

As the increasing use of composite and heterogeneous materials in practical engineering structures, the estimation of their effective properties plays a vital role in safety assessment as well as structural design. The elastic-plastic incremental method can be employed to predict the ultimate load and collapse mechanism of structures. However, direct method, e.g., limit analysis shows more effectively, i.e. the critical status of structures can be determined without any knowledge of whole loading path history [9, 237]. The first theoretical framework of limit analysis combined with homogenization technique for computation of heterogeneous microstructures was introduced in [115–117]. The numerical formulations using various mathematical solvers were developed then, for instance finite element method and linear algorithms [118], static direct methods and interior point algorithms [25, 119, 120] or kinematic formulations in combination with nonlinear programming [121–125]. Recently, with the use of finite element method and second order cone programming, a numerical procedure based on the combination of limit analysis and homogenization

[1] based on P. L. H. Ho, C. V. Le, and Phuong H. Nguyen. "Kinematic yield design computational homogenization of micro-structures using the stabilized iRBF mesh-free method," *Applied Mathematical Modelling*, submitted on Feb 2020.

theory for periodic materials was proposed in [126].

This study aim to develop a novel computational homogenization approach for upper bound limit analysis of microstructures using iRBF meshless method. The stability conforming nodal integration (SCNI) technique proposed in [166] is utilized to improve the performance of proposed approach. In addition, the plastic dissipation will be transformed into the form of a sum of norms and the resulting optimization are then formulated as conic one. The benchmark numerical examples will be considered and the good agreement in comparison to previous procedures proves the performance of present method.

6.2 Limit analysis based on homogenization theory

Consider a heterogeneous representative volume element $\Omega \in \mathbb{R}^2$ at every material point $\mathbf{x}$ in the the heterogeneous macroscopic-continuum $V \in \mathbb{R}^2$. The microstructure is subjected to the body force $\mathbf{f}$, the surface load $\mathbf{t}$ on the static boundary Γ_t and fixed by the displacement field $\mathbf{u}$ on the kinematic boundary Γ_u. Assuming that all constitutions of ductile composite are rigid-perfectly plastic and the strain of constitutions obey the normality rule. The kinematic approach in framework of limit analysis for computation homogenization described in [121–125, 183] will be taken into account in this study.

It is important to note that most of yield criterion can be expressed in the following form

$$\psi(\boldsymbol{\sigma}) = \sqrt{\boldsymbol{\sigma}^T \mathbf{P} \boldsymbol{\sigma}} - 1 \tag{6.1}$$

where $\mathbf{P}$ is the coefficient matrix consisting strength properties of materials. For orthotropic materials, Hill's criterion is often used; and $\mathbf{P}$ for plane stress problem is given by

$$\mathbf{P} = \begin{bmatrix} \kappa_{zx} + \kappa_{xy} & -\kappa_{xy} & 0 \\ -\kappa_{xy} & \kappa_{xy} + \kappa_{yz} & 0 \\ 0 & 0 & 3\eta_{xy} \end{bmatrix} \tag{6.2}$$

where the constants of material features can be expressed by

$$\kappa_{zx} = \frac{1}{2}\left[\frac{1}{\sigma_{pz}^2} + \frac{1}{\sigma_{px}^2} - \frac{1}{\sigma_{py}^2}\right]; \qquad \kappa_{xy} = \frac{1}{2}\left[\frac{1}{\sigma_{px}^2} + \frac{1}{\sigma_{py}^2} - \frac{1}{\sigma_{pz}^2}\right] \tag{6.3a}$$

$$\kappa_{yz} = \frac{1}{2}\left[\frac{1}{\sigma_{py}^2} + \frac{1}{\sigma_{pz}^2} - \frac{1}{\sigma_{px}^2}\right]; \qquad \eta_{xy} = \frac{1}{3\tau_{pxy}^2} \tag{6.3b}$$

with (σ_{px}, σ_{py}, σ_{pz}) are the uniaxial yield stresses related to three orthotropic dimensions (x, y, z); and τ_{xy} is the shear yield stress of materials.

For isotropic materials, the so-called von Mises criterion, a special case of Hill's criterion when $\sigma_{px} = \sigma_{py} = \sigma_{pz} = \sigma_p$ and $\tau_{pxy} = \dfrac{\sigma_p}{\sqrt{3}}$, is frequently applied; and matrix $\mathbf{P}$ for plane stress problem is given by

$$\mathbf{P} = \frac{1}{\sigma_p}\begin{bmatrix} 1 & -1/2 & 0 \\ -1/2 & 1 & 0 \\ 0 & 0 & 3 \end{bmatrix} \tag{6.4}$$

In framework of limit analysis, the strain rates are assumed to obey the normality rule; and therefore, the power of dissipation can be formulated in term of strain rates as

$$D(\boldsymbol{\epsilon}) = \int_\Omega \sqrt{\boldsymbol{\epsilon}^T \boldsymbol{\Theta} \boldsymbol{\epsilon}} \mathrm{d}\Omega = \int_\Omega \sqrt{(\mathbf{E} + \tilde{\boldsymbol{\epsilon}})^T \boldsymbol{\Theta} (\mathbf{E} + \tilde{\boldsymbol{\epsilon}})} \mathrm{d}\Omega \tag{6.5}$$

where $\boldsymbol{\Theta}$ is the inversion matrix of $\mathbf{P}$.

Omitting the body force $\mathbf{f}$ and applying the principle of microscopic virtual work (2.58), the normalization condition of external power can be rewritten as

$$F(\mathbf{u}) = \int_{\Gamma_t} \mathbf{t}^T \mathbf{u} \mathrm{d}\Gamma = \boldsymbol{\Sigma}^T \mathbf{E} = 1 \tag{6.6}$$

where $\boldsymbol{\Sigma}^T$ and $\mathbf{E}$ are the overall stress and strain.

Now, the kinematic limit formulation of computational homogenization analysis for a periodic micro-structure can be expressed as

$$\lambda^+ = \min \int_\Omega \sqrt{(\mathbf{E} + \tilde{\boldsymbol{\epsilon}})^T \boldsymbol{\Theta} (\mathbf{E} + \tilde{\boldsymbol{\epsilon}})} \mathrm{d}\Omega \tag{6.7a}$$

$$\text{s.t} \begin{cases} \boldsymbol{\Sigma}^T \mathbf{E} = 1 \\ \tilde{\mathbf{u}} \text{ periodic on } \Gamma_u \end{cases} \tag{6.7b}$$

The upper-bound of macroscopic limit strenth $\lambda^{+}\boldsymbol{\Sigma}$ can be determined by solving the nonlinear problem (6.7). The main difference of (6.7) in comparison with the formulation of kinematic limit analysis for structure is in the periodic boundary condition. Furthermore, it should be noted that present study only considers the continuous velocity fields; and if the velocity fields are assumed to be discontinuous, the dissipated power generated by discontinuities must be taken into account.

6.3 Discrete formulation using iRBF method

Following the homogenization theory, all variables related to the microscopic structures are split to two parts: mean fields averaged over RVE and fluctuation fields. In the kinematic formulation, the local microscopic fluctuation strain $\tilde{\boldsymbol{\epsilon}}(\mathbf{x})$ at point $\mathbf{x}$ can be calculated via the derivative of the fluctuation displacement $\tilde{u}(\mathbf{x})$ approximated using iRBF method as

$$\tilde{u}^h(\mathbf{x}) = \sum_{i=1}^{N} \Phi_i(\mathbf{x})\tilde{u}_i = \mathbf{N}\mathbf{d} \tag{6.8a}$$

$$\tilde{\boldsymbol{\epsilon}}(\mathbf{x}) = \sum_{i=1}^{N} \tilde{\Phi}_{i,\alpha}(\mathbf{x})\tilde{u}_i = \mathbf{B}\mathbf{d} \tag{6.8b}$$

where N is number of nodes scattered within problem domain; $\mathbf{N}$ denotes the iRBF shape function; $\mathbf{B}$ is the strain-displacement matrix consisting the smoothed version of shape function derivatives; and $\mathbf{d}$ is the nodal fluctuation displacement vector.

With the use of SCNI technique for the numerical integration, the plastic dissipation well-known as the objective function of the optimization problems can be expressed as

$$D_p(\boldsymbol{\epsilon}) = \sum_{i=1}^{N} \sigma_p A_i \sqrt{(\mathbf{E} + \mathbf{B}_i\mathbf{d})^T \boldsymbol{\Theta} (\mathbf{E} + \mathbf{B}_i\mathbf{d})} \tag{6.9}$$

where σ_p is the yield stress of material, A_i is the area of the i^{th} nodal representative domain created using Voronoi diagrams.

In this study, the optimization problem will be formulated in form of second order cone programming (SOCP) ensuring it can be solved using the highly efficient solves. Hence, a form of sum of norms can be used to calculate the internal

dissipation power as

$$D_p(\boldsymbol{\epsilon}) = \sum_{i=1}^{N} \sigma_p A_i \|\boldsymbol{\rho}_i\| \tag{6.10}$$

where $\|.\|$ denotes the Euclidean norm and $\boldsymbol{\rho}$ is the vector of additional variables defined by

$$\boldsymbol{\rho}_i = \mathbf{Q}^T(\mathbf{E} + \mathbf{B}_i\mathbf{d}) \tag{6.11}$$

with $\mathbf{Q}$ denotes the Cholesky factor of $\boldsymbol{\Theta}$.

Next, the periodic feature of the fluctuation displacement for nodes on the boundary of RVE needs to be enforced. Denoting Γ^+ and Γ^- for the positive and negative boundaries such that $\Gamma^+ \cup \Gamma^- = \Gamma$ and $\Gamma^+ \cap \Gamma^- = \varnothing$, the periodic condition for every pair of points $\{\mathbf{x}^+, \mathbf{x}^-\}$ on two opposite boundaries can be expressed as

$$\tilde{\mathbf{u}}(\mathbf{x}^+) - \tilde{\mathbf{u}}(\mathbf{x}^-) = 0 \tag{6.12}$$

Assembling to the global matrix, equation (6.12) can be rewritten as

$$\mathbf{C}\mathbf{d} = 0 \tag{6.13}$$

Finally, by introducing the auxiliary variables $(t_1, t_2, \ldots, t_N)$, the optimization problem can be formulated in form of conic programming as follows

$$\lambda^+ = \min \sum_{i=1}^{N} \sigma_p A_i \|\boldsymbol{\rho}_i\| \tag{6.14a}$$

$$\text{s.t} \begin{cases} \boldsymbol{\Sigma}^T\mathbf{E} = 1 \\ \mathbf{C}\mathbf{d} = 0 \\ \|\boldsymbol{\rho}_i\| \leq t_i, \quad i = 1, 2, \ldots, N \end{cases} \tag{6.14b}$$

The numerical implementation of the proposed approach is shown in Figure 6.1.

6.4 Numerical examples

In this section, various benchmark problems of computational homogenization for limit analysis, in which the numerical solutions are available, will be investigated to illustrate the performance of proposed method. A square RVE of $a \times a = 1 \times 1$

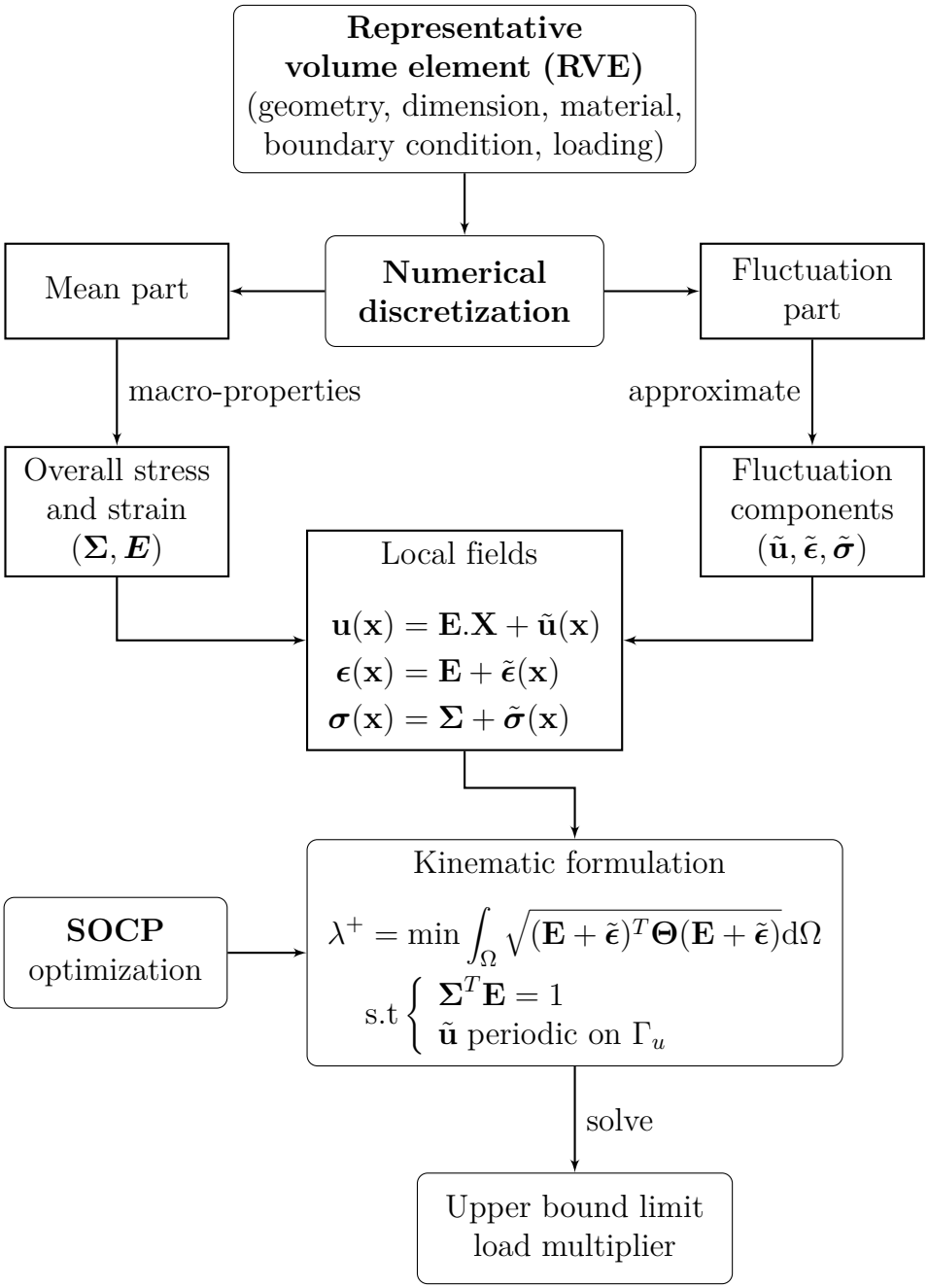

Figure 6.1: Kinematic limit analysis of materials.

mm, and the shape parameters ($\alpha_s = 0.00001$, $\beta_s = 3$) are used for all examples. The plane stress model is assumed and number of variables N_{var} in the problem is equal to $6 \times N + 3$. The resultant optimization problems are solved using the commercial software package Mosek on a 2.8 GHz Intel Core i7 PC running Window 10.

6.4.1 Perforated materials

Estimating load-bearing capacity of perforated materials treated as a special composite plays an important role in engineering structural design. In this example, two perforated material models including a rectangular and a circle hole at center are considered. The RVE is subjected to an orthogonal macroscopic stress $(\Sigma_{11}, \Sigma_{22})$ in plane as shown in Figure 6.2, where θ is the angle between the principle stress and x-axis. The matrix materials and yield stresses of rectangular and circular hole RVEs are summarized in Table 6.1, and the behavior of both material models is assumed to obey the von Mises yield criterion. Figure 6.3 illustrates the scheme of nodal discretization using Voronoi diagram. The problems have been investigated using kinematic formulation in [121, 122, 126] and quasi-static formulation in [120].

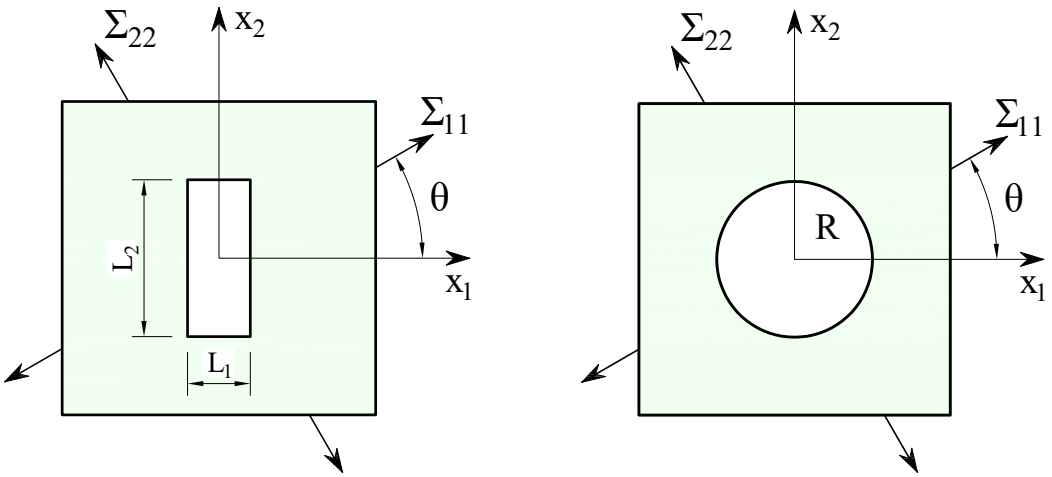

(a) Rectangular hole RVE (b) Circular hole RVE

Figure 6.2: RVEs of perforated materials: geometry, loading and dimension

Table 6.1: Perforated materials: the given data

Material models	Matrix material	Yield stress σ_p
RVE with rectangular hole	Aluminium (Al)	137 MPa
RVE with circular hole	Mild steel $(St3s)$	273 MPa

In case of rectangular hole RVE, the problem is considered with different sizes of hole: $(L_1 \times L_2 = 0.1 \times 0.5$ mm) and $(L_1 \times L_2 = 0.1 \times 0.7$ mm). Table 6.2 shows the numerical solutions using iRBF procedure in comparison with those in [122, 126]. From the table, it can be observed that present method provides the highly-accurate solution with low computational cost. Number of variables in present formulation is

less than those used in [126], while the numerical result is approximate. Moreover, taking advantage of the cone-based algorithm, present resultant optimization problem can be solved rapidly, the CPU-time taken in whole solving process is much lower than those in [122] using iterative algorithm. The good agreement of present solutions compared with previous results reported in [122, 126] using numerical as well as experimental procedures is expressed one more time in Figure 6.4 where the macroscopic uniaxial strength Σ_{11} for the case of loading angle $\theta = 0^o$ corresponding to two different sizes of rectangular hole are plotted. In addition, it can be seen from both sub-figures that the upper-bound solutions obtained using present iRBF approach are slightly lower (better) than available those in other studies.

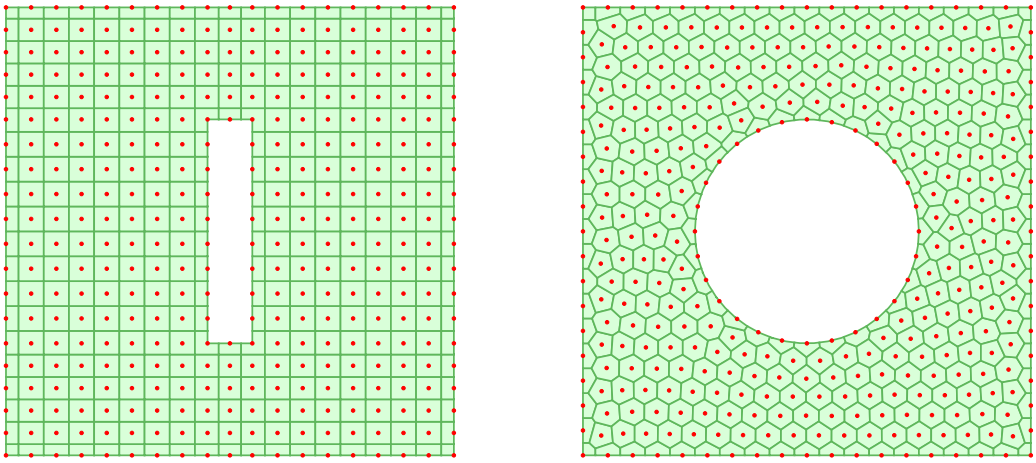

(a) Rectangular hole RVE ($L_1 \times L_2 = 0.1 \times 0.5$ mm)

(b) Circular hole RVE ($R = 0.25 \times a$)

Figure 6.3: RVEs of perforated materials: nodal discretization using Voronoi cells

Table 6.2: Rectangular hole RVE ($L_1 \times L_2 = 0.1 \times 0.5$ mm, $\theta = 0^o$)

Author and approach	Σ_{11}/σ_p	$sdof$	CPU-Time (s)
Present study, iRBF	0.5591	5246	10
Li et al. [122], FEM	0.5600	1920	95
Le et al. [126], FEM	0.5561	8140	6

$sdof$ denotes the total system degrees of freedom

Next, the effect of microscopic hole on the overall strength of perforated materials is investigated. The RVE with circular hole is considered with various variable dimensions of perforation and loading angles. The uniaxial macroscopic strengths

Σ_{11} and the limit strength domains in plane (x_1, x_2) are plotted in Figures 6.5 and 6.6, respectively. Obviously, from Figure 6.6, it is reasonable that the effective macroscopic strength decreases when increasing ratio R/a. Again, present solutions well agree with available those in [121, 126], see Figure 6.5.

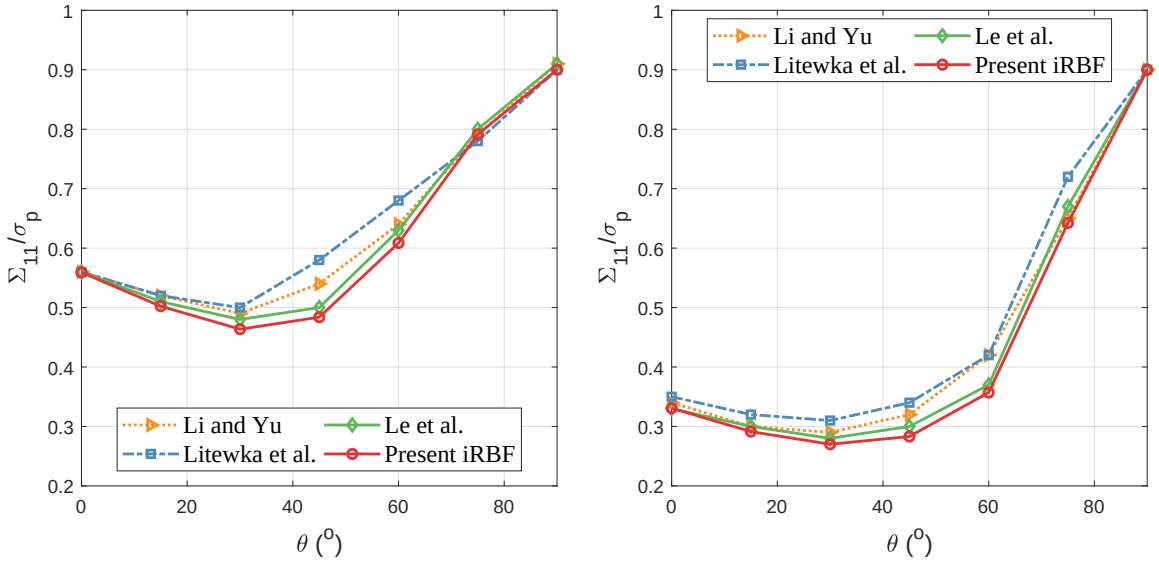

(a) $L_1 \times L_2 = 0.1 \times 0.5$ mm (b) $L_1 \times L_2 = 0.1 \times 0.7$ mm

Figure 6.4: Rectangular hole RVE: limit uniaxial strength Σ_{11} in comparison with other procedures

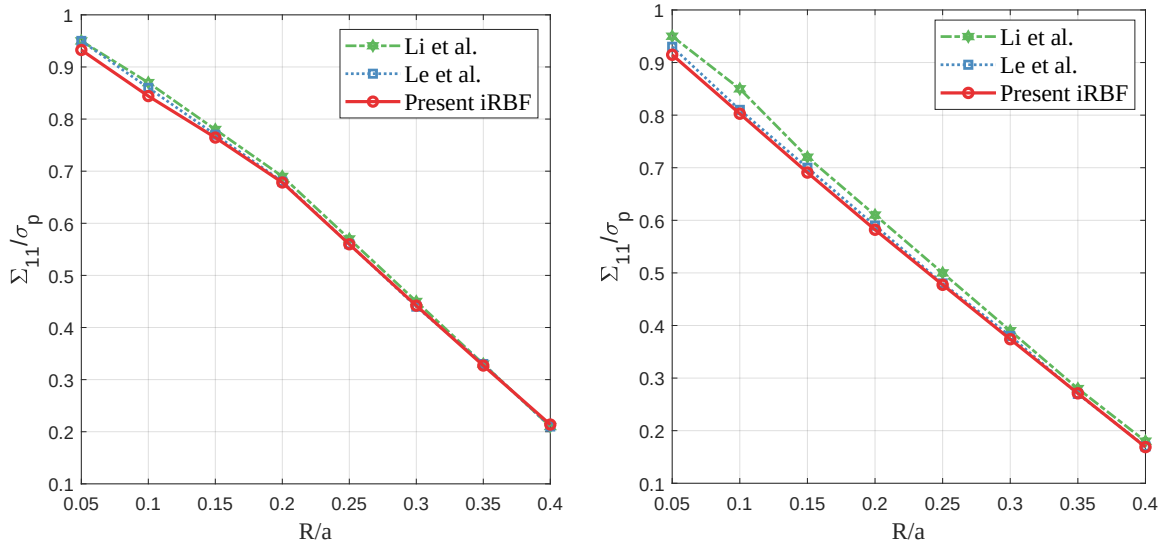

(a) $\theta = 0^o$ (b) $\theta = 45^o$

Figure 6.5: Circular hole RVE: limit uniaxial strength Σ_{11} in comparison with other procedures

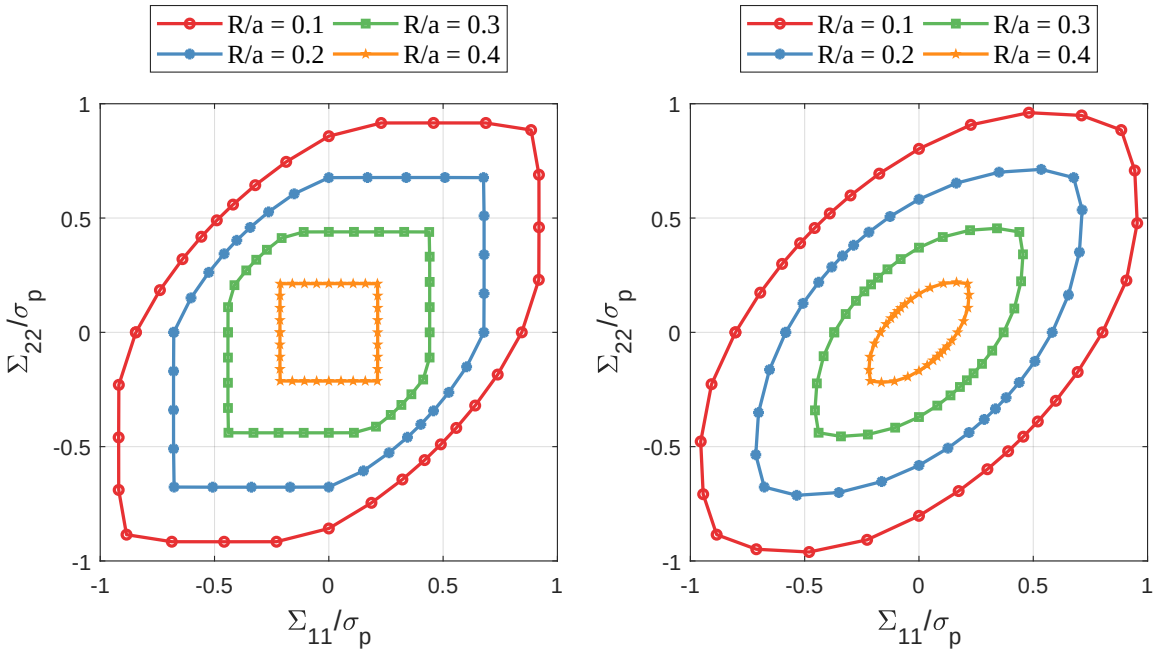

(a) $\theta = 0^o$ (b) $\theta = 45^o$

Figure 6.6: Circular hole RVE: limit macroscopic strength domain with different values of fraction R/a and loading angle θ

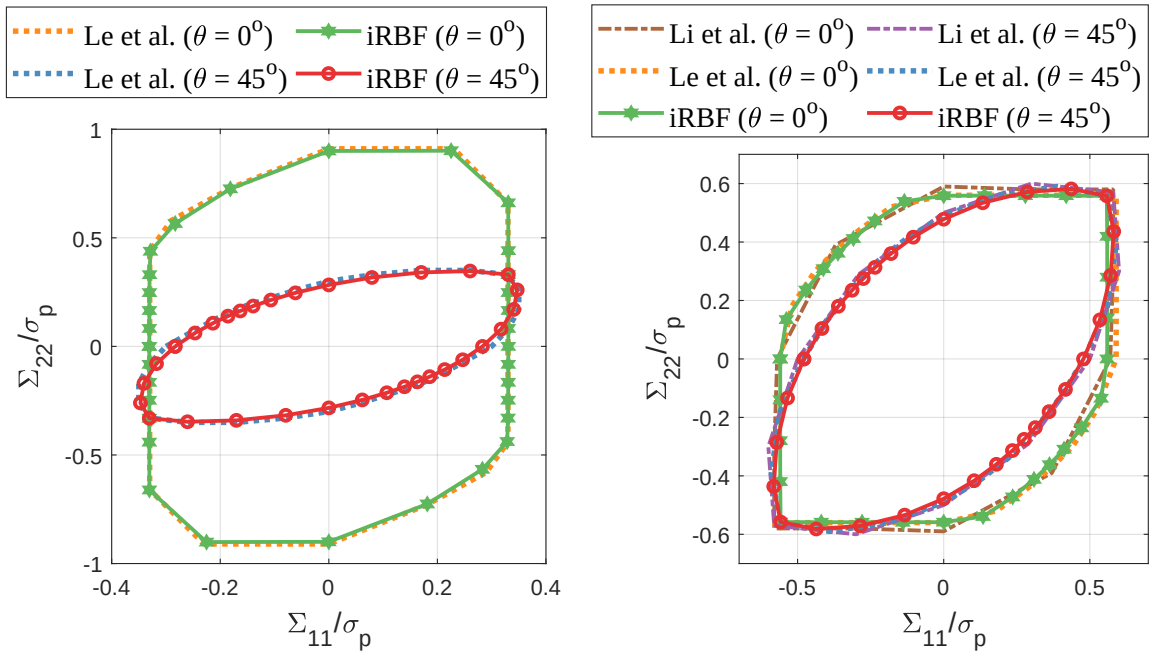

(a) Rectangular hole RVE (b) Circular hole RVE

Figure 6.7: Perforated materials: macroscopic strength domain at limit state

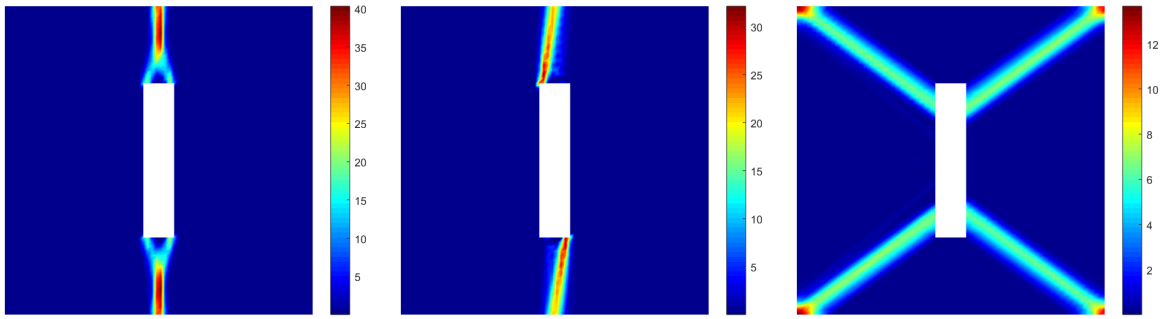

(a) $\theta = 0^o$ (b) $\theta = 45^o$ (c) $\theta = 90^o$

Figure 6.8: Rectangular hole RVE ($L_1 \times L_2 = 0.1 \times 0.5$ mm): the distribution of plastic dissipation

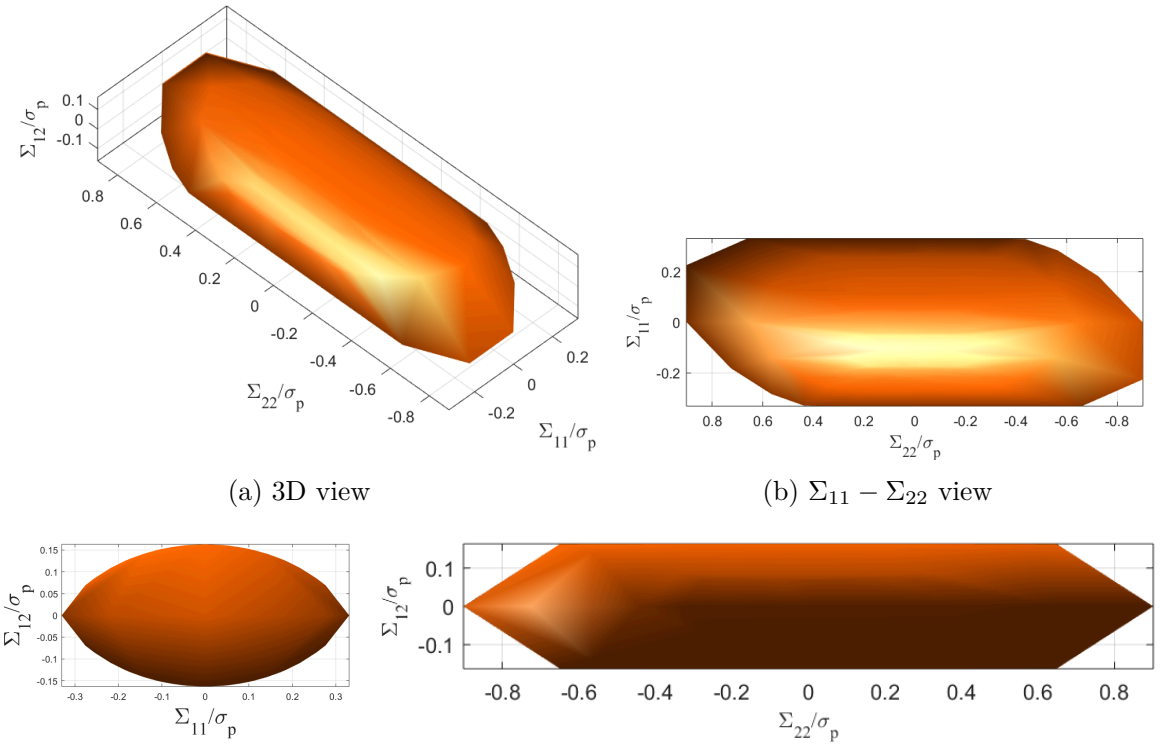

(a) 3D view (b) $\Sigma_{11} - \Sigma_{22}$ view

(c) $\Sigma_{11} - \Sigma_{12}$ view (d) $\Sigma_{22} - \Sigma_{12}$ view

Figure 6.9: Rectangular hole RVE: macroscopic strength domain under three-dimensions loads ($\Sigma_{11}, \Sigma_{12}, \Sigma_{22}$)

In addition, the approximate macroscopic strength domain of perforated materials with rectangular hole ($L_1 \times L_2 = 0.1 \times 0.7$ mm) and circle hole ($R = 0.25 \times a$) for angles of $\theta = 0^o$ and $\theta = 45^o$ are illustrated in Figure 6.7. The strength in Σ_{22} direction is greater than that in Σ_{11} direction in case of rectangular hole RVE, whereas those are equivalent in case of circular hole RVE. Figures 6.9 and 6.11 plot

the macroscopic strength domain in limit state of both perforated models under three-dimensions of applied loading $(\Sigma_{11}, \Sigma_{22}, \Sigma_{12})$. The plastic dissipation distributions representing the failure mechanism of RVEs are also presented in Figures 6.8 and 6.10.

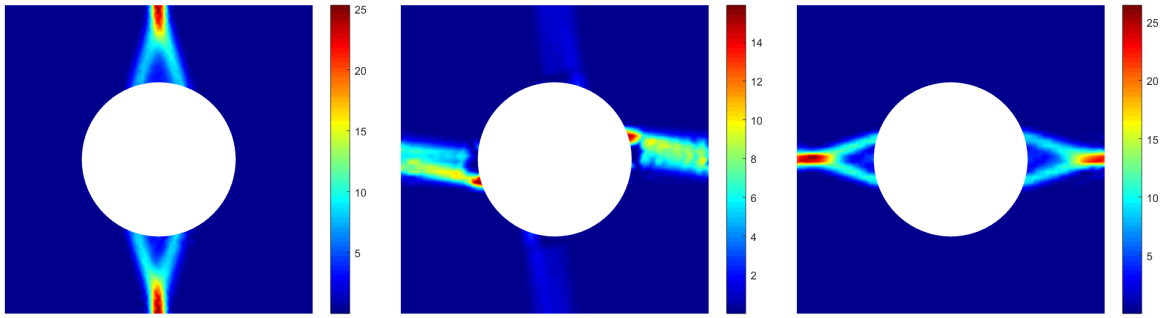

(a) $\theta = 0^o$ (b) $\theta = 45^o$ (c) $\theta = 90^o$

Figure 6.10: Circular hole RVE ($R = 0.25 \times a$): the distribution of plastic dissipation

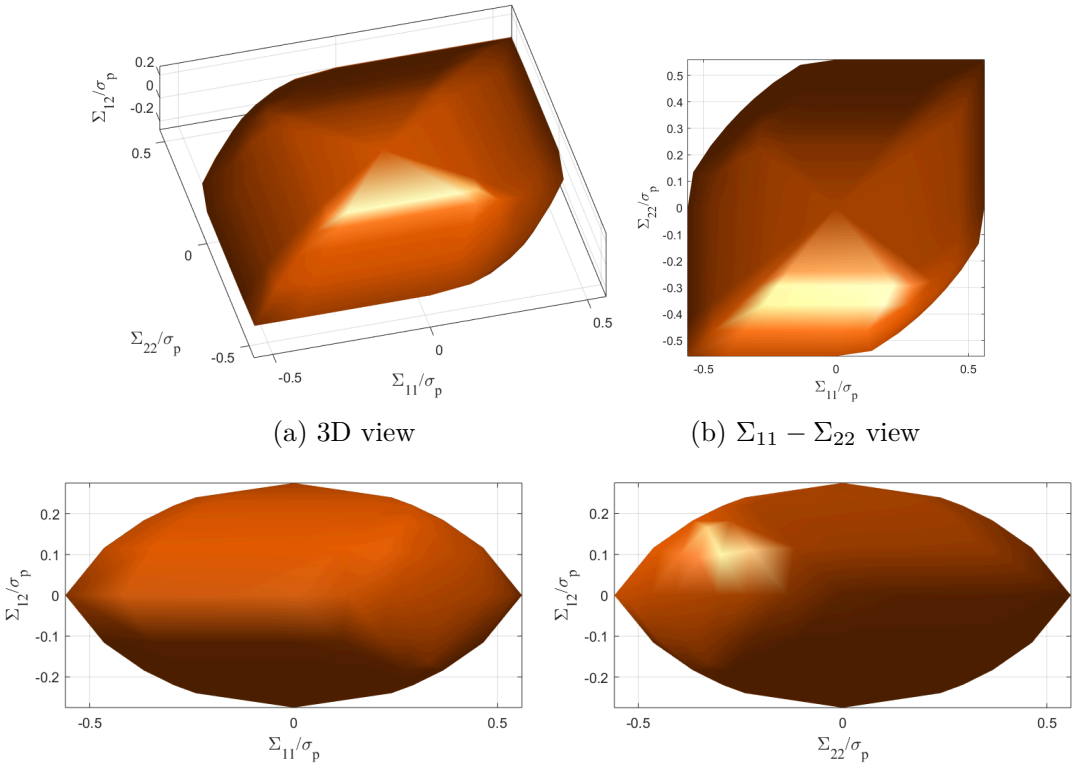

(a) 3D view (b) $\Sigma_{11} - \Sigma_{22}$ view

(c) $\Sigma_{11} - \Sigma_{12}$ view (d) $\Sigma_{22} - \Sigma_{12}$ view

Figure 6.11: Circular hole RVE: macroscopic strength domain under three-dimensions loads $(\Sigma_{11}, \Sigma_{12}, \Sigma_{22})$

6.4.2 Metal with cavities

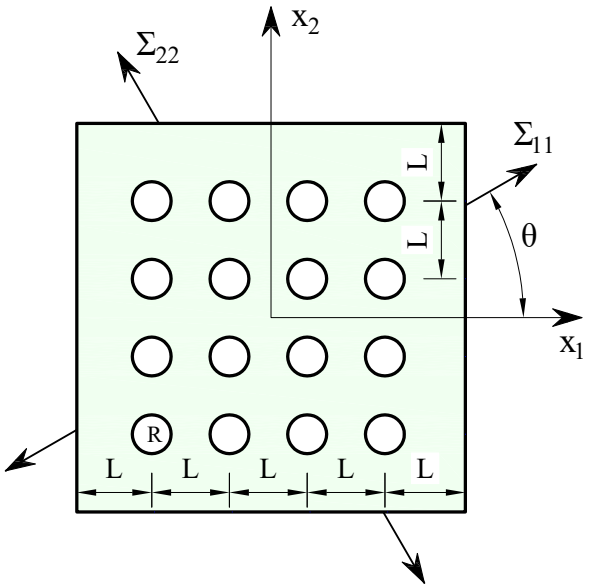

Figure 6.12: Metal sheet with cavities: geometry and loading

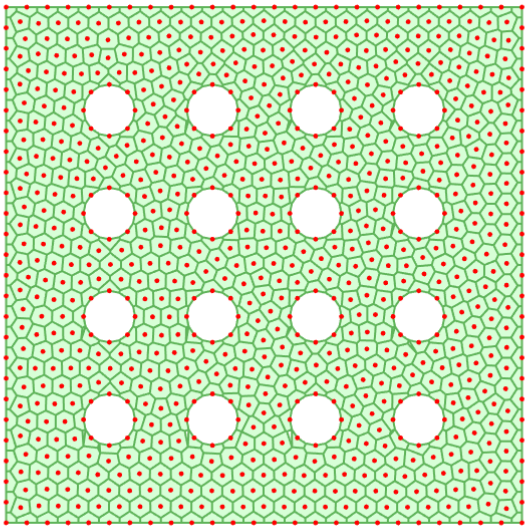

(a) Nodal discretization

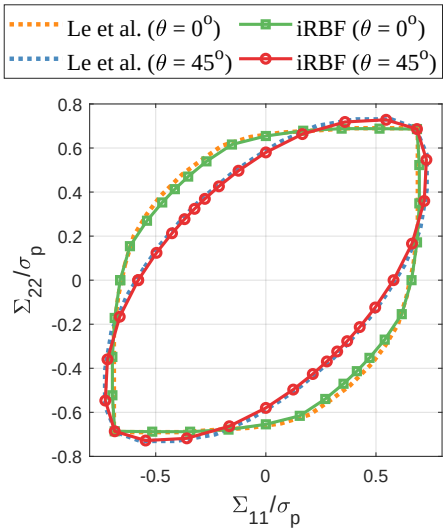

(b) Limit strength domain of macroscopic load: iRBF versus FEM [126]

Figure 6.13: Metal with cavities: nodal discretization and macroscopic strength domain

This example examines a perforated metal sheet with 4×4 holes regularly arranged in plane (x_1, x_2) as seen in Figure 6.12. The sheet of metal has dimension $a \times a$, the radius of holes and the distances are chosen such that $L/a = 0.2$ and $R/a = 0.05$. The square pattern is subjected to a set of orthogonal load $(\Sigma_{11}, \Sigma_{22})$,

in which the angle made by Σ_{11} and x_1-axis is θ. Assuming that material obeys the von Mises criterion. The nodal discretization of computational domain is presented in Figure 6.13(a).

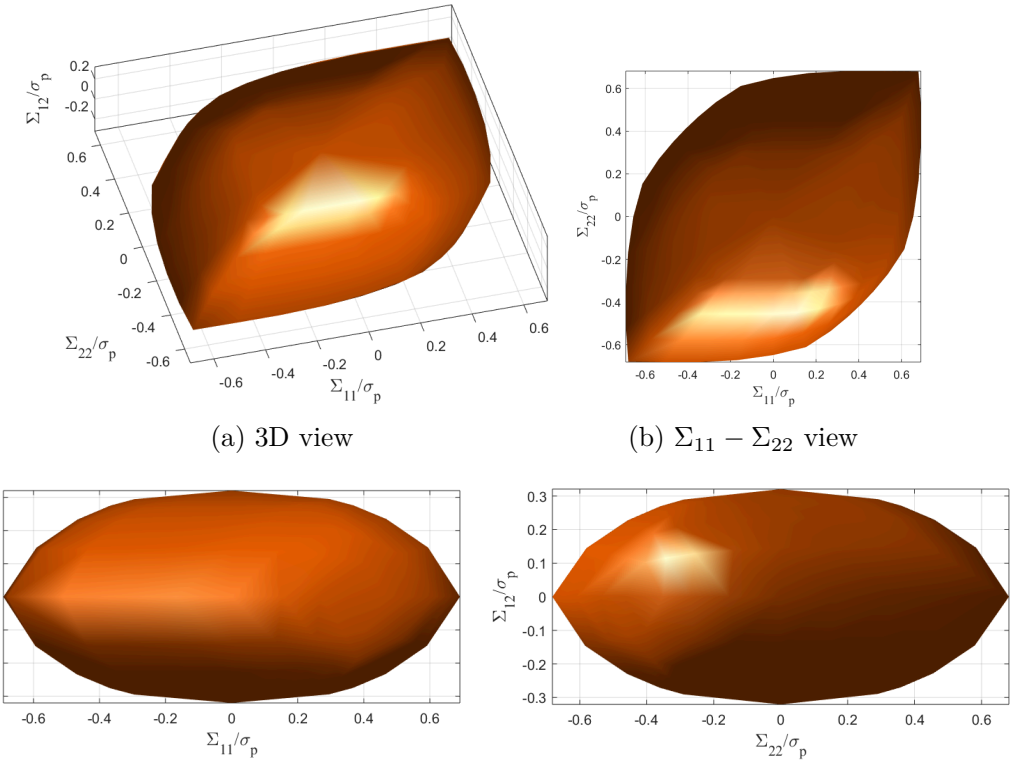

(a) 3D view (b) $\Sigma_{11} - \Sigma_{22}$ view

(c) $\Sigma_{11} - \Sigma_{12}$ view (d) $\Sigma_{22} - \Sigma_{12}$ view

Figure 6.14: Metal with cavities: macroscopic strength domain under three-dimensions loads $(\Sigma_{11}, \Sigma_{12}, \Sigma_{22})$

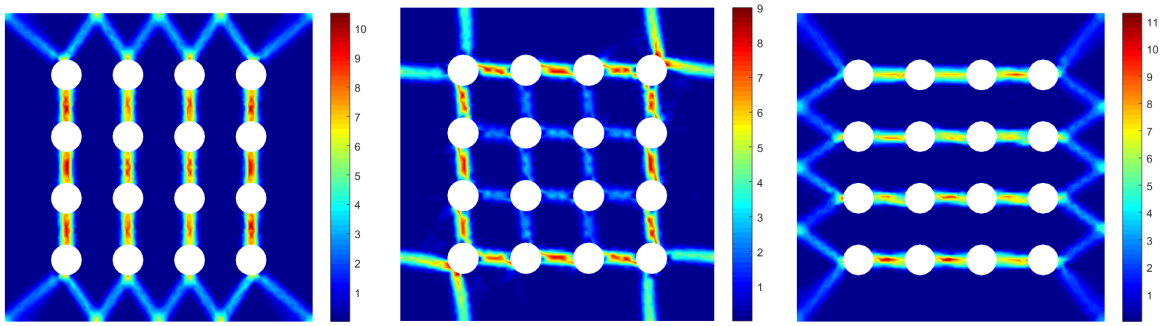

(a) $\theta = 0$ (b) $\theta = 45^o$ (c) $\theta = 90^o$

Figure 6.15: Metal with cavities: the distribution of plastic dissipation

The problem has been study in [126], and the comparison of the approximate macroscopic strength domain obtained by iRBF method and those reported in [126]

is expressed in Figure 6.13(b). From the figure, it can be observed that present solutions well agree with results in [126]. The limit domain of macroscopic strength for case of three dimension of applied load $(\Sigma_{11}, \Sigma_{22}, \Sigma_{12})$ are presented in Figure 6.14. The distribution of plastic dissipation corresponding to different values of loading angle θ are also plotted in Figure 6.15. It is easy to see that the yield zone makes the lines connecting holes and the boundary of RVE.

6.4.3 Perforated material with different arrangement of holes

This section considers a perforated material with two circular holes arranged such that the line connecting their centroid forms with x_1 axis an angle φ, and the effect of hole's arrangement on the bearing capacity of macro-structures is investigated. The micro-structure is subjected to the macroscopic tensile load as Figure 6.16.

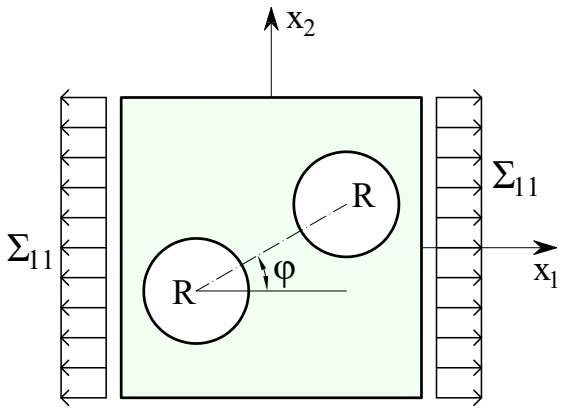

Figure 6.16: Perforated material with two hole: geometry and loading

Denoting V_f for the volume fraction of void, the centroid's coordinates of holes and their radius can be determined by

$$\begin{aligned} x_{1i} &= \pm(0.05 + R)\cos\varphi, \quad \text{i=1,2} \\ y_{1i} &= \pm(0.05 + R)\sin\varphi, \quad \text{i=1,2} \end{aligned} \qquad \text{and} \quad R = \sqrt{\frac{V_f}{2\pi}} \tag{6.17}$$

Various values of angle φ for different volume of voids are studied. Figure 6.17 clearly illustrates the decrease of macroscopic tensile strength when increasing the angle φ for all cases of V_f. The numerical solutions are also compared with those reported in [126], and the agreement of solutions demonstrates the resonability of present results. The plastic dissipation distribution for the volume fraction $V_f = 0.2$

are plotted in Figure 6.18. The results point out that the failure mechanism as well as the the strength of macro-structures is significantly affected by the change of the void's location in micro-scale level.

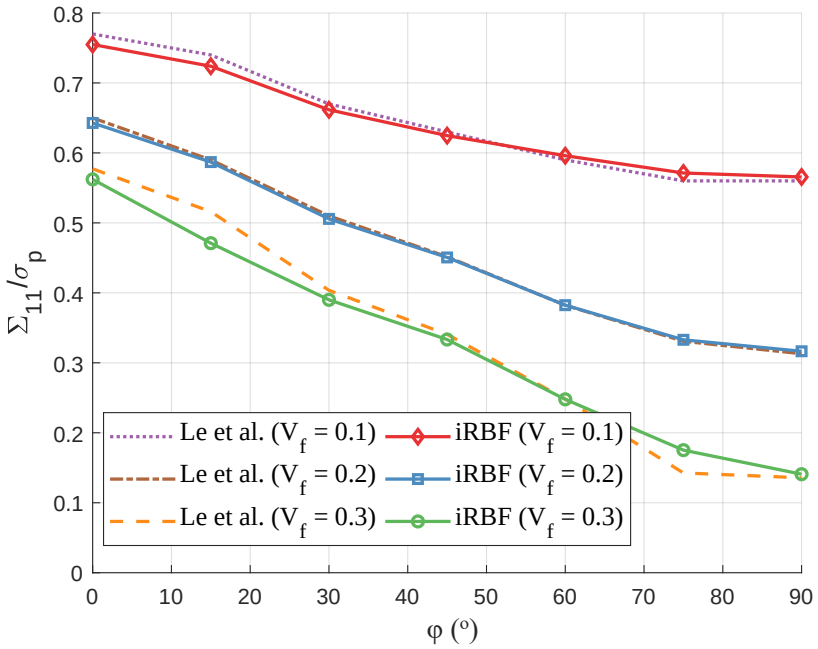

Figure 6.17: Perforated material with two hole: the comparison of macroscopic strengths obtained using iRBF and FEM in [126]

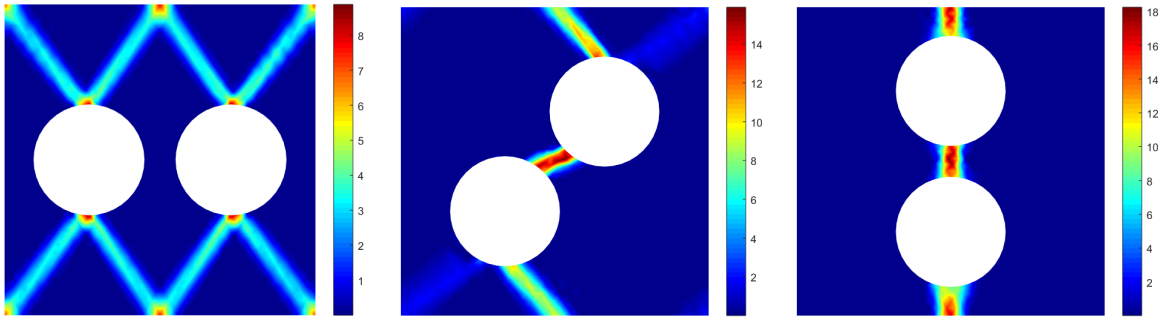

(a) $\varphi = 0^0$ (b) $\varphi = 45^o$ (c) $\varphi = 90^o$

Figure 6.18: Perforated material with two hole: the distribution of plastic dissipation

6.5 Conclusions

The plastic limit strength and the collapse mechanism of materials has been studied using the combination of direct analysis and homogenization theory. By

means of second-order cone programming and the iRBF approximation, the resulting optimization problems are kept in minimum size and solved rapidly. The good agreement of numerical solutions in comparison with other studies shows the computational efficiency of proposed method. In future work, the plane strain or three-dimensions problems, in where the volumetric locking phenomena is required to be handled, are extended. In addition, more complicate effects, e.g. material interfaces, multiple crack or even variable loading should be considered.

Chapter 7

Discussions, conclusions and future work

In this thesis, a novel numerical method employing the combination of the integrated radial basis function-based mesh-free method and second-order cone programming is developed for limit and shakedown analysis. The application of proposed approach for various problems regarding to structures and materials has been investigated in chapters 3, 4, 5 and 6. The current chapter expresses several discussions on the major issues arising during the course of the research, thereby both advantages and disadvantages of present procedure are outlined. Then, the contributions of this study are summarized, and several suggestions for future work are recommended.

7.1 Discussions

7.2 The convergence and reliability of obtained solutions

In this thesis, the iRBF method is developed for both displacement and equilibrium formulations of direct analysis, for which the strictly lower-bound and upper-bound models are applied in chapters 3, 4 and 6, whereas the quasi-lower bound one is employed in chapter 5.

Theoretically, for all models used, the numerical solutions converge to the exact value when increasing the nodal distribution, but using different formulations, the convergence behaviour is different as illustrated in Figure 7.1. Usually, the upper bound solutions approach to the actual collapse load multiplier from above, while the lower bound results converge from bellow as seen in chapters 3 and 4. However, owing to the approximation of displacement field and equilibrium equations are satisfied in a weak form, the equilibrium formulation in chapter 5 provides solu-

tions converging from above. It is interesting to note that although the analytical solutions are not available for almost practical engineering problems, the mean values of numerical solutions independently obtained using reliable upper bound and lower bound estimations can be recommended as actual safety loads for the use in structural design.

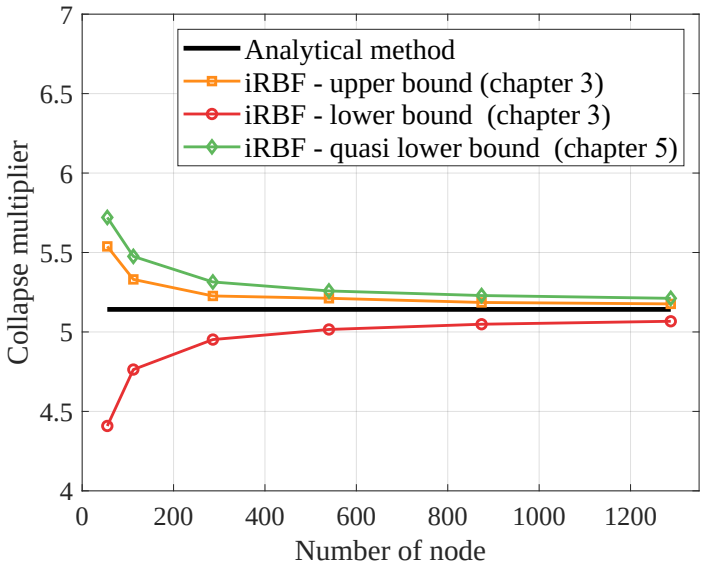

Figure 7.1: Convergent study (Prandtl's problem in chapters 3 and 5)

The numerical solutions of limit and shakedown analysis for various benchmark problems using the iRBF method with 2D and 3D discretizations have been reported in this thesis. In several problems, e.g. in sections 3.3.1, 4.3.1, 5.3.1 and 5.3.2, present solutions are priorly compared to the available analytical those in the literature in order to examine the accuracy of numerical results. It is important to note that, all relative errors are less than 1%, especially in sections 4.3.1, and 5.3.2, these errors are approximate 0%. The good agreement of proposed method in comparison with other studies, in which both analytical and numerical schemes are used, demonstrates the reliability of the approach.

7.2.1 The advantages of present method

As clarified, the most attractive feature of direct methods is the capability to assess the ultimate state of structures or materials without the step-by-step analysis, and not only safety load multipliers but also collapse mechanics of the structural systems are determined effectively. The positives of proposed method are offered by

a robust numerical approximation scheme and a powerful mathematical tool, that will be discussed following.

For one thing, there is the matter of the mesh in numerical discretization. As known, physical problems are usually expressed in terms of partial differential equations (PDEs), but that cannot be solved with analytical approach in almost situations. As a result, PDEs need to be treated using approximations typically based upon different types of discretizations. Traditionally, a favorite scheme, which is commonly employed in mesh-base methods, e.g. FEM, FVM or BEM, is that the physical domain is subdivided into a finite discrete elements connected together at nodes. The priori definition of nodal connectivity is known as the mesh permitting the compatibility of the interpolation and making the resulting approximation be continuous. In general, mesh-based methods are robust particularly for mechanical analysis; however, the creation of the mesh may become the major one of the total cost in whole process of the numerical implementation. On contrary, from the practical standpoint, the absence of the mesh in iRBF method is an attractive feature, decreasing the computational cost of such problems.

One more competitive advantage of iRBF method in comparison with mesh-based ones as well as other mesh-free schemes gains from the shape function. In traditional numerical procedures as FEM, the shape function of a node has low-order and only affects on elements attached to it, while in the meshless methods, the shape function can be flexibly constructed, i.e. the ability to create overlapping nodal influent domain increasing the continuity of approximation, or the initiative in choosing the order of functions. In mesh-free methods, the high-order shape function not only help to provide the highly accurate solution with rapid convergent rate, but also gives the effective treatment for the volumetric locking phenomena in solid mechanics problems. In this study, the iRBF method is constructed based on the multiple integration. As a result, its order is higher than other meshless ones, e.g. RPIM when using similar basis function. The better performance of present method compared to RPIM has been reported in section 5.3.1, i.e., iRBF method takes less CPU-time to provide more accurate and rapidly convergent results than RPIM when using the same nodal distribution.

Moreover, with the use of iRBF method in combination with second order cone programming and collocation procedure, number of variables required for the resulting optimization problems can be reduced significantly. It is worth noting that

using present formulation, the optimization problems with thousand variables can be speedily solved in seconds. The advantage of proposed approach in terms of computational cost was clearly discussed in chapters 3, 4, 5 and 6. For instance, in chapter 4, an application to limit state analysis of reinforced concrete slabs has been presented. There is only transverse velocity in need to be approximated; therefore the total number of variables in the resultant optimization problem is kept minimum, i.e. equal to the number of discretized nodes in the problem domain. In section 4.3.1, present method was compared with a finite element method named CS-HCT [208] and a mesh-free one so-called EFG [209]. Clearly, the solutions from three methods converge to similar values, but generally, iRBF formulation shows more efficiently than those of [208, 209] (both CPU-time and number of variables).

In addition, the advantage of the iRBF method over the EFG and almost mesh-free approaches is that iRBF shape function satisfies Kronecker-delta property; and therefore, there is no need of any special treatment when enforcing boundary conditions.

Last but not least is the improvement of iRBF method itself using stabilized conforming nodal integration technique. The collocation method is employed in this thesis, meaning that all conditions are directly satisfied at discretized nodes in problem domain. However, in chapter chapters 3 and 4, with the use of classical iRBF formulation, the global nodal influent domain is employed to ensure the accuracy of solutions, resulting in dense matrices included in optimization problems. Whereas, using iRBF method combined with SCNI scheme, which is so-called stabilized iRBF, in chapters 5 and 6, only the local domain is required in the approximation, and those matrices become sparse, decreasing the computer memory and CPU-time in solving process significantly. The advantage of stabilized iRBF in comparison with classical iRBF is clearly pointed out in section 5.3.1. It can be observed that solutions obtained from both models of iRBF method converge to the analytical one, but the local iRBF formulation with the support of SCNI provides the improvement of computational efficiency concerning accuracy and time taken for resulting optimization problem when using similar basis (nodal distribution and shape parameter).

7.2.2 The disadvantages of present method

The advantages and disadvantages of iRBF method are generated from the key difference of mesh-free procedures and mesh-based ones, i.e. the shape function and strategy to construct it. In previous section, the positive features of proposed method are discussed, now the negative those will be focused on.

Generally, the high-order shape function makes iRBF method as well as mesh-free ones more advantageous compared to mesh-base procedures to provide the accurate solutions with the speed convergence. The only disadvantage here is that it takes more computational run-time, and thus the cost of these process is still high. However, that is not the major obstacle of this study since the biggest challenge of direct analysis is dealing with the optimization problems accounting the most of overall cost. Employing the combination of stabilized iRBF approach and primal-dual interior-point SOCP algorithm, the resulting formulation is kept in minimum size and then solved rapidly using the highly efficient solvers.

Another limitation of meshless methods preventing the acceptance of the engineering community is that there are several factors affecting on the accuracy of outcomes must be priorly selected, for instance, the influence domain size or the coefficients of the shape function. A set of factors for one case may not work correctly for another ones, i.e., in case of elastic analysis, the dimensionless parameters should be chosen as $(\alpha_s = 10^{-5} \div 2.5, \beta_s = 3)$; whereas in direct analysis, those values are given as $(\alpha_s = 10^{-5} \div 2, \beta_s = 6)$ for structure scale and $(\alpha_s = 10^{-5}, \beta_s = 3)$ for material scale. It is difficult to find out a unified standard of approximation properties for all practical problems. In literature, the gap for choice is determined by trial and error.

In short, besides many advantages of computational aspect, there are several matters needed to be overcome in iRBF as well as other mesh-free approximation techniques. However, it should be realized that mesh-free methods are still in their infancy. They are being continuously improved to be integrated into commercial software packages for structural design.

7.3 Conclusions

The major objective of the research is to develop a robust numerical approach for direct analysis of structures and materials widely used in practical engineering, resulting in the use of iRBF-based meshless procedure and the primal-dual second order cone programming algorithm in the thesis. Detailed conclusions on specific problems are presented in chapters 3, 4, 5 and 6. This chapter will give the outline of the remarkable points following.

Firstly, this is the first time the iRBF mesh-free method combined with stability conforming nodal integration (SCNI) is developed to deal with the problems in the area of limit and shakedown analysis of structures and materials. The iRBF shape function is used to approximate the displacement as well as stress fields. The advantages of such procedure can be summarized as follows

- Unlike the traditional iRBF approach, for which the constrains in problems are imposed at various Gauss points, using the collocation method and SCNI scheme in this study, the kinematic and equilibrium conditions as well as the numerical integration in resulting optimization problems can be directly applied at scattered nodes, making proposed method truly mesh-free and reducing the size of formulated problems.

- The high-order iRBF shape functions are constructed on the overlapping influence domains, thus the enforcement of discontinuous condition at the interfaces of neighbour computational cells is not necessary.

- The high-order iRBF shape functions help to keep total number of variables to a minimum, i.e. for the kinematic discretization of bending slabs in chapter 4, only one degree of freedom (deflection) needs to be approximated instead of three those (deflection and two rotations) as in finite element method.

- The shape function satisfies Kronecker-delta property, which is absent in almost meshless procedures. As a result, the essential boundary conditions in problems can be similarly imposed as in finite element formulation. This characteristic also makes the matrices spare, decreasing the CPU run-time in whole solving process.

Secondly, by mean of conic algorithm, the largest obstacle in direct analysis is

overcome. The optimization problems are cast as second order cone programming, and then solved using an efficient commercial software package named Mosek. The numerical examples investigated in the thesis show that with the use of primal-dual interior point algorithm, a problem with thousand variables can be solved in seconds, proving that present method can be applied for large scale problems in engineering practice.

In conclusion, the combination of stabilized iRBF-based mesh-free method and SOCP algorithm results in a robust numerical procedure for limit and shakedown analysis, for which not only the safety loads are rapidly determined, but also the collapse mechanics of structures and the yield surface of heterogeneous materials are effectively captured. The good agreement in comparison with the analytical approach as well as other numerical schemes in literature fully justifies the computational effects of proposed method.

7.4 Suggestions for future work

Although present research has met most of initial objectives, there are several issues needed to be overcome in future works, and there are some techniques are able to be applied to improve the computational aspect of proposed method. Following extensions are recommended for further development of present work.

As mentioned, in iRBF procedures as well as other mesh-free methods, the shape parameters and influent domain size impact on the accuracy and stability of outcomes significantly. However, those factors are variable, and there are not any common standard for choice yet. In most studies, the well-known strategy is selecting form a gap determining by trial and error. It is important to find out an efficient algorithm to optimize those values and discover an appropriate interval for almost problems. That is interesting topic to be taken into account in further studies.

Taking advantage of a positive feature of mesh-free methods, i.e. the absence of the mesh in numerical discretization, the adaptive technique, especially *h-adaptivity*, may be easily applied for the implementation of iRBF procedure. The natural conforming property of mesh-free approximations make the use of *h-adaptivity*, for which only nodes have to be added, comparably simple. Also, conceptually, the application of *p-adaptivity* in meshless methods is simpler than in mesh-based ones, there are only additional enrichment is required to be added to the basis function.

Based on a posterior error estimation, adaptive scheme will automatically refine at indicated locations, e.g. plastic zone, and leave out the refinement at other regions within the problem domain. Consequently, the convergence rate is improved, and the cost of computation can be reduced. It would be relevant to extend adaptive strategy to iRBF formulation for direct analysis of engineering structures.

Moreover, there are various practical engineering problems for which this thesis cannot cover, for instance, fracture problem - an interesting topic in solid mechanics. In fact, traditional methods as FEM are not well suit for the treatment of discontinuities which do not coincide to the original mesh line, leading to the development of the so-call eXtended Finite Element Method (XFEM) which is demonstrated to be an effective solution for crack problem. In further studies, an extension of enrich technique from XFEM to iRBF approximation could be a good idea for limit and shakedown analysis of fracture structures using iRBF approach.

Furthermore, in computational homogenization analysis of materials, only plane stress problems are investigated. In future works, the plane strain or three dimensions problems, where the volumetric locking needed to be handled, will be extended. The more complicate effects such as variable, cyclic or repeat loading, or even materials with diverse constitutes including material interfaces, multiple crack may be also considered in the problems.

List of publications

The results from parts of thesis have been presented at the national & international conferences and published in the domestic & international journals.

International peer-reviewed journals

1. P. L. H. Ho, C. V. Le, and T. Tran-Cong, "Displacement and equilibrium mesh-free formulation based on integrated radial basis functions for dual yield design," *Engineering Analysis with Boundary Elements*, vol. 71, pp. 92–100, Oct. 2016.

2. P. L. H. Ho, C. V. Le, and T. Tran-Cong, "Limit state analysis of reinforced concrete slabs using an integrated radial basis function based mesh-free method," *Applied Mathematical Modelling*, vol. 53, pp. 1–11, Jan. 2018.

3. P. L. H. Ho, and C. V. Le, "A stabilized iRBF mesh-free method for quasi-lower bound shakedown analysis of structures," *Computers and Structures*, vol. 228, pp. 106157, 2020.

4. P. L. H. Ho, C. V. Le, and Phuong H. Nguyen. "Kinematic yield design computational homogenization of micro-structures using the stabilized iRBF mesh-free method," *Applied Mathematical Modelling*, revised.

Domestic journals

1. P. L. H. Ho, C. V. Le, and H. D. Phan, "A computational homogenization analysis of materials using the stabilized mesh-free method based on the radial basis functions," *Journal of Science and Technology in Civil Engineering*, vol. 14(1), pp. 65-76, 2020.

International conferences

1. P. L. H. Ho, C. V. Le, and T. Tran-Cong, "Upper-bound limit analysis of plane problems using radial basis function based mesh-free method," *In proceedings of The 2nd International Conference on Computational Science and Engineering*, Ho-Chi-Minh City, Vietnam, Aug. 2014.

2. P. L. H. Ho, and C. V. Le, "Computation of lower bound limit load using radial point interpolation method," *In proceedings of The International Conference On Multiphysical Interaction And Environment*, Vinhlong, Vietnam, Mar. 2015.

National conferences

1. P. L. H. Ho, and C. V. Le, "A multiple basis functions based mesh-free method for lower bound limit analysis," *National conference of Solid Mechanics*, Da-Nang, 06-07/08/2015.

2. P. L. H. Ho, C. V. Le, and T. Tran-Cong, "The shakedown state analysis of structures using an equilibrium mesh-free formulation based on the integrated radial basis functions," *The 10th National conference on Mechanics*, Hanoi, 8-9/12/2017.

3. P. L. H. Ho, P. H. Nguyen, C. V. Le, H. D. Phan, and T. Tran-Cong, "A computational homogenization analysis of materials using the integrated radial basis functions-based meshless method," *The 2nd National conference on Engineering Mechanics*, Hanoi, 6/4/2019.

4. P. L. H. Ho, C. V. Le, and H. D. Phan, "A computational homogenization analysis of materials using the stabilized mesh-free method based on the radial basis functions," *The 3rd Conference on Civil Technology*, Ho-Chi-Minh City, 20/9/2019.

Bibliography

[1] D. Drucker, W. Prager, and H. Greenberg, "Extended limit design theorems for continuous media," *Quarterly of applied mathematics*, vol. 9, no. 4, pp. 381–389, 1952.

[2] R. Hill, "The mathematical theory of plasticity," *Bull. Amer. Math. Soc*, vol. 58, pp. 507–512, 1952.

[3] W. Prager, "Limit analysis: the development of a concept," *Problems of Plasticity*, pp. 3–24, 1972.

[4] J. B. Martin, *Plasticity: fundamentals and general results*. MIT press, 1975.

[5] P. G. Hodge, "Plastic analysis of structures," 1959.

[6] P. Hodge Jr, "The mises yield condition for rotationally symmetric shells," *Quarterly of Applied Mathematics*, vol. 18, no. 4, pp. 305–311, 1961.

[7] P. G. Hodge, *Limit analysis of rotationally symmetric plates and shells*. Prentice-Hall, 1963.

[8] C. Massonnet and M. Save, *Calcul plastique des constructions: Structures dépendant d'un paramètre*. Centre Belgo-Luxembourgeois d'Information de l'Acier, 1967.

[9] M. A. Save, C. E. Massonnet, and C. Massonnet, *Plastic analysis and design of plates, shells and disks*, vol. 15. North-Holland, 1972.

[10] C. Massonnet, "Calcul plastique des constructions," tech. rep., Nelissen, 1976.

[11] J. Chakrabarty and W. Drugan, "Theory of plasticity," *Journal of Applied Mechanics*, vol. 55, p. 253, 1988.

[12] W. Chen and D. Han, "Plasticity for structural engineers. 1988," *Springer, New York*.

[13] J. Lubliner, "1990, plasticity theory. macmillan publishing company, new york,"

[14] E. Melan, *Theorie statisch unbestimmter Systeme aus ideal-plastischem Baustoff*. Holder-Pichler-Tempsky in Komm., 1936.

[15] W. T. Koiter, "General theorems for elastic plastic solids," *Progress of Solid Mechanics*, pp. 167–221, 1960.

[16] A. Sawczuk, "On incremental collapse of shells under cyclic loading," *Theory of Thin Shells*, pp. 328–340, 1969.

[17] D. A. Gokhfeld and O. Charniavsky, *Limit analysis of structures at thermal cycling*, vol. 4. Springer Science & Business Media, 1980.

[18] J. A. Konig, "On upper bounds to shakedown loads," *ZAMM-Journal of Applied Mathematics and Mechanics/Zeitschrift für Angewandte Mathematik und Mechanik*, vol. 59, no. 8, pp. 349–354, 1979.

[19] G. Maier, "Shakedown theory in perfect elastoplasticity with associated and nonassociated flow-laws: a finite element, linear programming approach," *Meccanica*, vol. 4, no. 3, pp. 250–260, 1969.

[20] S. Pycko and G. Maier, "Shakedown theorems for some classes of nonassociative hardening elastic-plastic material models," *International Journal of Plasticity*, vol. 11, no. 4, pp. 367–395, 1995.

[21] M. Heitzer, G. Pop, and M. Staat, "Basis reduction for the shakedown problem for bounded kinematic hardening material," *Journal of Global Optimization*, vol. 17, no. 1-4, pp. 185–200, 2000.

[22] D. Weichert, "On the influence of geometrical nonlinearities on the shakedown of elastic-plastic structures," *International Journal of Plasticity*, vol. 2, no. 2, pp. 135–148, 1986.

[23] D. Weichert and A. Hachemi, "Influence of geometrical nonlinearities on the shakedown of damaged structures," *International Journal of Plasticity*, vol. 14, no. 9, pp. 891–907, 1998.

[24] C. Polizzotto and G. Borino, "Shakedown and steady-state responses of elastic-plastic solids in large displacements," *International journal of solids and structures*, vol. 33, no. 23, pp. 3415–3438, 1996.

[25] D. Weichert, A. Hachemi, and F. Schwabe, "Shakedown analysis of composites," *Mech. Res. Commun.*, vol. 26, pp. 309–18, 1999.

[26] X.-Q. Feng and D. Gross, "A global/local shakedown analysis method of elastoplastic cracked structures," *Engineering fracture mechanics*, vol. 63, no. 2, pp. 179–192, 1999.

[27] A. Hachemi and D. Weichert, "Numerical shakedown analysis of damaged structures," *Computer Methods in Applied Mechanics and Engineering*, vol. 160, no. 1-2, pp. 57–70, 1998.

[28] M. Belouchrani and D. Weichert, "An extension of the static shakedown theorem to inelastic cracked structures," *International journal of mechanical sciences*, vol. 41, no. 2, pp. 163–177, 1999.

[29] M. Kleiber and J. Konig, "Incremental shakedown analysis in the case of thermal effects," *International Journal for Numerical Methods in Engineering*, vol. 20, no. 9, pp. 1567–1573, 1984.

[30] G. Borino, "Consistent shakedown theorems for materials with temperature dependent yield functions," *International Journal of Solids and Structures*, vol. 37, no. 22, pp. 3121–3147, 2000.

[31] P. D. Chinh, "Shakedown theory for elastic-perfectly plastic bodies revisited," *International journal of mechanical sciences*, vol. 45, no. 6-7, pp. 1011–1027, 2003.

[32] C. V. Le, T. Tran, and D. Pham, "Rotating plasticity and nonshakedown collapse modes for elastic–plastic bodies under cyclic loads," *International Journal of Mechanical Sciences*, vol. 111, pp. 55–64, 2016.

[33] E. Anderheggen and H. Knopfel, "Finite element limit analysis using linear programming," *International Journal of Solids and Structures*, vol. 8, no. 12, pp. 1413–1431, 1972.

[34] M. Cohn, "Engineering plasticity by mathematical programming," in *Proc. NATO Advanced Study Institute*, pp. 94–134, Pergamon Press, 1977.

[35] N. D. Hung, "Cepao—an automatic program for rigid-plastic and elastic-plastic analysis and optimization of frame structures," *Engineering Structures*, vol. 6, no. 1, pp. 33–51, 1984.

[36] S. Sloan, "Lower bound limit analysis using finite elements and linear programming," *International Journal for Numerical and Analytical Methods in Geomechanics*, vol. 12, no. 1, pp. 61–77, 1988.

[37] G. Maier, "A matrix structural theory of piecewise linear elastoplasticity with interacting yield planes," *Meccanica*, vol. 5, no. 1, pp. 54–66, 1970.

[38] F. Tin-Loi, "A yield surface linearization procedure in limit analysis," *Journal of Structural Mechanics*, vol. 18, no. 1, pp. 135–149, 1990.

[39] E. Christiansen, "Limit analysis of collapse states," *Handbook of numerical analysis*, vol. 4, pp. 193–312, 1996.

[40] V. F. Gaudrat, "A newton type algorithm for plastic limit analysis," *Computer methods in applied mechanics and engineering*, vol. 88, no. 2, pp. 207–224, 1991.

[41] N. Zouain, J. Herskovits, L. A. Borges, and R. A. Feijoo, "An iterative algorithm for limit analysis with nonlinear yield functions," *International Journal of Solids and Structures*, vol. 30, no. 10, pp. 1397–1417, 1993.

[42] Y. Liu, Z. Cen, and B. Xu, "Numerical limit analysis of cylindrical shells with part-through slots," *International journal of pressure vessels and piping*, vol. 64, no. 1, pp. 73–82, 1995.

[43] K. D. Andersen, "An efficient newton barrier method for minimizing a sum of euclidean norms," *SIAM Journal on Optimization*, vol. 6, no. 1, pp. 74–95, 1996.

[44] K. D. Andersen, E. Christiansen, and M. L. Overton, "Computing limit loads by minimizing a sum of norms," *SIAM Journal on Scientific Computing*, vol. 19, no. 3, pp. 1046–1062, 1998.

[45] D. Mackenzie and J. Boyle, "A method of estimating limit loads by iterative elastic analysis. i—simple examples," *International Journal of Pressure Vessels and Piping*, vol. 53, no. 1, pp. 77–95, 1992.

[46] A. Ponter and K. Carter, "Limit state solutions, based upon linear elastic solutions with a spatially varying elastic modulus," *Computer Methods in Applied Mechanics and Engineering*, vol. 140, no. 3-4, pp. 237–258, 1997.

[47] G. Maier, J. Pastor, A. Ponter, and D. Weichert, "Direct methods in limit and shakedown analysis," 2003.

[48] M. Boulbibane and A. Ponter, "Limit loads for multilayered half-space using the linear matching method," *Computers and Geotechnics*, vol. 32, no. 7, pp. 535–544, 2005.

[49] Y. Nesterov and A. Nemirovskii, *Interior-point polynomial algorithms in convex programming*, vol. 13. Siam, 1994.

[50] E. D. Andersen, C. Roos, and T. Terlaky, "On implementing a primal-dual interior-point method for conic quadratic optimization," *Mathematical Programming*, vol. 95, no. 2, pp. 249–277, 2003.

[51] A. Ben-Tal and A. Nemirovski, *Lectures on modern convex optimization: analysis, algorithms, and engineering applications*, vol. 2. Siam, 2001.

[52] J. Renegar, *A mathematical view of interior-point methods in convex optimization*, vol. 3. Siam, 2001.

[53] A. Makrodimopoulos and C. Bisbos, "Shakedown analysis of plane stress problems via socp," 2003.

[54] C. Bisbos, A. Makrodimopoulos, and P. M. Pardalos, "Second-order cone programming approaches to static shakedown analysis in steel plasticity," *Optimization Methods and Software*, vol. 20, no. 1, pp. 25–52, 2005.

[55] A. Makrodimopoulos, "Remarks on some properties of conic yield restrictions in limit analysis," *International Journal for Numerical Methods in Biomedical Engineering*, vol. 26, no. 11, pp. 1449–1461, 2010.

[56] P. G. Hodge and T. Belytschko, "Numerical methods for the limit analysis of plates," *Journal of Applied Mechanics*, vol. 35, no. 4, pp. 796–802, 1968.

[57] N. D. Hung, "Direct limit analysis via rigid-plastic finite elements," *Computer Methods in Applied Mechanics and Engineering*, vol. 8, no. 1, pp. 81–116, 1976.

[58] K. Krabbenhoft and L. Damkilde, "Lower bound limit analysis of slabs with nonlinear yield criteria," *Computers & structures*, vol. 80, no. 27-30, pp. 2043–2057, 2002.

[59] A. Lyamin and S. Sloan, "Lower bound limit analysis using non-linear programming," *International Journal for Numerical Methods in Engineering*, vol. 55, no. 5, pp. 573–611, 2002.

[60] C. V. Le, H. Nguyen-Xuan, and H. Nguyen-Dang, "Upper and lower bound limit analysis of plates using fem and second-order cone programming," *Computers & Structures*, vol. 88, no. 1-2, pp. 65–73, 2010.

[61] E. Anderheggen, "Finite element analysis assuming rigid-ideal-plastic material behavior," in *Finite Element Analysis Assuming Rigid-Ideal-Plastic Material Behavior*, pp. 1–17, Springer, 1977.

[62] K. Krabbenhoft, A. V. Lyamin, M. Hjiaj, and S. W. Sloan, "A new discontinuous upper bound limit analysis formulation," *International Journal for Numerical Methods in Engineering*, vol. 63, no. 7, pp. 1069–1088, 2005.

[63] A. Capsoni and L. Corradi, "A finite element formulation of the rigid–plastic limit analysis problem," *International Journal for Numerical Methods in Engineering*, vol. 40, no. 11, pp. 2063–2086, 1997.

[64] J. Bleyer and P. De Buhan, "On the performance of non-conforming finite elements for the upper bound limit analysis of plates," *International Journal for Numerical Methods in Engineering*, vol. 94, no. 3, pp. 308–330, 2013.

[65] A. Capsoni, "A mixed finite element model for plane strain limit analysis computations," *Communications in numerical methods in engineering*, vol. 15, no. 2, pp. 101–112, 1999.

[66] X. Yu and F. Tin-Loi, "A simple mixed finite element for static limit analysis," *Computers & structures*, vol. 84, no. 29-30, pp. 1906–1917, 2006.

[67] T. Belytschko, "Plane stress shakedown analysis by finite elements," *International Journal of Mechanical Sciences*, vol. 14, no. 9, pp. 619–625, 1972.

[68] V. Carvelli, Z. Cen, Y. Liu, and G. Maier, "Shakedown analysis of defective pressure vessels by a kinematic approach," *Archive of Applied Mechanics*, vol. 69, no. 9-10, pp. 751–764, 1999.

[69] A.-M. Yan and H. Nguyen-Dang, "Kinematical shakedown analysis with temperature-dependent yield stress," *International Journal for Numerical Methods in Engineering*, vol. 50, no. 5, pp. 1145–1168, 2001.

[70] D. Vu, A. Yan, and H. Nguyen-Dang, "A primal–dual algorithm for shakedown analysis of structures," *Computer Methods in Applied Mechanics and Engineering*, vol. 193, no. 42-44, pp. 4663–4674, 2004.

[71] D. K. Vu, M. Staat, and I. T. Tran, "Analysis of pressure equipment by application of the primal-dual theory of shakedown," *Communications in Numerical Methods in Engineering*, vol. 23, no. 3, pp. 213–225, 2007.

[72] J.-W. Simon, "Direct evaluation of the limit states of engineering structures exhibiting limited, nonlinear kinematical hardening," *International Journal of Plasticity*, vol. 42, pp. 141–167, 2013.

[73] J.-W. Simon and D. Weichert, "Numerical lower bound shakedown analysis of engineering structures," *Computer Methods in Applied Mechanics and Engineering*, vol. 200, no. 41-44, pp. 2828–2839, 2011.

[74] J.-W. Simon and D. Weichert, "Shakedown analysis of engineering structures with limited kinematical hardening," *International Journal of Solids and Structures*, vol. 49, no. 15-16, pp. 2177–2186, 2012.

[75] J.-W. Simon and D. Weichert, "Shakedown analysis with multidimensional loading spaces," *Computational Mechanics*, vol. 49, no. 4, pp. 477–485, 2012.

[76] J.-W. Simon and D. Weichert, "Interior-point method for lower bound shakedown analysis of von mises-type materials," in *Limit State of Materials and Structures*, pp. 103–128, Springer, 2013.

[77] T. Tran, C. Le, D. Pham, and H. Nguyen-Xuan, "Shakedown reduced kinematic formulation, separated collapse modes, and numerical implementation," *International Journal of Solids and Structures*, vol. 51, no. 15-16, pp. 2893–2899, 2014.

[78] C. V. Le, H. Nguyen-Xuan, H. Askes, S. P. Bordas, T. Rabczuk, and H. Nguyen-Vinh, "A cell-based smoothed finite element method for kinematic limit analysis," *International Journal for Numerical Methods in Engineering*, vol. 83, no. 12, pp. 1651–1674, 2010.

[79] C. V. Le, H. Nguyen-Xuan, H. Askes, T. Rabczuk, and T. Nguyen-Thoi, "Computation of limit load using edge-based smoothed finite element method and second-order cone programming," *International Journal of Computational Methods*, vol. 10, no. 01, p. 1340004, 2013.

[80] T. N. Tran, G. Liu, H. Nguyen-Xuan, and T. Nguyen-Thoi, "An edge-based smoothed finite element method for primal–dual shakedown analysis of structures," *International Journal for Numerical Methods in Engineering*, vol. 82, no. 7, pp. 917–938, 2010.

[81] H. Nguyen-Xuan, T. Rabczuk, T. Nguyen-Thoi, T. Tran, and N. Nguyen-Thanh, "Computation of limit and shakedown loads using a node-based smoothed finite element method," *International Journal for Numerical Methods in Engineering*, vol. 90, no. 3, pp. 287–310, 2012.

[82] P. Ho, C. Le, and T. Chu, "The equilibrium cell-based smooth finite element method for shakedown analysis of structures," *International Journal of Computational Methods*, vol. 16, no. 05, p. 1840013, 2019.

[83] G. Maier and C. Polizzotto, "A boundary element approach to limit analysis," *Boundary Elements*, pp. 551–566, 1983.

[84] T. Panzeca, "Shakedown and limit analysis by the boundary integral equation method," *European journal of mechanics. A. Solids*, vol. 11, no. 5, pp. 685–699, 1992.

[85] X. Zhang, Y. Liu, and Z. Cen, "Boundary element methods for lower bound limit and shakedown analysis," *Engineering Analysis with Boundary Elements*, vol. 28, no. 8, pp. 905–917, 2004.

[86] Y. Liu, X. Zhang, and Z. Cen, "Numerical determination of limit loads for three-dimensional structures using boundary element method," *European Journal of Mechanics-A Solids*, vol. 23, no. 1, pp. 127–138, 2004.

[87] Y. Liu, X. Zhang, and Z. Cen, "Lower bound shakedown analysis by the symmetric galerkin boundary element method," *International Journal of Plasticity*, vol. 21, no. 1, pp. 21–42, 2005.

[88] S.-T. Zhou and Y.-H. Liu, "Upper-bound limit analysis based on the natural element method," *Acta Mechanica Sinica*, vol. 28, no. 5, pp. 1398–1415, 2012.

[89] S. Zhou, Y. Liu, and S. Chen, "Upper bound limit analysis of plates utilizing the c1 natural element method," *Computational Mechanics*, vol. 50, no. 5, pp. 543–561, 2012.

[90] S. Chen, Y. Liu, and Z. Cen, "Lower-bound limit analysis by using the efg method and non-linear programming," *International Journal for Numerical Methods in Engineering*, vol. 74, no. 3, pp. 391–415, 2008.

[91] S. Chen, Y. Liu, and Z. Cen, "Lower bound shakedown analysis by using the element free galerkin method and non-linear programming," *Computer Methods in Applied Mechanics and Engineering*, vol. 197, no. 45-48, pp. 3911–3921, 2008.

[92] C. V. Le, M. Gilbert, and H. Askes, "Limit analysis of plates using the efg method and second-order cone programming," *International Journal for Numerical Methods in Engineering*, vol. 78, no. 13, pp. 1532–1552, 2009.

[93] C. V. Le, M. Gilbert, and H. Askes, "Limit analysis of plates and slabs using a meshless equilibrium formulation," *International Journal for Numerical Methods in Engineering*, vol. 83, no. 13, pp. 1739–1758, 2010.

[94] C. V. Le, H. Askes, and M. Gilbert, "Adaptive element-free galerkin method applied to the limit analysis of plates," *Computer Methods in Applied Mechanics and Engineering*, vol. 199, no. 37-40, pp. 2487–2496, 2010.

[95] C. Le, H. Askes, and M. Gilbert, "A locking-free stabilized kinematic efg model for plane strain limit analysis," *Computers & Structures*, vol. 106, pp. 1–8, 2012.

[96] F. Liu and J. Zhao, "Upper bound limit analysis using radial point interpolation meshless method and nonlinear programming," *International Journal of Mechanical Sciences*, vol. 70, pp. 26–38, 2013.

[97] J. D. Eshelby, "The determination of the elastic field of an ellipsoidal inclusion, and related problems," *Proceedings of the Royal Society of London. Series A. Mathematical and Physical Sciences*, vol. 241, no. 1226, pp. 376–396, 1957.

[98] J. R. Willis, "Variational and related methods for the overall properties of composites," in *Advances in applied mechanics*, vol. 21, pp. 1–78, Elsevier, 1981.

[99] P. P. Castaneda and P. Suquet, "Nonlinear composites," in *Advances in applied mechanics*, vol. 34, pp. 171–302, Elsevier, 1997.

[100] A. Bensoussan, J.-L. Lions, G. Papanicolaou, and T. Caughey, "Asymptotic analysis of periodic structures," *Journal of Applied Mechanics*, vol. 46, p. 477, 1979.

[101] E. Sánchez-Palencia, "Non-homogeneous media and vibration theory," *Lecture notes in physics*, vol. 127, 1980.

[102] S. Suresh, *Fundamentals of metal-matrix composites*. Elsevier, 2013.

[103] C. Huet, "Application of variational concepts to size effects in elastic heterogeneous bodies," *Journal of the Mechanics and Physics of Solids*, vol. 38, no. 6, pp. 813–841, 1990.

[104] P. SQUET, "Local and global aspects in the mathematical theory of plasticity," *Plasticity today*, pp. 279–309, 1985.

[105] R. Smit, W. Brekelmans, and H. Meijer, "Prediction of the mechanical behavior of nonlinear heterogeneous systems by multi-level finite element modeling," *Computer methods in applied mechanics and engineering*, vol. 155, no. 1-2, pp. 181–192, 1998.

[106] F. Feyel and J.-L. Chaboche, "Fe2 multiscale approach for modelling the elastoviscoplastic behaviour of long fibre sic/ti composite materials," *Computer methods in applied mechanics and engineering*, vol. 183, no. 3-4, pp. 309–330, 2000.

[107] V. Kouznetsova, W. Brekelmans, and F. Baaijens, "An approach to micro-macro modeling of heterogeneous materials," *Computational mechanics*, vol. 27, no. 1, pp. 37–48, 2001.

[108] S. Ghosh, K. Lee, and S. Moorthy, "Multiple scale analysis of heterogeneous elastic structures using homogenization theory and voronoi cell finite element method," *International Journal of Solids and Structures*, vol. 32, no. 1, pp. 27–62, 1995.

[109] S. Ghosh, K. Lee, and S. Moorthy, "Two scale analysis of heterogeneous elastic-plastic materials with asymptotic homogenization and voronoi cell finite element model," *Computer methods in applied mechanics and engineering*, vol. 132, no. 1-2, pp. 63–116, 1996.

[110] C. Miehe, J. Schroder, and J. Schotte, "Computational homogenization analysis in finite plasticity simulation of texture development in polycrystalline materials," *Computer methods in applied mechanics and engineering*, vol. 171, no. 3-4, pp. 387–418, 1999.

[111] G. Sfantos and M. Aliabadi, "Multi-scale boundary element modelling of material degradation and fracture," *Computer Methods in Applied Mechanics and Engineering*, vol. 196, no. 7, pp. 1310–1329, 2007.

[112] I. Ahmadi and M. Aghdam, "A truly generalized plane strain meshless method for combined normal and shear loading of fibrous composites," *Engineering Analysis with Boundary Elements*, vol. 35, no. 3, pp. 395–403, 2011.

[113] L. Li, P. Wen, and M. Aliabadi, "Meshfree modeling and homogenization of 3d orthogonal woven composites," *Composites Science and Technology*, vol. 71, no. 15, pp. 1777–1788, 2011.

[114] P. M. Suquet, "Elements of homogenization for inelastic solid mechanics, homogenization techniques for composite media," *Lecture notes in physics*, vol. 272, p. 193, 1985.

[115] D. Buhan, "A homogenization approach to the yield strength of composite materials," *European Journal of Mechanics, A/Solids*, vol. 10, no. 2, pp. 129–154, 1991.

[116] A. Taliercio, "Lower and upper bounds to the macroscopic strength domain of a fiber-reinforced composite material," *International journal of plasticity*, vol. 8, no. 6, pp. 741–762, 1992.

[117] A. Taliercio and P. Sagramoso, "Uniaxial strength of polymeric-matrix fibrous composites predicted through a homogenization approach," *International Journal of Solids and Structures*, vol. 32, no. 14, pp. 2095–2123, 1995.

[118] P. Francescato and J. Pastor, "Lower and upper numerical bounds to the off-axis strength of unidirectional fiber-reinforced composites by limit analysis methods," *European journal of mechanics. A. Solids*, vol. 16, no. 2, pp. 213–234, 1997.

[119] D. Weichert, A. Hachemi, and F. Schwabe, "Application of shakedown analysis to the plastic design of composites," *Archive of Applied Mechanics*, vol. 69, no. 9-10, pp. 623–633, 1999.

[120] H. Zhang, Y. Liu, and B. Xu, "Plastic limit analysis of ductile composite structures from micro-to macro-mechanical analysis," *Acta Mechanica Solida Sinica*, vol. 22, no. 1, pp. 73–84, 2009.

[121] H. Li, Y. Liu, X. Feng, and Z. Cen, "Limit analysis of ductile composites based on homogenization theory," *Proceedings of the Royal Society of London. Series A: Mathematical, Physical and Engineering Sciences*, vol. 459, no. 2031, pp. 659–675, 2003.

[122] H. Li and H. Yu, "Limit analysis of composite materials based on an ellipsoid yield criterion," *International journal of plasticity*, vol. 22, no. 10, pp. 1962–1987, 2006.

[123] H. Li, "Limit analysis of composite materials with anisotropic microstructures: A homogenization approach," *Mechanics of Materials*, vol. 43, no. 10, pp. 574–585, 2011.

[124] H. Li, "Microscopic limit analysis of cohesive-frictional composites with non-associated plastic flow," *European Journal of Mechanics-A/Solids*, vol. 37, pp. 281–293, 2013.

[125] H. Li, "A microscopic nonlinear programming approach to shakedown analysis of cohesive–frictional composites," *Composites Part B: Engineering*, vol. 50, pp. 32–43, 2013.

[126] C. V. Le, P. H. Nguyen, H. Askes, and D. Pham, "A computational homogenization approach for limit analysis of heterogeneous materials," *International Journal for Numerical Methods in Engineering*, vol. 112, no. 10, pp. 1381–1401, 2017.

[127] S. Li and W. K. Liu, "Meshfree and particle methods and their applications," *Applied Mechanics Reviews*, vol. 55, no. 1, pp. 1–34, 2002.

[128] T.-P. Fries, H. Matthies, *et al.*, "Classification and overview of meshfree methods," 2004.

[129] R. A. Gingold and J. J. Monaghan, "Smoothed particle hydrodynamics: theory and application to non-spherical stars," *Monthly notices of the royal astronomical society*, vol. 181, no. 3, pp. 375–389, 1977.

[130] L. B. Lucy, "A numerical approach to the testing of the fission hypothesis," *The astronomical journal*, vol. 82, pp. 1013–1024, 1977.

[131] L. D. Libersky and A. G. Petschek, "Smooth particle hydrodynamics with strength of materials," in *Advances in the free-Lagrange method including contributions on adaptive gridding and the smooth particle hydrodynamics method*, pp. 248–257, Springer, 1991.

[132] T. Belytschko, Y. Y. Lu, and L. Gu, "Element-free galerkin methods," *International journal for numerical methods in engineering*, vol. 37, no. 2, pp. 229–256, 1994.

[133] P. Lancaster and K. Salkauskas, "Surfaces generated by moving least squares methods," *Mathematics of computation*, vol. 37, no. 155, pp. 141–158, 1981.

[134] W. K. Liu, S. Jun, and Y. F. Zhang, "Reproducing kernel particle methods," *International journal for numerical methods in fluids*, vol. 20, no. 8-9, pp. 1081–1106, 1995.

[135] C. A. Duarte and J. T. Oden, "An hp adaptive method using clouds," *Computer methods in applied mechanics and engineering*, vol. 139, no. 1-4, pp. 237–262, 1996.

[136] J. M. Melenk and I. Babuska, "The partition of unity finite element method: basic theory and applications," *Computer methods in applied mechanics and engineering*, vol. 139, no. 1-4, pp. 289–314, 1996.

[137] S. N. Atluri and T. Zhu, "A new meshless local petrov-galerkin (mlpg) approach in computational mechanics," *Computational mechanics*, vol. 22, no. 2, pp. 117–127, 1998.

[138] M. Arroyo and M. Ortiz, "Local maximum-entropy approximation schemes: a seamless bridge between finite elements and meshfree methods," *International journal for numerical methods in engineering*, vol. 65, no. 13, pp. 2167–2202, 2006.

[139] R. Sibson, "A vector identity for the dirichlet tessellation," in *Mathematical Proceedings of the Cambridge Philosophical Society*, vol. 87, pp. 151–155, Cambridge University Press, 1980.

[140] J. Braun and M. Sambridge, "A numerical method for solving partial differential equations on highly irregular evolving grids," *Nature*, vol. 376, no. 6542, p. 655, 1995.

[141] N. Sukumar, B. Moran, and T. Belytschko, "The natural element method in solid mechanics," *International journal for numerical methods in engineering*, vol. 43, no. 5, pp. 839–887, 1998.

[142] R. L. Hardy, "Multiquadric equations of topography and other irregular surfaces," *Journal of geophysical research*, vol. 76, no. 8, pp. 1905–1915, 1971.

[143] R. Franke, "Scattered data interpolation: tests of some methods," *Mathematics of computation*, vol. 38, no. 157, pp. 181–200, 1982.

[144] J. Duchon, "Splines minimizing rotation-invariant semi-norms in sobolev spaces," in *Constructive theory of functions of several variables*, pp. 85–100, Springer, 1977.

[145] E. J. Kansa, "Multiquadrics—a scattered data approximation scheme with applications to computational fluid-dynamics—i surface approximations and partial derivative estimates," *Computers & Mathematics with applications*, vol. 19, no. 8-9, pp. 127–145, 1990.

[146] E. J. Kansa, "Multiquadrics—a scattered data approximation scheme with applications to computational fluid-dynamics—ii solutions to parabolic, hyperbolic and elliptic partial differential equations," *Computers & mathematics with applications*, vol. 19, no. 8-9, pp. 147–161, 1990.

[147] C. K. Lee, X. Liu, and S. C. Fan, "Local multiquadric approximation for solving boundary value problems," *Computational Mechanics*, vol. 30, no. 5-6, pp. 396–409, 2003.

[148] H. Wendland, "Meshless galerkin methods using radial basis functions," *Mathematics of Computation of the American Mathematical Society*, vol. 68, no. 228, pp. 1521–1531, 1999.

[149] G. Liu and Y. Gu, "A local radial point interpolation method (lrpim) for free vibration analyses of 2-d solids," *Journal of Sound and vibration*, vol. 246, no. 1, pp. 29–46, 2001.

[150] N. Mai-Duy and T. Tran-Cong, "Numerical solution of differential equations using multiquadric radial basis function networks," *Neural Networks*, vol. 14, no. 2, pp. 185–199, 2001.

[151] N. Mai-Duy and T. Tran-Cong, "Numerical solution of navier–stokes equations using multiquadric radial basis function networks," *International journal for numerical methods in fluids*, vol. 37, no. 1, pp. 65–86, 2001.

[152] N. Mai-Duy and T. Tran-Cong, "Approximation of function and its derivatives using radial basis function networks," *Applied Mathematical Modelling*, vol. 27, no. 3, pp. 197–220, 2003.

[153] N. Mai-Duy and T. Tran-Cong, "An efficient indirect rbfn-based method for numerical solution of pdes," *Numerical Methods for Partial Differential Equations: An International Journal*, vol. 21, no. 4, pp. 770–790, 2005.

[154] T. Belytschko and T. Black, "Elastic crack growth in finite elements with minimal remeshing," *International journal for numerical methods in engineering*, vol. 45, no. 5, pp. 601–620, 1999.

[155] N. Moës, J. Dolbow, and T. Belytschko, "A finite element method for crack growth without remeshing," *International journal for numerical methods in engineering*, vol. 46, no. 1, pp. 131–150, 1999.

[156] G.-R. Liu, *Meshfree methods: moving beyond the finite element method*. CRC press, 2009.

[157] G. E. Fasshauer, *Meshfree approximation methods with MATLAB*, vol. 6. World Scientific, 2007.

[158] C. Le, *Novel numerical procedures for limit analysis of structures: Mesh-free methods and mathematical programming*. PhD thesis, University of Sheffield, 2010.

[159] Y. Lu, T. Belytschko, and L. Gu, "A new implementation of the element free galerkin method," *Computer methods in applied mechanics and engineering*, vol. 113, no. 3-4, pp. 397–414, 1994.

[160] T. Belytschko, Y. Lu, L. Gu, and M. Tabbara, "Element-free galerkin methods for static and dynamic fracture," *International Journal of Solids and Structures*, vol. 32, no. 17-18, pp. 2547–2570, 1995.

[161] T. Zhu and S. Atluri, "A modified collocation method and a penalty formulation for enforcing the essential boundary conditions in the element free galerkin method," *Computational Mechanics*, vol. 21, no. 3, pp. 211–222, 1998.

[162] S. Atluri and T. Zhu, "New concepts in meshless methods," *International Journal for Numerical Methods in Engineering*, vol. 47, no. 1-3, pp. 537–556, 2000.

[163] A. Huerta and S. Fernandez-Mendez, "Enrichment and coupling of the finite element and meshless methods," *International Journal for Numerical Methods in Engineering*, vol. 48, no. 11, pp. 1615–1636, 2000.

[164] G. J. Wagner and W. K. Liu, "Application of essential boundary conditions in mesh-free methods: a corrected collocation method," *International Journal for Numerical Methods in Engineering*, vol. 47, no. 8, pp. 1367–1379, 2000.

[165] S. Beissel and T. Belytschko, "Nodal integration of the element-free galerkin method," *Computer methods in applied mechanics and engineering*, vol. 139, no. 1-4, pp. 49–74, 1996.

[166] J.-S. Chen, C.-T. Wu, S. Yoon, and Y. You, "A stabilized conforming nodal integration for galerkin mesh-free methods," *International journal for numerical methods in engineering*, vol. 50, no. 2, pp. 435–466, 2001.

[167] J.-S. Chen, M. Hillman, and M. Rüter, "An arbitrary order variationally consistent integration for galerkin meshfree methods," *International Journal for Numerical Methods in Engineering*, vol. 95, no. 5, pp. 387–418, 2013.

[168] C. Smith and M. Gilbert, "Application of discontinuity layout optimization to plane plasticity problems," *Proceedings of the Royal Society A: Mathematical, Physical and Engineering Sciences*, vol. 463, no. 2086, pp. 2461–2484, 2007.

[169] E. Christiansen and O. S. Pedersen, "Automatic mesh refinement in limit analysis," *International Journal for Numerical Methods in Engineering*, vol. 50, no. 6, pp. 1331–1346, 2001.

[170] L. Borges, N. Zouain, C. Costa, and R. Feijoo, "An adaptive approach to limit analysis," *International Journal of Solids and Structures*, vol. 38, no. 10-13, pp. 1707–1720, 2001.

[171] J. R. Q. Franco, A. R. Ponter, and F. B. Barros, "Adaptive fe method for the shakedown and limit analysis of pressure vessels," *European Journal of Mechanics-A/Solids*, vol. 22, no. 4, pp. 525–533, 2003.

[172] A. V. Lyamin and S. W. Sloan, "Mesh generation for lower bound limit analysis," *Advances in Engineering Software*, vol. 34, no. 6, pp. 321–338, 2003.

[173] W. Cecot, "Application of h-adaptive fem and zarka's approach to analysis of shakedown problems," *International journal for numerical methods in engineering*, vol. 61, no. 12, pp. 2139–2158, 2004.

[174] N. Ngo and F. Tin-Loi, "Shakedown analysis using the p-adaptive finite element method and linear programming," *Engineering structures*, vol. 29, no. 1, pp. 46–56, 2007.

[175] H. Ciria, J. Peraire, and J. Bonet, "Mesh adaptive computation of upper and lower bounds in limit analysis," *International journal for numerical methods in engineering*, vol. 75, no. 8, pp. 899–944, 2008.

[176] C. V. Le, "A stabilized discrete shear gap finite element for adaptive limit analysis of mindlin–reissner plates," *International Journal for Numerical Methods in Engineering*, vol. 96, no. 4, pp. 231–246, 2013.

[177] N. Pham-Sy, C. Tran, N. Mai-Duy, and T. Tran-Cong, "Parallel control-volume method based on compact local integrated rbfs for the solution of fluid flow problems," *CMES: Computer Modeling in Engineering and Sciences*, vol. 100, no. 5, pp. 363–397, 2014.

[178] P. B. Le, T. Rabczuk, N. Mai-Duy, and T. Tran-Cong, "A moving irbfn-based galerkin meshless method," *CMES: Computer Modeling in Engineering and Sciences*, vol. 66, no. 1, pp. 25–52, 2010.

[179] E. Christiansen, "Computation of limit loads," *International Journal for Numerical Methods in Engineering*, vol. 17, no. 10, pp. 1547–1570, 1981.

[180] E. Christiansen and K. Kortanek, "Computation of the collapse state in limit analysis using the lp primal affine scaling algorithm," *Journal of Computational and Applied Mathematics*, vol. 34, no. 1, pp. 47–63, 1991.

[181] K. D. Andersen and E. Christiansen, "Limit analysis with the dual affine scaling algorithm," *Journal of computational and Applied Mathematics*, vol. 59, no. 2, pp. 233–243, 1995.

[182] M. Chen, A. Hachemi, and D. Weichert, "A non-conforming finite element for limit analysis of periodic composites," *PAMM*, vol. 10, no. 1, pp. 405–406, 2010.

[183] V. Carvelli, G. Maier, and A. Taliercio, "Kinematic limit analysis of periodic heterogeneous media," *CMES(Computer Modelling in Engineering & Sciences)*, vol. 1, no. 2, pp. 19–30, 2000.

[184] A. Hachemi, M. Chen, G. Chen, and D. Weichert, "Limit state of structures made of heterogeneous materials," *International Journal of Plasticity*, vol. 63, pp. 124–137, 2014.

[185] J. Konig and M. Kleiber, "New method of shakedown analysis," *BULLETIN DE L ACADEMIE POLONAISE DES SCIENCES-SERIE DES SCIENCES TECHNIQUES*, vol. 26, no. 4, pp. 275–281, 1978.

[186] K.-J. Bathe, *Finite element procedures*. Klaus-Jurgen Bathe, 2006.

[187] S. Krenk, L. Damkilde, and O. Hoyer, "Limit analysis and optimal design of plates with equilibrium elements," *Journal of Engineering Mechanics*, vol. 120, no. 6, pp. 1237–1254, 1994.

[188] P. N. Poulsen and L. Damkilde, "Limit state analysis of reinforced concrete plates subjected to in-plane forces," *International Journal of Solids and Structures*, vol. 37, no. 42, pp. 6011–6029, 2000.

[189] L. Prandtl, "Uber die harte plastischer korper," *Nachrichten von der Gesellschaft der Wissenschaften zu Gottingen, Mathematisch-Physikalische Klasse*, vol. 1920, pp. 74–85, 1920.

[190] A. Makrodimopoulos and C. Martin, "Upper bound limit analysis using simplex strain elements and second-order cone programming," *International journal for numerical and analytical methods in geomechanics*, vol. 31, no. 6, pp. 835–865, 2007.

[191] M. Vicente da Silva and A. Antao, "A non-linear programming method approach for upper bound limit analysis," *International Journal for Numerical Methods in Engineering*, vol. 72, no. 10, pp. 1192–1218, 2007.

[192] S. Sloan and P. Kleeman, "Upper bound limit analysis using discontinuous velocity fields," *Computer Methods in Applied Mechanics and Engineering*, vol. 127, no. 1-4, pp. 293–314, 1995.

[193] T. Belytschko and P. G. Hodge, "Plane stress limit analysis by finite elements," *Journal of the Engineering Mechanics Division*, vol. 96, no. 6, pp. 931–944, 1970.

[194] Z. Pixin, L. Mingwan, and H. Kehchih, "A mathematical programming algorithm for limit analysis," *Acta Mechanica Sinica*, vol. 7, no. 3, pp. 267–274, 1991.

[195] X. Zhang, Y. Liu, Y. Zhao, and Z. Cen, "Lower bound limit analysis by the symmetric galerkin boundary element method and the complex method," *Computer Methods in Applied Mechanics and Engineering*, vol. 191, no. 17-18, pp. 1967–1982, 2002.

[196] J. C. Nagtegaal, D. M. Parks, and J. Rice, "On numerically accurate finite element solutions in the fully plastic range," *Computer methods in applied mechanics and engineering*, vol. 4, no. 2, pp. 153–177, 1974.

[197] F. Tin-Loi and N. Ngo, "Performance of the p-version finite element method for limit analysis," *International Journal of Mechanical Sciences*, vol. 45, no. 6-7, pp. 1149–1166, 2003.

[198] E. Christiansen and K. D. Andersen, "Computation of collapse states with von mises type yield condition," *International Journal for Numerical Methods in Engineering*, vol. 46, no. 8, pp. 1185–1202, 1999.

[199] A. Bottero, R. Negre, J. Pastor, and S. Turgeman, "Finite element method and limit analysis theory for soil mechanics problems," *Computer Methods in Applied Mechanics and Engineering*, vol. 22, no. 1, pp. 131–149, 1980.

[200] K. Krabbenhoft and L. Damkilde, "A general non-linear optimization algorithm for lower bound limit analysis," *International Journal for Numerical Methods in Engineering*, vol. 56, no. 2, pp. 165–184, 2003.

[201] H. Chan, "The collapse load of reinforced concrete plate," *International Journal for Numerical Methods in Engineering*, vol. 5, no. 1, pp. 57–64, 1972.

[202] J. Munro and J. Danro, "Yield line method by finite elements and linear programming," *Structural Engineer*, vol. 56, no. 2, 1978.

[203] A. Ramsay and D. Johnson, "Analysis of practical slab configurations using automated yield-line analysis and geometric optimization of fracture patterns," *Engineering structures*, vol. 20, no. 8, pp. 647–654, 1998.

[204] M. Gohnert, "Collapse load analysis of yield-line elements," *Engineering Structures*, vol. 22, no. 8, pp. 1048–1054, 2000.

[205] M. Gilbert, L. He, C. C. Smith, and C. V. Le, "Automatic yield-line analysis of slabs using discontinuity layout optimization," *Proceedings of the Royal Society A: Mathematical, Physical and Engineering Sciences*, vol. 470, no. 2168, p. 20140071, 2014.

[206] L. He and M. Gilbert, "Automatic rationalization of yield-line patterns identified using discontinuity layout optimization," *International Journal of Solids and Structures*, vol. 84, pp. 27–39, 2016.

[207] E. Maunder and A. Ramsay, "Equilibrium models for lower bound limit analyses of reinforced concrete slabs," *Computers & Structures*, vol. 108, pp. 100–109, 2012.

[208] C. V. Le, P. H. Nguyen, and T. Q. Chu, "A curvature smoothing hsieh–clough–tocher element for yield design of reinforced concrete slabs," *Computers & Structures*, vol. 152, pp. 59–65, 2015.

[209] C. V. Le, P. L. Ho, P. H. Nguyen, and T. Q. Chu, "Yield design of reinforced concrete slabs using a rotation-free meshfree method," *Engineering Analysis with Boundary Elements*, vol. 50, pp. 231–238, 2015.

[210] E. Onate and M. Cervera, "Derivation of thin plate bending elements with one degree of freedom per node: a simple three node triangle," *Engineering computations*, vol. 10, no. 6, pp. 543–561, 1993.

[211] F. Sabourin and M. Brunet, "Analysis of plates and shells with a simplified three node triangular element," *Thin-walled structures*, vol. 21, no. 3, pp. 209–223, 1995.

[212] F. Sabourin and M. Brunet, "Detailed formulation of the rotation-free triangular element "s3" for general purpose shell analysis," *Engineering computations*, vol. 23, no. 5, pp. 469–502, 2006.

[213] A. S. Al-Sabah and H. Falter, "Finite element lower bound "yield line" analysis of isotropic slabs using rotation-free elements," *Engineering Structures*, vol. 53, pp. 38–51, 2013.

[214] P. Krysl and T. Belytschko, "Analysis of thin plates by the element-free galerkin method," *Computational Mechanics*, vol. 17, no. 1-2, pp. 26–35, 1995.

[215] T. Q. Bui, T. N. Nguyen, and H. Nguyen-Dang, "A moving kriging interpolation-based meshless method for numerical simulation of kirchhoff plate problems," *International Journal for Numerical Methods in Engineering*, vol. 77, no. 10, pp. 1371–1395, 2009.

[216] X. Cui, G. Liu, G. Li, and G. Zhang, "A thin plate formulation without rotation dofs based on the radial point interpolation method and triangular cells," *International journal for numerical methods in engineering*, vol. 85, no. 8, pp. 958–986, 2011.

[217] X. Cui, G. Liu, and G. Li, "A smoothed hermite radial point interpolation method for thin plate analysis," *Archive of Applied Mechanics*, vol. 81, no. 1, pp. 1–18, 2011.

[218] M. P. Nielsen and L. C. Hoang, *Limit analysis and concrete plasticity*. CRC press, 2016.

[219] K. W. Johansen, *Yield-line theory*. Cement and Concrete Association, 1962.

[220] E. N. Fox, "Limit analysis for plates: the exact solution for a clamped square plate of isotropic homogeneous material obeying the square yield criteron and loaded by uniform pressure," *Philosophical Transactions of the Royal Society of London. Series A, Mathematical and Physical Sciences*, vol. 277, no. 1265, pp. 121–155, 1974.

[221] J. Groβ-Weege, "On the numerical assessment of the safety factor of elastic-plastic structures under variable loading," *International Journal of Mechanical Sciences*, vol. 39, no. 4, pp. 417–433, 1997.

[222] K. V. Spiliopoulos and K. D. Panagiotou, "A direct method to predict cyclic steady states of elastoplastic structures," *Computer Methods in Applied Mechanics and Engineering*, vol. 223, pp. 186–198, 2012.

[223] N. Zouain and R. SantAnna, "Computational formulation for the asymptotic response of elastoplastic solids under cyclic loads," *European Journal of Mechanics-A/Solids*, vol. 61, pp. 267–278, 2017.

[224] N. D. Hung and L. Palgen, "Shakedown analysis by displacement method and equilibrium finite element," *Transactions of the Canadian Society for Mechanical Engineering*, vol. 6, no. 1, pp. 34–40, 1980.

[225] F. Genna, "A nonlinear inequality, finite element approach to the direct computation of shakedown load safety factors," *International journal of mechanical sciences*, vol. 30, no. 10, pp. 769–789, 1988.

[226] N. Zouain, L. Borges, and J. L. Silveira, "An algorithm for shakedown analysis with nonlinear yield functions," *Computer Methods in Applied Mechanics and Engineering*, vol. 191, no. 23-24, pp. 2463–2481, 2002.

[227] P. L. Ho, C. V. Le, and T. Tran-Cong, "Displacement and equilibrium mesh-free formulation based on integrated radial basis functions for dual yield design," *Engineering Analysis with Boundary Elements*, vol. 71, pp. 92–100, 2016.

[228] L. Corradi and A. Zavelani, "A linear programming approach to shakedown analysis of structures," *Computer Methods in Applied Mechanics and Engineering*, vol. 3, no. 1, pp. 37–53, 1974.

[229] K. Krabbenhoft, A. Lyamin, and S. Sloan, "Bounds to shakedown loads for a class of deviatoric plasticity models," *Computational Mechanics*, vol. 39, no. 6, pp. 879–888, 2007.

[230] F. Gaydon and A. McCrum, "A theoretical investigation of the yield point loading of a square plate with a central circular hole," *Journal of the Mechanics and Physics of Solids*, vol. 2, no. 3, pp. 156–169, 1954.

[231] G. Garcea, G. Armentano, S. Petrolo, and R. Casciaro, "Finite element shakedown analysis of two-dimensional structures," *International journal for numerical methods in engineering*, vol. 63, no. 8, pp. 1174–1202, 2005.

[232] T. N. Tran *et al.*, "Limit and shakedown analysis of plates and shells including uncertainties," 2008.

[233] D. K. Vu, "Dual limit and shakedown analysis of structures," *Doctor thesis, University of Liege Faculty of Applied Sciences, Liege*, 2001.

[234] W. Prager and P. G. Hodge, *Theory of perfectly plastic solids*. Dover Publications, 1968.

[235] R. Casciaro and L. Cascini, "A mixed formulation and mixed finite elements for limit analysis," *International Journal for Numerical Methods in Engineering*, vol. 18, no. 2, pp. 211–243, 1982.

[236] A.-M. Yan, *Contributions to the direct limit state analysis of plastified and cracked structures*. PhD thesis, Universite de Liege, Faculte des Sciences appliquees, 1999.

[237] J. Salençon, *Yield design*. John Wiley & Sons, 2013.